Metal-insulator transition from combined disorder and interaction effects in Hubbard-like electronic lattice models with random hopping

Matthew S. Foster[1,*] and Andreas W. W. Ludwig[2]

[1]*Department of Physics, Columbia University, New York, New York 10027, USA*
[2]*Department of Physics, University of California, Santa Barbara, California 93106, USA*

We uncover a disorder-driven instability in the diffusive Fermi liquid phase of a class of many-fermion systems, indicative of a metal-insulator transition of first-order type, which arises solely from the competition between quenched disorder and interparticle interactions. Our result is expected to be relevant for sufficiently strong disorder in $d=3$ spatial dimensions. Specifically, we study a class of half-filled, Hubbard-like models for spinless fermions with (complex) random hopping and short-ranged interactions on bipartite lattices in $d \geq 2$. In a given realization, the hopping disorder breaks time-reversal invariance but preserves the special "nesting" symmetry responsible for the charge density wave instability of the ballistic Fermi liquid. This disorder may arise, e.g., from the application of a random magnetic field to the otherwise *clean* model. We derive a low-energy effective field theory description for this class of disordered, interacting fermion systems, which takes the form of a Finkel'stein nonlinear sigma model (FNLσM) (A. M. Finkel'stein, Zh. Eksp. Teor. Fiz. **84**, 168 (1983) [Sov. Phys. JETP **57**, 97 (1983)]). We analyze the FNLσM using a perturbative, one-loop renormalization group analysis controlled via an ϵ expansion in $d=2+\epsilon$ dimensions. We find that in $d=2$ dimensions, the interactions destabilize the conducting phase known to exist in the disordered, noninteracting system. The metal-insulator transition that we identify in $d > 2$ dimensions ($\epsilon > 0$) occurs for disorder strengths of order ϵ, and is therefore perturbatively accessible for $\epsilon \ll 1$. We emphasize that the disordered system has no localized phase in the absence of interactions, so that a localized phase and the transition into it can only appear due to the presence of the interactions.

I. INTRODUCTION

In many experimental situations, the effects of *both* static ("quenched") disorder and interparticle interactions may play comparatively important roles. These issues have, for example, come again to the forefront of debate in view of discussions centered around the fascinating yet still controversial "metal-insulator transition" observed in two-dimensional (2D) semiconductor inversion layers.[1] Unfortunately, theoretical descriptions of quantum many-particle systems incorporating both disorder and interactions are typically quite challenging and difficult to reliably analyze.

With this state of affairs in mind, in this paper, we apply a powerful analytical technique, known as the Finkel'stein nonlinear sigma model (FNLσM) formalism,[2,3] to a model of spinless lattice fermions subject simultaneously to both static disorder and short-ranged interactions. The isolated effects of disorder or interactions on the lattice model that we consider are already well understood yet still nontrivial. Our goal is to gain insight into the possible interplay between the Fermi liquid, the Mott insulating, and what we term the "Anderson–Mott"[4] insulating phases of interacting many-body Fermi systems in spatial dimensions $d \geq 2$. The FNLσM formalism admits a renormalization group analysis controlled via an ϵ expansion in $d=2+\epsilon$ dimensions, permitting us to address the following general questions within the context of our model: In the simultaneous presence of both disorder and interactions, (i) does a conducting phase occur in $d=2$, and (ii) is there a metal-insulator transition (MIT) in dimensions $d > 2$? If yes, what is its nature?

The primary purpose of this paper is to present a detailed derivation and a thorough discussion of results previously announced briefly in Ref. 5. A short summary of these results and an outline of this work appear below in Sec. I C.

A. Interactions and sublattice symmetry

We study a class of "Hubbard-like" models[6] for spinless fermions *at half-filling* on bipartite lattices, possessing short-ranged interparticle interactions and quenched disorder. We work in $d \geq 2$ spatial dimensions throughout. For concreteness, in this introduction, we consider the hypercubic lattice. By definition, any bipartite lattice may be subdivided into two interpenetrating sublattices, which we will distinguish with the labels A and B. The $d=2$ dimensional example of the square lattice is depicted in Fig. 1.

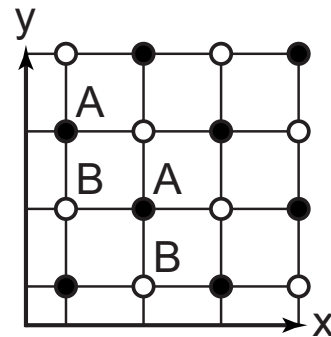Our starting point is the clean (zero-disorder), generalized Hubbard-like Hamiltonian

FIG. 1. The square lattice. Labels A and B denote sites belonging to the black and blank square sublattices, respectively.

165108-1

$$H_0 = -t\sum_{\langle ij\rangle} c_{Ai}^{\dagger}c_{Bj} + \text{H.c.} + V\sum_{\langle ij\rangle}\delta\hat{n}_{Ai}\delta\hat{n}_{Bj}$$
$$+ U\left(\sum_{\langle\langle ii'\rangle\rangle}\delta\hat{n}_{Ai}\delta\hat{n}_{Ai'} + \sum_{\langle\langle jj'\rangle\rangle}\delta\hat{n}_{Bj}\delta\hat{n}_{Bj'}\right), \quad (1.1)$$

where $c_{Ai}^{\dagger}$ and c_{Bj} are creation and annihilation operators for spinless fermions on the A and B sublattices of the bipartite lattice, respectively. Here, i and j index, respectively, the A and B sublattice sites, and the sums on $\langle ij\rangle$ run over all nearest-neighbor A-B lattice bonds, while the sums on $\langle\langle ii'\rangle\rangle$ and $\langle\langle jj'\rangle\rangle$ run over all next-nearest-neighbor (same sublattice) pairs of sites. The homogeneous hopping amplitude t is taken to be real. The operators $\delta\hat{n}_{A/B} \equiv (c_{A/B}^{\dagger}c_{A/B} - \frac{1}{2})$ denote deviations of the local sublattice (A or B) fermion densities from their value at half-filling. Finally, the interaction strengths V and U appearing in Eq. (1.1) couple to nearest-neighbor and next-nearest-neighbor density-density interactions, respectively.

The model at half-filling, given by Eq. (1.1), possesses the following special symmetry, which we refer to here as "sublattice" symmetry (SLS) [this symmetry is termed "chiral" in the classification scheme of Ref. 7 (see also Refs. 8–18)]: the Hubbard-like Hamiltonian in Eq. (1.1) is invariant under the transformation

$$c_{Ai} \to c_{Ai}^{\dagger}, \quad c_{Bj} \to -c_{Bj}^{\dagger}, \quad (1.2)$$

where we simultaneously complex conjugate all scalar terms in the Hamiltonian. [This transformation, like that of time reversal, is antiunitary. In the presence of time-reversal invariance (TRI), SLS is equivalent to the usual particle-hole symmetry.] As is well known, the Fermi surface[19] of the half-filled, noninteracting model, Eq. (1.1) with $U=V=0$, possesses perfect "nesting,"

$$\varepsilon(\mathbf{k}+\mathbf{K_N}) = -\varepsilon(\mathbf{k}), \quad (1.3)$$

where $\varepsilon(\mathbf{k})$ is the noninteracting band structure, and $\mathbf{K_N}$ is a nesting wave vector. For the hypercubic lattice with lattice spacing $a=1$, $\mathbf{K_N}$ takes the form

$$\mathbf{K_N} \equiv \pi(n_1, n_2, \ldots, n_d), \quad (1.4)$$

where the numbers $n_s = \pm 1$, with $s \in \{1, \ldots, d\}$. Figure 2 depicts the Brillouin zone (BZ) associated with the square lattice shown in Fig. 1. The set of nesting wave vectors $\{\mathbf{K_N}\}$ defined in Eq. (1.4) span the *sublattice* Brillouin zone (sBZ), appropriate to the A and B sublattices of the composite bipartite lattice. For the special case of the square lattice, the boundary of the sBZ also serves as the Fermi line at half-filling, shown in Fig. 2.

Nesting and SLS are tied together. Under the transformation given by Eq. (1.2), the hopping part of the Hamiltonian in Eq. (1.1) transforms as
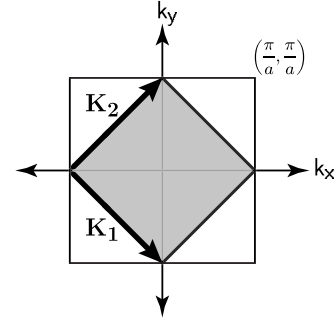

FIG. 2. BZ associated with the square lattice shown in Fig. 1. The shaded subregion is the sBZ appropriate to the A and B sublattices. This subregion also indicates the Fermi sea at half-filling, an attribute particular to the square lattice model. The nesting wave vectors $\mathbf{K_1}$ and $\mathbf{K_2}$ are reciprocal lattice vectors for the sBZ.

$$\int_{\text{BZ}}\frac{d^d\mathbf{k}}{(2\pi)^d}\varepsilon(\mathbf{k})c_{\mathbf{k}}^{\dagger}c_{\mathbf{k}} \to \int_{\text{BZ}}\frac{d^d\mathbf{k}}{(2\pi)^d}\varepsilon^*(\mathbf{k})c_{\mathbf{k}-\mathbf{K_N}}c_{\mathbf{k}-\mathbf{K_N}}^{\dagger}$$
$$= \int_{\text{BZ}}\frac{d^d\mathbf{k}}{(2\pi)^d}[-\varepsilon(\mathbf{k}+\mathbf{K_N})]c_{\mathbf{k}}^{\dagger}c_{\mathbf{k}}, \quad (1.5)$$

where $\mathbf{K_N}$ is a nesting wave vector as in Eq. (1.4), and

$$c_{\mathbf{k}} \equiv \sum_{i\in A}e^{-i\mathbf{k}\cdot\mathbf{R}_i}c_{Ai} + \sum_{j\in B}e^{-i\mathbf{k}\cdot\mathbf{R}_j}c_{Bj}. \quad (1.6)$$

Fermi surface nesting is, in a sense, the *defining* property of Hubbard-like models for interacting lattice fermions in $d \geq 2$ dimensions. It is the nesting condition which makes the ballistic Fermi liquid phase at half-filling in such models unstable to Mott insulating order in the presence of generic, arbitrarily weak interparticle interactions.[22–24] Nesting instabilities can occur for microscopically repulsive interparticle interaction strengths and arise through the exchange of the nesting momenta $\{\mathbf{K_N}\}$ through the particle-hole channel of these interactions. Such models may also exhibit the BCS superconducting instability,[25] which exists for any TRI Fermi liquid with (effectively) attractive pairing interactions. The ground state of such a half-filled, Hubbard-like model with weak but nonvanishing interactions is typically a Mott insulator, with lattice translational symmetry spontaneously broken at the nesting wavelength, a superconductor, or a mixture of these, such as a "supersolid."[22,24,26,27]

A simple calculation[23] using the random phase approximation (RPA) predicts that the Fermi liquid phase of the (nondisordered) model defined by Eq. (1.1) is unstable to charge density wave (CDW) order for any $V > U \geq 0$. The CDW state is a Mott insulator, in which a greater proportion of the fermion density resides on one sublattice than on the other. For the 2D case of the square lattice, the RPA calculation predicts a transition to the CDW state at a temperature

$$T_c \sim 2t\exp\left[-\pi\sqrt{\frac{t}{V-U}}\right] \quad (1.7)$$

in the weak coupling limit $0 \leq U < V \ll t$. Alternatively, a one-loop renormalization group (RG) calculation,[24] per-

formed on a low-energy effective field theory description of the model given by Eq. (1.1), shows that the effective CDW interaction strength, which we define here as

$$W_c \sim \frac{1}{2}(U - V) \qquad (1.8)$$

(corresponding to a staggered charge density), grows to large *negative* values under renormalization if its initial value $W_c^{(0)} < 0$, i.e., was negative to begin with. This run off to strong interaction coupling is taken to signal the onset of CDW formation.[28] These and analogous results regarding the Néel ground state of the half-filled, spin-1/2 Hubbard model in $d \geq 2$ are well established, and the latter have been further confirmed with extensive numerical work. (See, e.g., Refs. 22, 27, and 29.) The spinless Hubbard-like Hamiltonian in Eq. (1.1), on the other hand, has received less attention in the numerical literature; early Monte Carlo studies[23] of the 2D version of this Hamiltonian, with $U \equiv 0$, show the existence of a CDW ground state for positive V but were unable to access the weak coupling limit $V \to 0^+$.

B. Quenched disorder

Now, we turn to the incorporation of quenched (static) disorder into the model given by Eq. (1.1). First, note that the addition of on-site (or "diagonal") randomness, characterized by a strength λ_D, breaks sublattice symmetry [Eq. (1.2)] in every realization of disorder. Thus, turning on diagonal disorder is expected to destroy the CDW ground state,[30,31] at least for sufficiently weak interactions. [By keeping the disorder strength λ_D fixed, for example, we expect the absence of zero temperature CDW order in a window of (small) interaction strengths, e.g., for $0 \leq V < V_c(\lambda_D)$, with $U=0$.] The proximity of a Mott insulating phase to the *noninteracting* (ballistic) Fermi liquid is the most essential characteristic of the Hubbard-like lattice model defined in Eq. (1.1). We conclude that this characteristic is *lost* upon the incorporation of diagonal disorder. Studies of Hubbard-like models subject to diagonal disorder include those listed in Refs. 30–32 and Refs. 33–35 for spinless and spin-1/2 lattice fermions, respectively.

Instead, we consider the Hamiltonian in Eq. (1.1), weakly perturbed by purely "off-diagonal" randomness, which is taken to occur only in the intersublattice hopping amplitudes. Such a model is invariant under the SLS transformation [Eq. (1.2)] for each and every static realization of the disorder. We consider *complex* random (nearest-neighbor) hopping that breaks TRI. (Without interactions, the model is in the chiral symmetry class AIII of Ref. 7.) The full lattice Hamiltonian is given by $H = H_0 + \delta H$, where H_0 was defined in Eq. (1.1), and

$$\delta H = -\sum_{\langle ij \rangle} \delta t_{i,j} c_{Ai}^\dagger c_{Bj} + \text{H.c.} \qquad (1.9)$$

Here, the random part of the hopping matrix element, $\delta t_{i,j}$, is taken to be a Gaussian complex random variable with zero mean, independent on different lattice links. For our system of spinless fermions, this is consistent with the application of a random magnetic field to the otherwise *clean* model. For

noninteracting spin-1/2 fermion systems, with nearest-neighbor hopping on bipartite lattices at half-filling, in random orbital and/or Zeeman magnetic fields, a general classification is (briefly) mentioned in Sec. II B, with more details being provided in Appendix B. We will conclude from this classification that the results of this paper also apply to a related Hubbard-like model of spin-1/2 fermions, subject to an orbital magnetic field and to (homogeneous or random) spin-orbit coupling. Independent work on the effects of interparticle interactions on these and several other classes of disordered spin-1/2 fermions has very recently appeared in Ref. 36.

Our principal motivation for studying the model in Eqs. (1.1) and (1.9) is that, due to the presence of SLS, we expect both disorder and interparticle interactions to play important roles in the description of the low-energy physics. Because random hopping preserves the special SLS, our disordered model retains the nesting CDW instability of the associated clean system. This instability can therefore compete with the unusual localization physics arising from SLS in the disordered but noninteracting model (see below). The further assumption of broken TRI guarantees that we do not have to confront an additional superconducting instability.[3,22–24,37] We note that the effects of hopping disorder on the Néel ground state of the (slightly more complex) spin-1/2 Hubbard model at half-filling were studied numerically in Refs. 38 and 39, although these studies were limited to $d=2$.

A second motivating factor is that, interestingly, and as alluded to above, the presence of SLS radically changes the localization physics of the disordered, noninteracting random hopping model [Eqs. (1.1) and (1.9) with $V=U=0$]. SLS enables the random hopping model (RHM) to *evade* the phenomenon of Anderson localization. Specifically, the noninteracting system exhibits a critical, delocalized phase at the band center (half-filling) in one, two, and three dimensions for finite disorder strength, with a strongly divergent low-energy density of states (DOS) in $d=1,2$.[8–17] In particular, there is no MIT and no Anderson insulating phase in $d=3$ (in the absence of interactions). The essential features of random hopping model physics are summarized in Figs. 3 and 4. These figures apply, for example, to spinless lattice fermions with sublattice symmetry, with or without TRI (classes BDI and AIII, respectively),[7] in $d \geq 2$. Upon approaching the band center ($\varepsilon = 0$) in two dimensions, both the density of states $\nu(\varepsilon)$ and the localization length $\zeta(\varepsilon)$ strongly diverge, as indicated in Fig. 3. By contrast, RHMs in $d > 2$ support a diffusive metallic phase,[9,12] characterized by a band of delocalized states with energies $|\varepsilon| < \varepsilon_c$, represented by the shaded regions in Fig. 4. ($\varepsilon = \pm\varepsilon_c$ are particle and hole mobility edges.) While ε_c is expected to decrease monotonically with increasing disorder, as indicated by the arrows along the dashed boundaries of the shaded region in Figs. 4(a) and 4(b), it is believed that in $d > 2$, there always remains a region of delocalized states of finite thickness in energy, centered around $\varepsilon = 0$, for any finite disorder strength in a non-interacting system with SLS.

Indeed, random hopping models have been of significant theoretical interest in the recent past both because of the unusual delocalization physics described above and also because these models have proven amenable to a variety of
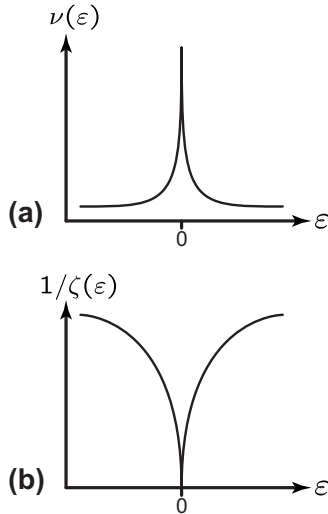
FIG. 3. Features of RHM physics in two dimensions in the *absence* of interparticle interactions. (a) and (b) depict the qualitative energy (ε) dependence of the density of states ν and inverse localization length $1/\zeta$, respectively, in the chiral (Ref. 7) orthogonal (BDI) and unitary (AIII) class RHMs in $d=2$. Both ν and ζ diverge upon approaching the band center, taken to occur at $\varepsilon=0$ (Refs. 9, 12, and 13).

powerful analytical techniques in $d \leq 2$, with many exact and/or nonperturbative features now understood.[8,13,15,17] This situation should be contrasted with our understanding of the conventional noninteracting ("Wigner–Dyson") MIT, which is based largely on perturbative analytical results in $d > 2$ using the ϵ expansion.[40]
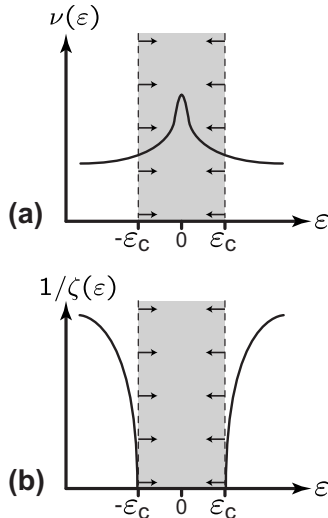

FIG. 4. Same as Fig. 3 but for spatial dimensionalities $d > 2$, e.g., noninteracting random hopping model physics in three dimensions. Here, the shaded area represents a band of extended (delocalized) states; ε_c is the mobility edge. Increasing the strength of the random hopping disorder narrows the region of extended states in $d > 2$, as indicated by the arrows in (a) and (b). The DOS is finite, albeit parametrically enhanced at the band center (Refs. 9 and 12).

C. Summary of results and outline

In this work, we analyze the stability of the diffusive Fermi liquid phase of the Hubbard-like model defined by Eqs. (1.1) and (1.9) in the simultaneous presence of both disorder and interactions. We derive a low-energy, continuum field theory description of this system, which takes the form of a (class AIII)[7] FNLσM.[2,3] We employ the Schwinger–Keldysh[41] method in order to ensemble average over realizations of the hopping disorder. The FNLσM contains parameters which specify the random hopping disorder and the interparticle interaction strengths. We compute the one-loop renormalization group flow equations for these parameters using a Wilsonian frequency-momentum shell background field methodology.[2] We then discuss the physics of our model in (i) $d=2$ and (ii) $d>2$ dimensions. We now briefly discuss our results:

For the 2D case, we find that the conducting phase of the disordered, noninteracting system is destabilized by the interactions. By contrast, such a phase, a metallic "diffusive Fermi liquid," does exist (trivially) in $d>2$; we identify what we call an Anderson–Mott disorder-driven instability of this metallic diffusive Fermi liquid. This instability arises *solely* from the competition between disorder and short-ranged interactions and is perturbatively controlled via an ϵ expansion in $d=2+\epsilon$. The instability that we find is indicative of a first-order MIT; it occurs for disorder strengths of order ϵ, and is therefore perturbatively accessible for $\epsilon \ll 1$. We expect our result to be relevant for the Hubbard-like model in Eqs. (1.1) and (1.9) in three spatial dimensions ($\epsilon=1$) for sufficiently strong disorder, and we stress that this Anderson–Mott instability is clearly distinct from the pure Mott nesting instability, which is driven solely by interactions (and not by disorder), although the latter also appears in the phase diagram of our model (see Fig. 23). The noninteracting random hopping model, Eqs. (1.1) and (1.9) with $V=U=0$, has no localized phase with disorder in the absence of interactions (see, e.g., Sec. V A 1); therefore, a localized phase can only appear due to the presence of the interactions. The discovery of this disorder-driven, interaction-mediated diffusive Fermi liquid instability was previously announced in Ref. 5. In this paper, we present a derivation of this result, a detailed analysis of the phase diagram of the model, and we discuss our findings in view of previously known results for other related disordered and interacting fermion systems.

We note that the ϵ expansion is employed in this work as a technical tool in the continuum FNLσM description and should be thought of as a controlled approximation scheme to access the physics of the disordered, interacting Hubbard-like Hamiltonian in Eqs. (1.1) and (1.9) in three dimensions. Clearly, we cannot easily define a bipartite lattice fermion model in a fractional number of $d=2+\epsilon$ dimensions; instead, we work with a continuum field theory, the FNLσM, argued to capture the low-energy physics of the lattice model in *both* two dimensions ($\epsilon=0$) and three dimensions ($\epsilon=1$), whose internal structure is constrained by the crucial SLS [Eq. (1.2)]. The field theory action of the continuum FNLσM [displayed in Eqs. (2.48)–(2.51), Sec. II A 4] can be analytically continued between integer dimensions in the usual way. The internal structure of the FNLσM, and thus SLS, is pre-

served under this continuation; it is SLS then that gives meaning to such an interpolation between lattice models in disparate integer dimensions. The Anderson–Mott instability of the diffusive Fermi liquid identified in this work occurs for perturbatively accessible, weak disorder strengths only for $\epsilon \ll 1$, i.e., in $2 < d \leq 3$. We *conjecture* that this instability also exists in the three-dimensional (3D) FNLσM, and should therefore be found (i.e., via numerics) in the 3D Hubbard-like lattice fermion model. This conjecture cannot be directly proven here since the instability of the 3D FNLσM, if it exists, would occur in the strong coupling regime.

The organization of this paper is as follows.

In Sec. II, we formulate a Schwinger–Keldysh[41] path integral representation for the lattice model given by Eqs. (1.1) and (1.9); we then derive the low-energy, continuum FNLσM description. The technical content of our work appears in Secs. III and IV. We set up our one-loop, frequency-momentum shell renormalization group calculation in Sec. III, specifying the parametrization of the FNLσM and stating the necessary diagrammatic Feynman rules. The actual one-loop calculation is chronicled in Sec. IV. We analyze and discuss our results in Sec. V. The reader less interested in calculational details may skip Secs. III and IV entirely and proceed from the end of Sec. II directly to Sec. V.

A variety of elaborations, extensions, and technical details are relegated to the Appendixes. In Appendix A, we relate the structure of the continuum FNLσM to that of the noninteracting random hopping model [Eqs. (1.1) and (1.9), with $U = V = 0$] via a symmetry analysis. Appendix B describes the random matrix symmetry classification (along the lines of Ref. 42) of disordered, bipartite lattice models for spin-1/2 electrons. (See also Sec. II B.) Appendix C provides a surprising alternative interpretation of the class AIII Finkel'stein NLσM, studied in this paper, in terms of the spin-1/2 quasiparticles of a spin-triplet, *p*-wave superconductor. This quasiparticle system may be defined directly in the continuum, without reference to a "microscopic" lattice model or an additional sublattice symmetry. Finally, Appendix D collects the loop integrals required in the RG calculation presented in Sec. IV.

II. FINKEL'STEIN NONLINEAR SIGMA MODEL FORMULATION

In this section, we derive the class AIII FNLσM description of the Hubbard-like lattice model given by Eqs. (1.1) and (1.9) using the Schwinger–Keldysh[41] method to perform the disorder averaging. The results of the derivation are provided below in Eqs. (2.48)–(2.50) and interpreted in the discussion following these equations.

A. Class AIII Finkel'stein nonlinear sigma model

1. Schwinger–Keldysh path integral

To begin, we envisage a zero temperature, $(d+1)$-dimensional real time-ordered (T-ordered) path integral Z_T for the model defined in Eqs. (1.1) and (1.9). As usual, we need to normalize this path integral to unity in order to perform the ensemble average over realizations of the hopping disorder. We employ the Schwinger–Keldysh (Keldysh) method,[41] which exploits the identity $1/Z_T = Z_{\bar{T}}$, where $Z_{\bar{T}}$ is an anti-time-ordered ($\bar{T}$-ordered) path integral for the same model. We write the Keldysh generating function[41]

$$Z \equiv Z_T Z_{\bar{T}} = \int \mathcal{D}\bar{c}\,\mathcal{D}c\, e^{i(S_1 + S_2)}, \qquad (2.1)$$

where the noninteracting action is given by

$$\begin{aligned} S_1 = \sum_{a=1,2} \xi^a \int d\omega \Bigg(&\sum_{\langle ij \rangle} t_{i,j} \bar{c}^a_{Ai}(\omega) c^a_{Bj}(\omega) + \text{H.c.} \\ &+ \sum_{i \in A} \bar{c}^a_{Ai}(\omega)[\omega + i\xi^a \eta\, \text{sgn}(\omega)] c^a_{Ai}(\omega) \\ &+ \sum_{j \in B} \bar{c}^a_{Bj}(\omega)[\omega + i\xi^a \eta\, \text{sgn}(\omega)] c^a_{Bj}(\omega) \Bigg), \end{aligned} \qquad (2.2)$$

with $t_{i,j} \equiv t + \delta t_{i,j}$. The interactions reside in

$$\begin{aligned} S_2 = \sum_{a=1,2} \xi^a \int dt \Bigg(&-V \sum_{\langle ij \rangle} n^a_{Ai}(t) n^a_{Bj}(t) - U \sum_{\langle\langle ii' \rangle\rangle} n^a_{Ai}(t) n^a_{Ai'}(t) \\ &- U \sum_{\langle\langle jj' \rangle\rangle} n^a_{Bj}(t) n^a_{Bj'}(t) \Bigg). \end{aligned} \qquad (2.3)$$

The generating functional defined by Eq. (2.1) is an integral over the Grassmann fields $\bar{c}^a_{iA}$, c^a_{iA}, and $\bar{c}^a_{jB}$, c^a_{jB}, defined on the A and B sublattices of the bipartite lattice. In Eqs. (2.2) and (2.3), indices $\{i, i'\}$ and $\{j, j'\}$ label A and B sublattice sites, respectively, while the "Keldysh" species index $a \in 1, 2$ denotes the T-ordered ($a = 1$) and $\bar{T}$-ordered ($a = 2$) branches of the theory. The number ξ^a takes the values

$$\xi^a = \begin{cases} 1, & a = 1 \ (T \text{ ordered}) \\ -1, & a = 2 \ (\bar{T} \text{ ordered}). \end{cases} \qquad (2.4)$$

The factors $i\xi^a \eta\, \text{sgn}(\omega)$ in Eq. (2.2) are frequency integration pole prescriptions appropriate to T- and $\bar{T}$-ordered correlation functions, with $\eta \to 0^+$. Finally, the density fields in Eq. (2.3) are defined via $n^a_{Ai/Bj}(t) \equiv \bar{c}^a_{Ai/Bj}(t) c^a_{Ai/Bj}(t)$.[43]

The FNLσM that we are after is a matrix field theory; it therefore makes good sense to introduce a compactifying matrix notation at this early stage. We think of the field $c_{Ai/Bj}$ ($\bar{c}_{Ai/Bj}$) as a column (row) vector with a single "superindex," which is a direct product of frequency $\{\omega\}$ and Keldysh $\{a\}$ indices: e.g., $c_{Ai} \to c^a_{Ai}(\omega)$. In the Keldysh formalism, it is often useful to further divide frequency into a product of (discrete) sign and (continuous) modulus spaces: $\omega = |\omega|\text{sgn}(\omega)$. Next, we introduce two commuting sets of Pauli matrices: the matrix $\hat{\Sigma}_m$ acts in the $\text{sgn}(\omega)$ space, while the matrix $\hat{\xi}_n$ acts in the Keldysh species ($T/\bar{T}$) space, with $m, n \in \{1, 2, 3\}$. By employing the conventional basis for all Pauli matrices, we identify $\hat{\Sigma}_3 \to \text{sgn}\,\omega\, \delta_{\omega,\omega'} \delta^{a,a'}$ and $\hat{\xi}_3 \to \xi^a \delta_{\omega,\omega'} \delta^{a,a'}$, with $\delta_{\omega,\omega'} \equiv 2\pi\delta(\omega - \omega')$. Finally, we define the single-particle energy matrix $\hat{\omega} \equiv |\hat{\omega}|\hat{\Sigma}_3$, with $|\hat{\omega}| \to |\omega|\delta_{\omega,\omega'} \delta^{a,a'}$.

We make a change of variables $\bar{c}_{Ai/Bj} \rightarrow \bar{c}_{Ai/Bj}\hat{\xi}_3$ and rewrite the noninteracting sector [Eq. (2.2)] of the Keldysh action as

$$S_1 \equiv S_1^0 + \delta S_1. \tag{2.5}$$

The clean bipartite hopping model appears in the term

$$S_1^0 = \int_{sBZ} \frac{d^d\mathbf{k}}{(2\pi)^d} \left(\begin{bmatrix} \bar{c}_{A\mathbf{k}} & \bar{c}_{B\mathbf{k}} \end{bmatrix} \begin{bmatrix} i\eta\hat{\Sigma}_3\hat{\xi}_3 & -\varepsilon(\mathbf{k}) \\ -\varepsilon(\mathbf{k}) & i\eta\hat{\Sigma}_3\hat{\xi}_3 \end{bmatrix} \begin{bmatrix} c_{A\mathbf{k}} \\ c_{B\mathbf{k}} \end{bmatrix} \right.$$

$$\left. + \begin{bmatrix} \bar{c}_{A\mathbf{k}} & \bar{c}_{B\mathbf{k}} \end{bmatrix} \begin{bmatrix} \hat{\Sigma}_3|\hat{\omega}| & 0 \\ 0 & \hat{\Sigma}_3|\hat{\omega}| \end{bmatrix} \begin{bmatrix} c_{A\mathbf{k}} \\ c_{B\mathbf{k}} \end{bmatrix} \right) \tag{2.6}$$

$$\equiv \bar{c}[\hat{\Sigma}_3|\hat{\omega}| + i\eta\hat{\Sigma}_3\hat{\xi}_3 - \hat{\sigma}_1\varepsilon(\hat{\mathbf{k}})]c. \tag{2.7}$$

The momentum integration in Eq. (2.6) is taken over the sBZ; $\varepsilon(\mathbf{k})$ is the clean energy band structure.[44] Equation (2.7) gives the most compact representation that we will use for the clean, noninteracting action. Here, we have introduced a third set of Pauli matrices, $\hat{\sigma}_m$, $m \in \{1,2,3\}$, acting in the sublattice flavor $\{A, B\}$ space, and we have also promoted momentum to an operator, $\mathbf{k} \rightarrow \hat{\mathbf{k}}$. The column vector c carries indices in the momentum $\mathbf{k}$, mod energy $|\omega|$, sgn(ω) (Σ), sublattice flavor (σ), and Keldysh (ξ) spaces, i.e., $c \rightarrow c_{A/B\mathbf{k}}^a(\omega)$ with all indices displayed. The disorder is relegated to the perturbation

$$\delta S_1 = \sum_{\langle ij \rangle} (\bar{c}_{Ai}\delta t_{i,j}c_{Bj} + \bar{c}_{Bj}\delta t_{i,j}^* c_{Ai}). \tag{2.8}$$

2. Disorder averaging and Hubbard–Stratonovich decoupling

We now ensemble average over realizations of the complex random hopping amplitudes $\{\delta t_{i,j}\}$ appearing in Eq. (2.8). In order to simplify the derivation of the FNLσM, we employ the following artifice: we assume that of the z_c nearest-neighbor bonds surrounding a given site i belonging to the A sublattice of the bipartite lattice under study, only *one* such bond is disordered. (z_c is the coordination number.) We further assume that the same type of bond (specified by its orientation) is made random at each and every A site, thus allowing a unique, orientationally homogeneous pairing (dimer covering) of the A and B sublattice sites of the bipartite lattice. An example of such a pairing is provided for the square lattice in Fig. 5. This seemingly pathological constraint on the disorder distribution allows for the quickest derivation of the low-energy effective field theory.

With such a pairing established between each A sublattice site i and its associated B sublattice site $j(i)$, we have

$$\delta t_{i,j} = \begin{cases} \delta t_{i,j(i)}, & j = j(i) \\ 0, & j \neq j(i). \end{cases} \tag{2.9}$$

We take the "dimerized" bond amplitudes $\{\delta t_{i,j(i)}\}$ to be Gaussian random variables, independent on different nearest-neighbor lattice links $\langle ij(i) \rangle$, and identically distributed with the following purely real mean and variance:
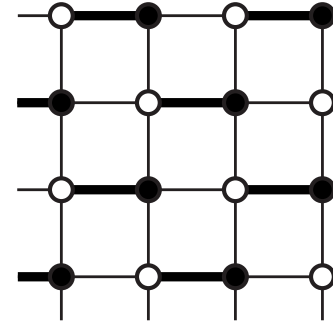

FIG. 5. Homogeneous pairing (dimer covering) of nearest-neighbor sites on the square lattice.

$$\overline{\delta t_{i,j(i)}} = \delta t_{\text{dim}} \tag{2.10}$$

and

$$\overline{\delta t_{i,j(i)}^* \delta t_{i,j(i)}} = \lambda^{(m)}, \tag{2.11}$$

respectively. The overbars in Eqs. (2.10) and (2.11) denote disorder averaging. Although we will be ultimately interested in the limit of zero mean bond dimerization, it will prove convenient in the interim to retain $\delta t_{\text{dim}} \neq 0$. The superscript "(m)" appearing on the right-hand side of Eq. (2.11) stands for microscopic, indicating that the quantity $\lambda^{(m)}$ is defined at the lattice scale. Using Eqs. (2.8)–(2.11), we define the disorder-averaged action $\overline{\delta S_1}$ via

$$e^{i\overline{\delta S_1}} \equiv \int |\mathcal{D}\delta t|^2 \exp\left[\frac{-1}{\lambda^{(m)}} \sum_{i \in A} |\delta t_{i,j(i)} - \delta t_{\text{dim}}|^2 + i\delta S_1 \right]$$

$$= \exp\left(\frac{\lambda^{(m)}}{2} \sum_{i \in A} \text{Tr}[\hat{\mathcal{A}}_i^2] + i\delta S_{\text{dim}} \right), \tag{2.12}$$

with

$$\hat{\mathcal{A}}_i \equiv \begin{bmatrix} 0 & \hat{A}_i \\ \hat{A}_{j(i)}^\dagger & 0 \end{bmatrix} = \frac{\hat{\sigma}_1 + i\hat{\sigma}_2}{2}\hat{A}_i + \frac{\hat{\sigma}_1 - i\hat{\sigma}_2}{2}\hat{A}_{j(i)}^\dagger, \tag{2.13}$$

where we have defined

$$\hat{A}_i \rightarrow A_{i\omega,\omega'}^{a,a'} \equiv c_{Ai}^a(\omega)\bar{c}_{Ai}^{a'}(\omega'), \tag{2.14a}$$

$$\hat{A}_{j(i)}^\dagger \rightarrow A_{j\omega,\omega'}^{\dagger a,a'} \equiv c_{Bj}^a(\omega)\bar{c}_{Bj}^{a'}(\omega'). \tag{2.14b}$$

In Eq. (2.12), Tr denotes a matrix trace over indices in the sublattice flavor (σ), frequency (ω), and Keldysh (ξ) spaces. The field $\hat{\mathcal{A}}_i$, introduced in Eq. (2.12), is a matrix of fermion bilinears; Eq. (2.13) details the sublattice flavor space decomposition of $\hat{\mathcal{A}}_i$ in terms of the purely off-diagonal Pauli matrices $\hat{\sigma}_1$ and $\hat{\sigma}_2$. Although they occupy the off-diagonal blocks of $\hat{\mathcal{A}}_i$, the fields $\hat{A}_i$ and $\hat{A}_{j(i)}^\dagger$ actually describe fermion degrees of freedom residing *entirely* on the A and B sublattices, respectively, as shown in Eqs. (2.14a) and (2.14b). $\hat{A}_i$ and $\hat{A}_{j(i)}^\dagger$ each carry frequency $\{\omega, \omega'\}$ and Keldysh species

$\{a, a'\}$ indices. Finally, a nonzero mean bond dimerization δt_{dim} [Eq. (2.10)] gives rise to the following homogeneous term in Eq. (2.12):

$$\delta S_{\text{dim}} = \delta t_{\text{dim}} \sum_i (\bar{c}_{Ai} c_{Bj(i)} + \bar{c}_{Bj(i)} c_{Ai})$$

$$= -\bar{c}[\hat{\sigma}_1 \phi_R(\hat{\mathbf{k}}) + \hat{\sigma}_2 \phi_I(\hat{\mathbf{k}})]c. \qquad (2.15)$$

The second line of Eq. (2.15) expresses δS_{dim} in momentum space; here, we have adopted the same compact notation employed in Eq. (2.7). The functions $\phi_R(\mathbf{k})$ and $\phi_I(\mathbf{k})$ in Eq. (2.15) are real and imaginary components of the "dimerization" function

$$\phi_R(\mathbf{k}) + i\phi_I(\mathbf{k}) \equiv -\delta t_{\text{dim}} e^{i\mathbf{k}\cdot\mathbf{n}}. \qquad (2.16)$$

In this equation, $\mathbf{n}$ is a unit vector pointing in the direction determined by the chosen bond dimerization [see Eqs. (2.9) and (2.10) and Fig. 5].

We have adopted a suggestive notation in Eqs. (2.14a) and (2.14b) to denote the pure sublattice fields $\hat{A}_i$ and $\hat{A}_{j(i)}^\dagger$. Consider the following spatially uniform deformation of these fermion bilinears:

$$\hat{A}_i \rightarrow \hat{U}_A \hat{A}_i \hat{U}_B^\dagger, \quad \hat{A}_{j(i)}^\dagger \rightarrow \hat{U}_B \hat{A}_{j(i)}^\dagger \hat{U}_A^\dagger, \qquad (2.17)$$

where $\hat{U}_A$ and $\hat{U}_B$ are independent unitary transformations in $|\omega| \otimes \Sigma \otimes \xi$ (frequency $\otimes$ Keldysh) space:

$$\hat{U}_A^\dagger \hat{U}_A = \hat{U}_B^\dagger \hat{U}_B = \hat{1}_{|\omega| \otimes \Sigma \otimes \xi}. \qquad (2.18)$$

The transformation in Eq. (2.17) is clearly a symmetry of the disorder-averaged action $\overline{\delta S}_1$, as can be seen from Eqs. (2.12)–(2.15). In fact, there is a direct relationship between this transformation and the symmetry structure of the noninteracting Keldysh action [Eqs. (2.7) and (2.8)] in every fixed realization of the static disorder; the connection is articulated in Appendix A. Equation (2.17) suggests that we may regard $\hat{A}_{j(i)}^\dagger$ as the "Hermitian adjoint" of its associated nearest neighbor $\hat{A}_i$, justified on length scales much larger than the lattice spacing. The identification $\hat{A}_{j(i)}^\dagger \sim \hat{A}_i^\dagger$ implies the Hermiticity of the composite matrix field in Eq. (2.13): $\hat{\mathcal{A}}_i^\dagger \sim \hat{\mathcal{A}}_i$.

Next, we decouple all four fermion terms appearing in the disorder-averaged and interacting sectors of the theory with bosonic Hubbard–Stratonovich fields. In the disorder-averaged sector [Eq. (2.12)], we write

$$\exp\left(\frac{\lambda^{(m)}}{2} \sum_{i \in A} \text{Tr}[\hat{\mathcal{A}}_i^2]\right)$$

$$= \int \mathcal{D}\hat{\mathcal{Q}} \exp\left(\sum_{i \in A} \text{Tr}\left[\frac{-1}{2\lambda^{(m)}} \hat{\mathcal{Q}}_i^2 + \hat{\mathcal{Q}}_i \hat{\mathcal{A}}_i\right]\right). \qquad (2.19)$$

The matrix field $\hat{\mathcal{Q}}_i$ is taken to be Hermitian and purely off-diagonal in sublattice flavor space, i.e.,

$$\hat{\mathcal{Q}}_i \equiv \begin{bmatrix} 0 & \hat{Q}_i \\ \hat{Q}_{j(i)}^\dagger & 0 \end{bmatrix} = \frac{\hat{\sigma}_1 + i\hat{\sigma}_2}{2} \hat{Q}_i + \frac{\hat{\sigma}_1 - i\hat{\sigma}_2}{2} \hat{Q}_{j(i)}^\dagger, \qquad (2.20)$$

with

$$\hat{Q}_i \rightarrow Q_{i\omega,\omega'}^{a,a'}, \quad \hat{Q}_{j(i)}^\dagger \sim \hat{Q}_i^\dagger \rightarrow Q_{i\omega,\omega'}^{\dagger a,a'}. \qquad (2.21)$$

[Compare Eqs. (2.13), (2.14a), and (2.14b).]

Turning to the interacting sector, we rewrite Eq. (2.3) as

$$S_2 = -\sum_{a=1,2} \frac{\xi^a}{2} \int dt\, N^{\mathsf{T}a}(t) \hat{\mathcal{X}} N^a(t), \qquad (2.22)$$

where the superscript "T" denotes the matrix transpose operation, and

$$\hat{\mathcal{X}} \equiv \begin{bmatrix} U\hat{x} & V\hat{y} \\ V\hat{y}^\mathsf{T} & U\hat{x} \end{bmatrix} \qquad (2.23)$$

is a matrix in sublattice flavor space (σ), with elements involving the position space coupling functions $\hat{x}$ and $\hat{y}$ (defined below), while the fermion sublattice densities are encoded in the vector

$$N^a(t) \rightarrow \begin{bmatrix} n_A^a(t) \\ n_B^a(t) \end{bmatrix}. \qquad (2.24)$$

We have suppressed all position space indices in Eqs. (2.22)–(2.24). In Eq. (2.23), the function $\hat{y} \rightarrow y_{i,j}$ ($\hat{x} \rightarrow x_{i,i'}$) equals unity for pairs of nearest-neighbor (next-nearest-neighbor) lattice sites $\{i, j\}$ ($\{i, i'\}$) and vanishes otherwise. Now, we decouple

$$e^{iS_2} = \int \mathcal{D}\rho \exp\left(\sum_{a=1,2} i \int dt \left[\frac{\xi^a}{2} \rho^{\mathsf{T}a}(t) \hat{\mathcal{X}}^{-1} \rho^a(t) \right. \right.$$

$$\left. \left. + \rho^{\mathsf{T}a}(t) N^a(t)\right]\right), \qquad (2.25)$$

where

$$\rho^a(t) \rightarrow \begin{bmatrix} \rho_A^a(t) \\ \rho_B^a(t) \end{bmatrix}. \qquad (2.26)$$

Again, we have suppressed all position space indices in Eqs. (2.25) and (2.26).

3. Saddle point and gradient expansion

Gathering together the homogeneous hopping [Eq. (2.7)], mean bond dimerization [Eq. (2.15)], disorder-averaged [Eq. (2.19)], and interacting [Eq. (2.25)] pieces of our theory, we perform the Gaussian integral over the fermion fields and finally arrive at the following effective field theory:

$$Z = \int \mathcal{D}\hat{\mathcal{Q}}\mathcal{D}\rho \exp[-S_Q - S_\rho - S_{\text{DET}}], \qquad (2.27)$$

where

$$S_Q = \frac{1}{2\lambda^{(m)}} \sum_{i \in A} \text{Tr}[\hat{\mathcal{Q}}_i^2], \qquad (2.28)$$

$$S_\rho = \sum_{a=1,2} \frac{-i\xi^a}{2} \int dt \rho^{\text{T}a}(t) \hat{\mathcal{X}}^{-1} \rho^a(t), \qquad (2.29)$$

and

$$S_{\text{DET}} = -\text{Tr}(\ln[G_0^{-1} + i\hat{\sigma}_1 \hat{\mathcal{Q}} + \rho]). \qquad (2.30)$$

The trace in Eq. (2.30) is performed over indices in the position, sublattice flavor (σ), mod energy $|\omega|$, sgn(ω) (Σ), and Keldysh species (ξ) spaces. The operator G_0^{-1} in Eq. (2.30) represents the inverse of the (Keldysh) single-particle Green function for the clean, noninteracting hopping model described by Eq. (2.7), incorporating, in addition, the mean bond dimerization from Eq. (2.15):

$$G_0^{-1} = \hat{\Sigma}_3 |\hat{\omega}| + i\eta\hat{\Sigma}_3\hat{\xi}_3 - \hat{\sigma}_1[\varepsilon(\hat{\mathbf{k}}) + \phi_R(\hat{\mathbf{k}})] - \hat{\sigma}_2 \phi_I(\hat{\mathbf{k}}). \qquad (2.31)$$

The functions ϕ_R and ϕ_I are real and imaginary parts of the dimerization function defined by Eq. (2.16).

We look for a spatially homogeneous saddle point solution to the action given by Eqs. (2.28) and (2.30) in terms of the matrix field $\hat{\mathcal{Q}}$, with $\rho = \phi_R = \phi_I = 0$ in Eqs. (2.30) and (2.31) (i.e., ignoring the interparticle interactions and considering the limit of zero mean bond dimerization). In the low-energy and long-time limit $|\omega| \to 0$, the structure of the saddle point solution is determined by the pole prescription piece (the term proportional to η) in Eq. (2.31). We make the standard ansatz

$$\hat{\mathcal{Q}}_{\text{SP}} \equiv \frac{1}{2\tau} \hat{\sigma}_1 \hat{\Sigma}_3 \hat{\xi}_3, \qquad (2.32)$$

with τ the elastic scattering lifetime due to the disorder. Then, the saddle point condition reduces to the usual self-consistent Born approximation (SCBA) for the elastic decay rate $1/\tau$:

$$\frac{1}{\lambda^{(m)}} = \int_{\text{sBZ}} \frac{d^d\mathbf{k}}{(2\pi)^d} \left[\varepsilon^2(\mathbf{k}) + \frac{1}{(2\tau)^2} \right]^{-1}. \qquad (2.33)$$

For the 2D case of the square lattice (with its concomitant van Hove singularities at half-filling), Eq. (2.33) gives

$$\frac{1}{2\tau} \sim \frac{\lambda^{(m)}}{2\pi t} \ln\left(\frac{t^2}{\lambda^{(m)}} \right) \qquad (2.34)$$

in the weak disorder limit $\lambda^{(m)} \ll t^2$.

Next, we consider fluctuations about the saddle point solution given by Eq. (2.32). Dominant within the diffusive metallic phase are the long-wavelength, low-energy Goldstone (diffusion) modes that preserve the saddle point norm $1/2\tau$. These modes are generated by applying a slowly spatially varying generalization of the symmetry transformation in Eqs. (2.17) and (2.18) to $\hat{\mathcal{Q}}_{\text{SP}}$. (See also Appendix A.) In terms of the sublattice flavor space decomposition [Eq. (2.20)], we define

$$\hat{\mathcal{Q}}(\mathbf{r}) \equiv \frac{\hat{\sigma}_1 + i\hat{\sigma}_2}{4\tau} \hat{Q}(\mathbf{r}) + \frac{\hat{\sigma}_1 - i\hat{\sigma}_2}{4\tau} \hat{Q}^\dagger(\mathbf{r}), \qquad (2.35)$$

where

$$\hat{Q}(\mathbf{r}) = \hat{U}_A(\mathbf{r}) \hat{Q}_{\text{SP}} \hat{U}_B^\dagger(\mathbf{r}), \qquad (2.36a)$$

$$\hat{Q}^\dagger(\mathbf{r}) = \hat{U}_B(\mathbf{r}) \hat{Q}_{\text{SP}} \hat{U}_A^\dagger(\mathbf{r}), \qquad (2.36b)$$

and

$$\hat{Q}_{\text{SP}} = \hat{\Sigma}_3 \hat{\xi}_3. \qquad (2.37)$$

Alternatively, we note that Eqs. (2.18), (2.36a), (2.36b), and (2.37), imply the unitary constraint

$$\hat{Q}^\dagger(\mathbf{r}) \hat{Q}(\mathbf{r}) = \hat{1}_{|\omega| \otimes \Sigma \otimes \xi}. \qquad (2.38)$$

Our FNLσM will therefore be a field theory of the unitary matrix $\hat{Q}(\mathbf{r}) \to \hat{Q}_{\omega,\omega'}^{a,a'}(\mathbf{r})$.

Finally, we assemble the action for the FNLσM from the components given by Eqs. (2.28)–(2.30). The unitary constraint [Eq. (2.38)] renders S_Q in Eq. (2.28) an irrelevant constant, so we concentrate on S_{DET} in Eq. (2.30). By keeping only the most relevant terms in a gradient expansion, one obtains

$$S_{\text{DET}} \sim i2\tau \int d^d\mathbf{r}\, \text{Tr}((\hat{\Sigma}_3 |\hat{\omega}| + i\eta\hat{\Sigma}_3\hat{\xi}_3)[\hat{Q}^\dagger(\mathbf{r}) + \hat{Q}(\mathbf{r})])$$
$$+ (2\bar{v}_F\tau)^2 \int d^d\mathbf{r}\, \text{Tr}(\nabla\hat{Q}^\dagger(\mathbf{r}) \cdot \nabla\hat{Q}(\mathbf{r})) + S_{\text{DET}}^{\text{dim}} + S_I, \qquad (2.39)$$

where the terms $S_{\text{DET}}^{\text{dim}}$ and S_I are defined below in Eqs. (2.40) and (2.45), respectively. Here, $\bar{v}_F$ is the average Fermi velocity (at half-filling), while the elastic scattering lifetime τ is determined by the SCBA [Eq. (2.33)].

The second term on the second line of Eq. (2.39) is a perturbation arising from the presence of a nonzero mean bond dimerization $\delta t_{\text{dim}} \neq 0$ [Eq. (2.10)]:

$$S_{\text{DET}}^{\text{dim}} \equiv \mathfrak{c} \frac{\delta t_{\text{dim}}}{t} \int d^d\mathbf{r}\, \text{Tr}[\hat{Q}^\dagger(\mathbf{r}) \nabla \hat{Q}(\mathbf{r})] \cdot \mathbf{n}, \qquad (2.40)$$

where the unit vector $\mathbf{n}$, originally introduced in Eq. (2.16), specifies the orientation of the mean bond dimerization and $\mathfrak{c}$ is a constant.

Consider the local vector operator

$$i\nabla\Phi(\mathbf{r}) \equiv \text{Tr}[\hat{Q}^\dagger(\mathbf{r}) \nabla \hat{Q}(\mathbf{r})], \qquad (2.41)$$

where $\Phi(\mathbf{r})$ is the $U(1)$ phase of the unitary matrix field $\hat{Q}(\mathbf{r})$. Equation (2.40) implies that $i\nabla\Phi(\mathbf{r})$ provides a coarse-grained measure of the local bond dimerization, i.e., of the orientation of the strongest nearest-neighbor hopping bonds within a neighborhood of size of the elastic scattering length, in the sublattice symmetric random hopping model.

Given this interpretation, we can generalize Eq. (2.40) to the case of a perturbation involving a static random vector field $\mathbf{n} \to \mathbf{n}_{\text{dim}}(\mathbf{r})$:

$$S_{\text{DET}}^{\text{dim}} \rightarrow \int d^d\mathbf{r} \, \text{Tr}[\hat{Q}^\dagger(\mathbf{r}) \, \boldsymbol{\nabla} \, \hat{Q}(\mathbf{r})] \cdot \mathbf{n}_{\text{dim}}(\mathbf{r}). \quad (2.42)$$

In Eq. (2.42), $\mathbf{n}_{\text{dim}}(\mathbf{r})$ is taken to vary in both orientation and magnitude and represents long-wavelength, quenched orientation fluctuations in the bond strength dimerization of the random hopping. Since Eq. (2.42) is consistent with the sublattice symmetry of the underlying lattice model, its effects should be included in the low-energy effective theory on the grounds of universality.

We take $\mathbf{n}_{\text{dim}}(\mathbf{r})$ to be a Gaussian random variable of vanishing mean, delta function correlated with the variance

$$\overline{n_{\text{dim}}^i(\mathbf{r}) n_{\text{dim}}^j(\mathbf{r}')} = \lambda_A \delta^{i,j} \delta^{(d)}(\mathbf{r} - \mathbf{r}'). \quad (2.43)$$

Using Eqs. (2.42) and (2.43), we define the disorder-averaged action $\overline{S_{\text{DET}}^{\text{dim}}}$ via[45]

$$e^{-\overline{S_{\text{DET}}^{\text{dim}}}} \equiv \int \mathcal{D}\mathbf{n}_{\text{dim}} \exp\left[\frac{-1}{2\lambda_A} \int d^d\mathbf{r} \, \mathbf{n}_{\text{dim}}^2(\mathbf{r}) + S_{\text{DET}}^{\text{dim}} \right]$$

$$= \exp\left(\frac{\lambda_A}{2} \int d^d\mathbf{r} [i \, \boldsymbol{\nabla} \, \Phi(\mathbf{r})]^2 \right), \quad (2.44)$$

where the operator $i\boldsymbol{\nabla}\Phi$ was defined in Eq. (2.41). In the low-energy effective field theory, then, the random hopping is characterized by the two parameters $\lambda^{(m)}$ [Eq. (2.11)] and λ_A [Eq. (2.43)]; the former sets the elastic scattering lifetime and the conductance,[9,12,13] and therefore reflects the microscopic structure of the random hopping up to small distance scales of order of the Fermi wavelength (responsible for elastic backscattering events involving large crystal momentum transfers), while the latter characterizes the orientational fluctuations of the random hopping at larger distance scales (of order of the mean free path).

The last term on the second line of Eq. (2.39) is due to the interactions and is given by

$$S_I \equiv i2\tau \sum_{a=1,2} \int dt d^d\mathbf{r} [\rho_A^a(t,\mathbf{r}) Q_{t,t}^{a,a}(\mathbf{r}) + \rho_B^a(t,\mathbf{r}) Q_{t,t}^{\dagger a,a}(\mathbf{r})].$$

$$(2.45)$$

Using Eq. (2.29), we can now perform the Gaussian integral over the auxiliary field ρ, leading to the result

$$S_I \rightarrow i \sum_{a=1,2} \frac{\xi^a}{2} \int dt d^d\mathbf{r} [Q_{t,t}^{a,a} \, Q_{t,t}^{\dagger a,a}] \begin{bmatrix} \Gamma_U & \Gamma_V \\ \Gamma_V & \Gamma_U \end{bmatrix} \begin{bmatrix} Q_{t,t}^{a,a} \\ Q_{t,t}^{\dagger a,a} \end{bmatrix},$$

$$(2.46)$$

where

$$\Gamma_U \sim (2\tau)^2 U, \quad \Gamma_V \sim (2\tau)^2 V \quad (2.47)$$

[cf. Eqs. (2.22) and (2.23)], and $1/\tau$ is the decay rate, Eqs. (2.33) and (2.34)].

4. Finkel'stein nonlinear sigma model and its coupling constants

By combining the results of the previous subsection, Eqs. (2.39), (2.44), and (2.46), we arrive at last to the final form of the FNLσM description of the Hubbard-like model de-

fined in Eqs. (1.1) and (1.9). The FNLσM is given by the functional integral

$$Z = \int \mathcal{D}\hat{Q} e^{-S_D - S_I}, \quad (2.48)$$

where

$$S_D = \frac{1}{2\lambda} \int d^d\mathbf{r} \, \text{Tr}(\boldsymbol{\nabla}\hat{Q}^\dagger(\mathbf{r}) \cdot \boldsymbol{\nabla}\hat{Q}(\mathbf{r}))$$

$$+ ih \int d^d\mathbf{r} \, \text{Tr}((\hat{\Sigma}_3|\hat{\omega}| + i\eta\hat{\Sigma}_3\hat{\xi}_3)[\hat{Q}^\dagger(\mathbf{r}) + \hat{Q}(\mathbf{r})])$$

$$- \frac{\lambda_A}{2\lambda^2} \int d^d\mathbf{r}(\text{Tr}[\hat{Q}^\dagger(\mathbf{r}) \, \boldsymbol{\nabla} \, \hat{Q}(\mathbf{r})])^2 \quad (2.49)$$

and

$$S_I = i \sum_{a=1,2} \xi^a \int dt d^d\mathbf{r}(2\Gamma_V Q_{t,t}^{\dagger a,a}(\mathbf{r}) Q_{t,t}^{a,a}(\mathbf{r})$$

$$+ \Gamma_U[Q_{t,t}^{a,a}(\mathbf{r}) Q_{t,t}^{a,a}(\mathbf{r}) + Q_{t,t}^{\dagger a,a}(\mathbf{r}) Q_{t,t}^{\dagger a,a}(\mathbf{r})]) \quad (2.50)$$

The field variable $\hat{Q}(\mathbf{r})$ in Eqs. (2.48)–(2.50) is a complex, infinite-dimensional unitary matrix,

$$\hat{Q}^\dagger(\mathbf{r})\hat{Q}(\mathbf{r}) = \hat{1}, \quad (2.51)$$

carrying Keldysh species ($\{a,a'\}$) and time ($\{t,t'\}$) or frequency ($\{\omega,\omega'\}$) indices:

$$\hat{Q}(\mathbf{r}) \rightarrow Q_{\omega,\omega'}^{a,a'}(\mathbf{r}) \quad \text{or} \quad \hat{Q}(\mathbf{r}) \rightarrow Q_{t,t'}^{a,a'}(\mathbf{r}). \quad (2.52)$$

In Eq. (2.48), $\mathcal{D}\hat{Q}$ is the invariant (Haar) functional measure for the group manifold associated with $\hat{Q}$. The matrix $\hat{Q}$ and its adjoint $\hat{Q}^\dagger$ may be interpreted as continuum versions of the *same-sublattice* fermion bilinears

$$Q_{t,t'}^{a,a'} \sim c_A^a(t)\bar{c}_A^{a'}(t'), \quad (2.53a)$$

$$Q_{t,t'}^{\dagger a,a'} \sim c_B^a(t)\bar{c}_B^{a'}(t'), \quad (2.53b)$$

which follows from Eqs. (2.13), (2.14a), (2.14b), (2.19), and (2.20). It is a peculiar feature of the random hopping model that the low-energy fluctuations on a given sublattice are described by a unitary, rather than a Hermitian matrix, familiar from other models.

The Tr in Eq. (2.49) denotes a matrix trace over Keldysh species and time or frequency indices; the diagonal Pauli matrices $\hat{\Sigma}_3 \rightarrow \text{sgn}\,\omega\delta_{\omega,\omega'}\delta^{a,a'}$ and $\hat{\xi}_3 \rightarrow \xi^a\delta_{\omega,\omega'}\delta^{a,a'}$ act in the $\text{sgn}(\omega)$ and Keldysh species spaces, respectively, while $|\hat{\omega}| \rightarrow |\omega|\delta_{\omega,\omega'}\delta^{a,a'}$ is a matrix of absolute frequencies. Here and in Eq. (2.50), the number ξ^a was defined in Eq. (2.4). The saddle point configuration $\hat{Q}(\mathbf{r})=\hat{Q}_{\text{SP}}$ was determined above in Eq. (2.37). The structure of $\hat{Q}_{\text{SP}}$ is set by the symmetry-breaking (Keldysh pole prescription) term, proportional to $\eta \rightarrow 0^+$, in Eq. (2.49).

The action given by Eq. (2.49) describes the low-energy diffusive physics of the noninteracting random hopping

model;[9,12,13] a replica version of the noninteracting sigma model with action S_D was originally studied by Gade and Wegner.[9] This noninteracting sector of the FNLσM is parametrized by three coupling strengths: λ, λ_A, and h. The coupling constant λ is a coarse-grained measure of the microscopic hopping disorder strength, $\lambda^{(m)}$ [Eq. (2.11)];[46] it can be shown that $1/\lambda$ is proportional to the dimensionless dc conductance g of the system.[2,3,40] The parameter λ_A gives a second measure of the disorder strength, unique to this "sublattice symmetry class," which strongly influences the behavior of the low-energy, disorder-averaged single-particle density of states.[9,12,13] [In Eq. (2.49), we have rescaled λ_A by a factor of $1/\lambda^2$ relative to Eq. (2.44), so that λ and λ_A now share the same naive "engineering" dimension. See also Sec. IV B.] As elaborated in the previous subsection, the parameter λ_A may be simply interpreted as characterizing the strength of long-wavelength, quenched orientational fluctuations of bond strength dimerization in the microscopic random hopping disorder. Finally, the parameter h in Eq. (2.49) is a dynamic scale factor, introduced here in order to track the scaling relationship between length and time as the model is renormalized.[2,3]

The interparticle interactions appear in the second term S_I, given by Eq. (2.50). With the advent of Eqs. (2.53a) and (2.53b), we may interpret $Q_{t,t}^{a,a}(\mathbf{r})$ and $Q_{t,t}^{\dagger a,a}(\mathbf{r})$ as continuum local density operators on the A and B sublattices, respectively. Then, the coarse-grained interaction strengths $\Gamma_V \propto V$ and $\Gamma_U \propto U$ in Eq. (2.50) couple to generic, short-ranged intersublattice and same-sublattice density-density interactions, respectively [compare to Eq. (1.1) above].

We use the RG to study the model defined by Eqs. (2.48)–(2.50). It will prove convenient to define the linear combinations of Γ_U and Γ_V,

$$\Gamma_s \equiv \frac{1}{2}(\Gamma_U + \Gamma_V), \quad \Gamma_c \equiv \frac{1}{2}(\Gamma_U - \Gamma_V). \qquad (2.54)$$

In the continuum FNLσM [Eq. (2.50)], the interaction strength Γ_s couples to the squared (*smooth*) local charge density, $[Q_{t,t}^{a,a}(\mathbf{r})+Q_{t,t}^{\dagger a,a}(\mathbf{r})]^2$, while Γ_c couples to the squared sublattice *staggered* charge density, $[Q_{t,t}^{a,a}(\mathbf{r})-Q_{t,t}^{\dagger a,a}(\mathbf{r})]^2$. In accordance with the discussion in the paragraph below Eq. (1.8) in Sec. I, we expect $\Gamma_c < 0$ to promote charge density wave formation, while $\Gamma_c > 0$ should suppress it.

We compute the one-loop flow equations for the coupling constants λ, λ_A, h, Γ_s, and Γ_c in the following two sections. We analyze and discuss our results in Sec. V. The reader less interested in calculational details may skip Secs. III and IV entirely and proceed immediately to Sec. V.

B. Related models for spin-1/2 fermions

To conclude this section, we briefly discuss some connections between various models of disordered (and possibly interacting) spin-1/2 fermions and their corresponding random matrix theory classification and sigma model descriptions. Details are provided in Appendixes B and C.

Consider a clean system of spinless or spinful fermions with homogeneous, real nearest-neighbor hopping on a bipartite lattice at half-filling. In both the spinless and spinful

cases, such a tight-binding model possesses three additional (non-space-time) discrete symmetries: TRI, SLS, and particle-hole (PH) symmetry. For spin-1/2 electrons, we also have spin $SU(2)$ rotational symmetry. Here, we *define* the unitary particle-hole transformation as a product of antiunitary time-reversal and sublattice symmetry transformations; as a result, in the spin-1/2 case, the PH transformation involves a spin flip—see Appendix B for details. The introduction of quenched disorder may break or preserve each of these internal invariances, and the resulting disordered (noninteracting) Hamiltonian can be classified using random matrix theory.[7,42]

Consider now the effect of random magnetic fields on the otherwise clean spin-1/2 hopping model. Here, it is crucial to distinguish between the cases of random orbital and random Zeeman magnetic fields. A random orbital field preserves spin $SU(2)$ rotational symmetry and SLS, while it breaks TRI and PH symmetry in every static disorder realization. A random Zeeman field, on the other hand, preserves PH but breaks TRI, SLS, and spin $SU(2)$ rotational symmetry (completely). These two cases actually fall into *different* symmetry classes of noninteracting, disordered quantum systems. In the classification scheme of Ref. 7, the random orbital field model, with SLS [and spin $SU(2)$] only, belongs to class AIII, while the random Zeeman field model, with PH only, belongs to class C. These results are derived in Appendix B. A model with both random Zeeman and orbital fields falls into the standard unitary Wigner–Dyson class A since all three of the discrete symmetries TRI, SLS, and PH are broken. As discussed in the Introduction, known (noninteracting) realizations of the chiral class AIII,[9–14,16] including the noninteracting version of the (spinless) model [Eqs. (1.1) and (1.9) with $U=V=0$] studied in this paper, possess a conducting phase with extended states in $d=2$ spatial dimensions. A system of noninteracting, spin-1/2 superconductor quasiparticles, with broken TRI and with spin $SU(2)$ rotational symmetry preserved in every instance of the static disorder, furnishes a better known realization of class C.[7,37,42,47–50] Noninteracting systems belonging to class C or A do not possess extended states in two dimensions,[40,47,51] except at their respective quantum Hall[50,52] transitions.

From this discussion, we conclude that the FNLσM that we study in this paper also applies to a related Hubbard-like model for spin-1/2 fermions, subject to a random *orbital* magnetic field and possessing strong spin-orbit coupling. Spin-orbit coupling is needed to suppress an additional hydrodynamic spin diffusion channel, which we do not treat in this work. The 2D half-filled, spin-1/2 Hubbard model subject to a random Zeeman field was studied numerically in Ref. 39. The effects of interparticle interactions in the context of the superconductor quasiparticle interpretation of class C were analyzed using the FNLσM in Ref. 37; see also Ref. 49. Very recently, Dell'Anna[36] has independently studied several universality classes of Finkel'stein NLσMs including realizations of both the particle-hole symmetric class C and the sublattice symmetric class AIII for electrically charged spin-1/2 fermions. In the latter case, Dell'Anna included the spin diffusion channel (i.e., assumed no spin-orbit coupling). His results are discussed briefly in the conclusion to this paper, Sec. V D. Finally, we note that different classes appear in the presence of TRI.[7,42]

Surprisingly, our AIII Finkel'stein NLσM equivalently describes a system of spin-1/2 superconductor quasiparticles, subject to disorder and interactions, with TRI and a $U(1)$ remnant of the spin $SU(2)$ rotational symmetry preserved in every static disorder realization. Such a (gapless) quasiparticle system could occur, e.g., in the polar phase of a p-wave, spin-triplet superconductor.[53,54] This quasiparticle system may be defined directly in the continuum, without reference to a lattice model or an additional sublattice and/or chiral symmetry. The connection is derived in Appendix C.

III. PARAMETRIZATION AND FEYNMAN RULES

We now turn to the setup of our perturbative, one-loop renormalization group calculation for the FNLσM defined by Eqs. (2.48)–(2.50). The actual RG computation follows in Sec. IV. Beyond developing the apparatus necessary for the RG, the material in this section also serves to further elucidate the structure of the sigma model description of sublattice symmetric disorder and interparticle interactions.

To begin, we shift the saddle point $\hat{\Sigma}_3\hat{\xi}_3$ [Eq. (2.37)] to the identity $\hat{1}$ via left group translation of the unitary matrix field $\hat{Q}(\mathbf{r})$,

$$\hat{Q}(\mathbf{r}) \rightarrow \hat{\Sigma}_3\hat{\xi}_3\hat{Q}(\mathbf{r}), \quad \hat{Q}^\dagger(\mathbf{r}) \rightarrow \hat{Q}^\dagger(\mathbf{r})\hat{\Sigma}_3\hat{\xi}_3. \quad (3.1)$$

The FNLσM action, Eqs. (2.49) and (2.50), becomes

$$S_D = \frac{1}{2\lambda} \int d^d\mathbf{r} \, \text{Tr}[\nabla\hat{Q}^\dagger \cdot \nabla\hat{Q}] - \frac{\lambda_A}{2\lambda^2} \int d^d\mathbf{r}[\text{Tr}(\hat{Q}^\dagger\nabla\hat{Q})]^2$$

$$+ ih \int d^d\mathbf{r} \, \text{Tr}((|\hat{\omega}|\hat{\xi}_3 + \hat{1}i\eta)(\hat{Q}^\dagger + \hat{Q})) \quad (3.2)$$

and

$$S_I = \sum_a i\xi^a \int \frac{d\omega_1}{2\pi}\frac{d\omega_2}{2\pi}\frac{d\omega_3}{2\pi}\frac{d\omega_4}{2\pi} d^d\mathbf{r}\,\delta_{1+3,2+4}(\Gamma_U[s_1s_3Q_{1,2}^{a,a}Q_{3,4}^{a,a}$$

$$+ s_2s_4Q_{1,2}^{\dagger a,a}Q_{3,4}^{\dagger a,a}] + 2\Gamma_V s_2s_3Q_{1,2}^{\dagger a,a}Q_{3,4}^{a,a}). \quad (3.3)$$

Equation (3.3) expresses S_I in frequency space, where we have implemented the compact notations

$$\delta_{1+3,2+4} \equiv \delta_{\omega_1+\omega_3,\omega_2+\omega_4},$$

$$Q_{1,2}^{a,a}(\mathbf{r}) \equiv Q_{\omega_1,\omega_2}^{a,a}(\mathbf{r}),$$

$$s_1 \equiv (\hat{\Sigma}_3)_{\omega_1,\omega_1} = \text{sgn}(\omega_1), \quad (3.4)$$

etc., i.e., numeric subscripts represent associated frequency labels.

The saddle point shift defined by Eq. (3.1) modifies only the symmetry-breaking term, proportional to h, in the noninteracting sector of the theory [cf. Eqs. (2.49) and (3.2)]. In contrast, the transformation in Eq. (3.1) inserts explicit factors of $s_is_j = \text{sgn}(\omega_i)\text{sgn}(\omega_j)$, $i, j \in \{1,2,3,4\}$, into all terms inhabiting the interacting sector S_I [Eqs. (2.50) and (3.3)]. Below, we show that these factors function as projection matrices, dividing the interaction-dressed diffusion modes into

smooth and sublattice staggered charge density diffuson channels, characterized by interaction strengths Γ_s and Γ_c, respectively. [See Eq. (2.54), as well as Eqs. (3.16a)–(3.18d).]

We now parametrize the FNLσM for the RG computation. We employ a Wilsonian frequency-momentum shell, background field methodology.[2] The first step is to split $\hat{Q}$ into "fast" $\hat{Q}_\mathsf{F}$ and "slow" $\hat{Q}_\mathsf{S}$ mode parts,

$$\hat{Q}(\mathbf{r}) \equiv \hat{Q}_\mathsf{F}(\mathbf{r})\hat{Q}_\mathsf{S}(\mathbf{r}) \equiv \hat{Q}_\mathsf{F}(\mathbf{r})[\hat{1} + \delta\hat{Q}_\mathsf{S}(\mathbf{r})], \quad (3.5)$$

where both the fast and slow matrix fields satisfy the unitary constraint [Eq. (2.51)]:

$$\hat{Q}_\mathsf{F}^\dagger(\mathbf{r})\hat{Q}_\mathsf{F}(\mathbf{r}) = \hat{Q}_\mathsf{S}^\dagger(\mathbf{r})\hat{Q}_\mathsf{S}(\mathbf{r}) = \hat{1}. \quad (3.6)$$

On the second line of Eq. (3.5), we have further decomposed[55] the slow mode field $\hat{Q}_\mathsf{S}$ into the homogeneous saddle point $\hat{1}$ plus the "small" perturbation $\delta\hat{Q}_\mathsf{S}(\mathbf{r}) \equiv \hat{Q}_\mathsf{S}(\mathbf{r}) - \hat{1}$.

We require a parametrization for the unitary fast mode field $\hat{Q}_\mathsf{F}$ in terms of some unconstrained coordinates; we choose geodetic coordinates on the group manifold,

$$\hat{Q}_\mathsf{F}(\mathbf{r}) \equiv \exp[i\hat{Y}(\mathbf{r})] \approx \hat{1} + i\hat{Y}(\mathbf{r}) + \cdots, \quad (3.7)$$

where $\hat{Y}^\dagger = \hat{Y}$ is a Hermitian matrix belonging to the Lie algebra that generates $\hat{Q}_\mathsf{F}$.

We now explain the meaning of the fast-slow decomposition defined by Eq. (3.5). The spatial Fourier transform of the slow mode fluctuation

$$\delta\hat{Q}_\mathsf{S}(\mathbf{k}) = \int d^d\mathbf{r} \exp(-i\mathbf{k}\cdot\mathbf{r})\delta\hat{Q}_\mathsf{S}(\mathbf{r}) \rightarrow \delta Q_{\mathsf{S}\omega,\omega'}^{a,a'}(\mathbf{k})$$

$$(3.8)$$

is taken to possess support within a cube of linear size $\tilde{\Lambda}$ in the (three-dimensional) absolute frequency and squared-momentum space $(|\omega|,|\omega'|,D\mathbf{k}^2)$; the cube encompasses the origin $|\omega|=|\omega'|=D\mathbf{k}^2=0$. Here,

$$D \equiv 1/(\lambda h) \quad (3.9)$$

is the effective diffusion constant. The linear size of the cube satisfies $\tilde{\Lambda} \ll 1/\tau \sim D/l^2$ (measured in energy units), where τ is the elastic scattering lifetime and l is the mean free path. We take the support of the fast mode coordinate

$$\hat{Y}(\mathbf{k}) = \int d^d\mathbf{r} \exp(-i\mathbf{k}\cdot\mathbf{r})\hat{Y}(\mathbf{r}) \rightarrow Y_{\omega,\omega'}^{a,a'}(\mathbf{k}) \quad (3.10)$$

to lie within a thin frequency-momentum shell enclosing the slow mode cube,

$$\tilde{\Lambda} \leq D\mathbf{k}^2 < \Lambda, \quad 0 \leq |\omega| < \Lambda, \quad 0 \leq |\omega'| < \Lambda, \quad (3.11a)$$

$$\tilde{\Lambda} \leq |\omega| < \Lambda, \quad 0 \leq D\mathbf{k}^2 < \Lambda, \quad 0 \leq |\omega'| < \Lambda, \quad (3.11b)$$
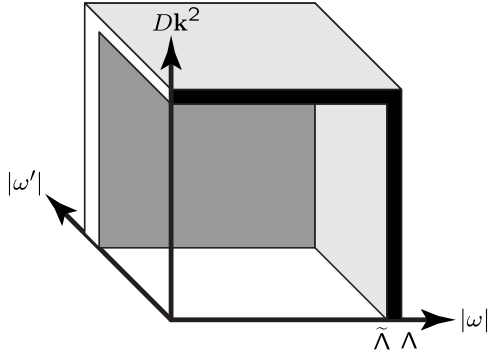
FIG. 6. Frequency-momentum shell of thickness $\Lambda - \tilde{\Lambda}$ supporting fast mode field coordinates $Y_{\omega,\omega'}^{a,a'}(\mathbf{k})$. The cubic volume of linear size $\tilde{\Lambda}$ enclosed by the shell supports the slow mode fields $\delta Q_{\mathsf{S}\omega,\omega'}^{a,a'}(\mathbf{k})$ and $\delta Q_{\mathsf{S}\omega,\omega'}^{\dagger a,a'}(\mathbf{k})$.

$$\tilde{\Lambda} \leq |\omega'| < \Lambda, \quad 0 \leq D\mathbf{k}^2 < \Lambda, \quad 0 \leq |\omega| < \Lambda,$$
$$(3.11c)$$

where $\Lambda/\tilde{\Lambda} \approx 1 + 2dl$ is a ratio of energy cutoffs, with $0 < dl \ll 1$. The regions of slow and fast mode supports are illustrated in Fig. 6. In the next section, we will integrate out the degrees of freedom in this shell and determine the resulting effect on the slow modes $\delta \hat{Q}_{\mathsf{S}}$.

By substituting the fast-slow decomposition [Eq. (3.5)] into the action in Eqs. (3.2) and (3.3) and expanding to second order[56] in the fast mode coordinates $\hat{Y}(\mathbf{r})$ using Eq. (3.7), the Keldysh generating functional Z [Eq. (2.48)] may be rewritten as

$$Z \sim \int \mathcal{D}\hat{Q}_{\mathsf{S}}\mathcal{D}\hat{Y} \exp(-S[\hat{Y}, \delta \hat{Q}_{\mathsf{S}}]).$$
$$(3.12)$$

We divide the action S in Eq. (3.12) into terms containing (i) only slow modes, (ii) only fast modes, and (iii) both fast and slow modes:

$$S = S_{\mathsf{S}}[\delta \hat{Q}_{\mathsf{S}}] + S_{\mathsf{F}}[\hat{Y}] + S_{\mathsf{F/S}}[\hat{Y}, \delta \hat{Q}_{\mathsf{S}}].$$
$$(3.13)$$

The pure slow mode sector of the theory is

$$S_{\mathsf{S}}[\delta \hat{Q}_{\mathsf{S}}] = S_D[\hat{Q} \to \hat{1} + \delta \hat{Q}_{\mathsf{S}}] + S_I[\hat{Q} \to \hat{1} + \delta \hat{Q}_{\mathsf{S}}],$$
$$(3.14)$$

with S_D and S_I as given by Eqs. (3.2) and (3.3). Of the remaining terms in Eq. (3.13), $S_{\mathsf{F}}[\hat{Y}]$ contains only fast mode degrees of freedom, while $S_{\mathsf{F/S}}[\hat{Y}, \delta \hat{Q}_{\mathsf{S}}]$ describes the coupling between the fast and slow mode fields.

To one-loop order, we need only retain terms in $S_{\mathsf{F}}[\hat{Y}]$ [Eq. (3.13)] to second order in $\hat{Y}(\mathbf{r})$, thereby obtaining the fast mode Gaussian diffusion propagator. We write

$$S_{\mathsf{F}} \equiv S_{\mathsf{F}}^{(D)} + S_{\mathsf{F}}^{(I)},$$
$$(3.15)$$

where the sector of the fast mode theory independent of the interparticle interactions is

$$S_{\mathsf{F}}^{(D)} = \frac{1}{2} \int d^d\mathbf{r} \left(\mathrm{Tr}\left[\frac{1}{\lambda}(\boldsymbol{\nabla}\hat{Y})^2 - ih(|\hat{\omega}|\hat{\xi}_3 + \hat{1}i\eta)\hat{Y}^2 \right. \right.$$
$$\left. \left. - ih\hat{Y}(|\hat{\omega}|\hat{\xi}_3 + \hat{1}i\eta)\hat{Y} \right] + \frac{\lambda_A}{\lambda^2}[\mathrm{Tr}(\boldsymbol{\nabla}\hat{Y})]^2 \right), \quad (3.16a)$$

while the interactions give rise to the term

$$S_{\mathsf{F}}^{(I)} = -\sum_a i\xi^a \int \frac{d\omega_1}{2\pi}\frac{d\omega_2}{2\pi}\frac{d\omega_3}{2\pi}\frac{d\omega_4}{2\pi}d^d\mathbf{r}(\delta_{1+3,2+4}$$
$$\times[\Gamma_s(s_1 - s_2)(s_3 - s_4) + \Gamma_c(s_1 + s_2)(s_3 + s_4)]Y_{1,2}^{a,a}Y_{3,4}^{a,a}).$$
$$(3.16b)$$

We have expressed $S_{\mathsf{F}}^{(I)}$, Eq. (3.16b) containing the interparticle interactions, in terms of the smooth and of the sublattice staggered (CDW) charge density interaction parameters Γ_s and Γ_c, defined by Eq. (2.54). In Eq. (3.16b), Γ_s and Γ_c couple to the frequency index tensors $(s_1 - s_2)(s_3 - s_4)\delta_{1+3,2+4}$ and $(s_1 + s_2)(s_3 + s_4)\delta_{1+3,2+4}$, respectively, which project out the channels of the propagator $\langle Y_{1,2}^{a,a}Y_{3,4}^{a,a}\rangle$ off-diagonal and diagonal in $\mathrm{sgn}(\omega)$ space, respectively. These channels are orthogonal, so that Eqs. (3.16a) and (3.16b) may be simply inverted to obtain the fast mode propagator for the theory. Note that all Keldysh indices must be identical to obtain a nonzero contribution from Eq. (3.16b).

The fast mode propagator cleanly decomposes into four disparate components; in terms of the spatial Fourier transform $\hat{Y}(\mathbf{k})$ defined via Eq. (3.10),

$$\langle Y_{1,2}^{a,b}(-\mathbf{k})Y_{3,4}^{c,d}(\mathbf{k})\rangle \equiv \mathsf{P}_\lambda + \mathsf{P}_A + \mathsf{P}_S + \mathsf{P}_C, \quad (3.17)$$

where the four symbols P_λ, P_A, P_S, and P_C represent the components

$$\mathsf{P}_\lambda = \Delta_{\mathcal{O}}^{a,b}(|\omega_1|, |\omega_2|, \mathbf{k})\delta^{a,d}\delta^{c,b}\delta_{1,4}\delta_{3,2}, \quad (3.18a)$$

$$\mathsf{P}_A = -\left[\frac{\lambda_A}{\lambda^2}\mathbf{k}^2\Delta_{\mathcal{O}}^{a,a}(|\omega_1|, |\omega_1|, \mathbf{k})\Delta_{\mathcal{O}}^{c,c}(|\omega_3|, |\omega_3|, \mathbf{k}) \right]$$
$$\times \delta^{a,b}\delta^{c,d}\delta_{1,2}\delta_{3,4}, \quad (3.18b)$$

$$\mathsf{P}_S = [2i\xi^a\Gamma_s(s_1 - s_2)(s_3 - s_4)\Delta_S^a(|\omega_1 - \omega_2|, \mathbf{k})$$
$$\times \Delta_{\mathcal{O}}^{a,a}(|\omega_1 - \omega_2|, 0, \mathbf{k})]\delta^{a,b}\delta^{a,d}\delta^{c,d}\delta_{1+3,2+4}, \quad (3.18c)$$

$$\mathsf{P}_C = \left[2i\xi^a\Gamma_c(s_1 + s_2)(s_3 + s_4) \right.$$
$$\left. \times \frac{\Delta_{\mathcal{O}}^{a,a}(|\omega_1|, |\omega_2|, \mathbf{k})\Delta_{\mathcal{O}}^{a,a}(|\omega_3|, |\omega_4|, \mathbf{k})}{1 + \gamma_c f^a(|\omega_1 - \omega_2|, \mathbf{k})} \right]$$
$$\times \delta^{a,b}\delta^{a,d}\delta^{c,d}\delta_{1+3,2+4}. \quad (3.18d)$$

Keldysh $\{a, b, \ldots\}$ and frequency $\{1, 2, \ldots\}$ indices in Eqs. (3.18a)–(3.18d) should be matched to those in Eq. (3.17). Components P_λ and P_A [Eqs. (3.18a) and (3.18b)] follow from the inversion of the disorder-only action in Eq. (3.16a), while P_S and P_C [Eqs. (3.18c) and (3.18d)] incorporate the interactions from Eq. (3.16b).
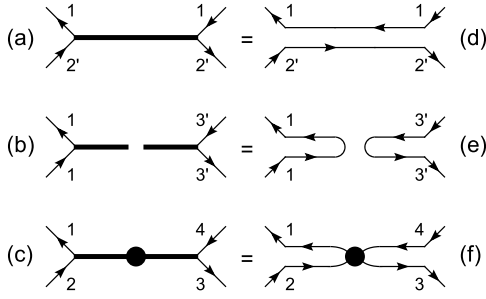
FIG. 7. Feynman rules I: fast mode propagator, from Eqs. (3.17)–(3.18d). Components of the disorder-only sector P_λ and P_A are depicted in (a) and (b), respectively; (c) represents the sum of interaction-dressed components $P_S + P_C$, which vanishes in the non-interacting limit. (d), (e), and (f) show that each thick line in (a), (b), and (c), respectively, can be understood as a pair of particle and hole lines, which carry counterpropagating arrows to indicate the flow of the conserved electric $U(1)$ current. The numeric labels represent the frequency indices of single fermion lines, while the primes denote the associated Keldysh species indices. The numeric labels with the same number of primes share the same Keldysh index, while the labels with different numbers of primes possess independent Keldysh indices.

The basic (heat) diffuson kernel in Eq. (3.18a) is

$$\Delta_{\mathcal{O}}^{a,b}(|\omega_1|,|\omega_2|,\mathbf{k}) \equiv \frac{1}{h}[D\mathbf{k}^2 - i(\xi^a|\omega_1| + \xi^b|\omega_2|)]^{-1},$$

$$(3.19)$$

with the diffusion constant D defined via Eq. (3.9). The diffuson matrix propagator P_λ in Eq. (3.18a) is pictured as a thick line segment in Fig. 7(a). As shown in Figs. 7(d)–7(f), each such thick line segment in Figs. 7(a)–7(c) can be taken to represent a *pair* of single fermion particle and hole lines, carrying counterpropagating arrows indicating the flow of the conserved electric $U(1)$ current [see, e.g., Eqs. (2.53a) and (2.53b)]. The numeric labels appearing along the terminating thin lines in Fig. 7(a) encode the frequency and Keldysh indices carried by the fast mode matrix fields $\hat{Y} \to Y_{\omega,\omega'}^{a,a'}$. These indices are propagated along (unbroken) thick line segments *without* mixing, as in Fig. 7(d). In both Figs. 7 and 8, we employ the following convention: different numerical labels encode independent frequency indices, and numerical labels carrying different numbers of primes indicate independent Keldysh species indices; numerical labels with the same number of primes represent indices that share the same Keldysh species.

Inversion of Eq. (3.16a) also gives the component P_A proportional to λ_A [Eq. (3.18b)], which has a different frequency and Keldysh index structure than the basic diffuson P_λ [Eq. (3.18a)]. P_A is depicted in Fig. 7(b). The inversion of Eq. (3.16a) gives only the sum of P_λ and P_A, i.e., terms up to first order in λ_A. We can try to build terms higher order in λ_A by cascading together multiple such sections, but it is clear from Figs. 7(b) and 7(e) that such a construction necessarily contains at least one closed "Keldysh" loop, defined here as a simultaneous Keldysh species index summation and fre-
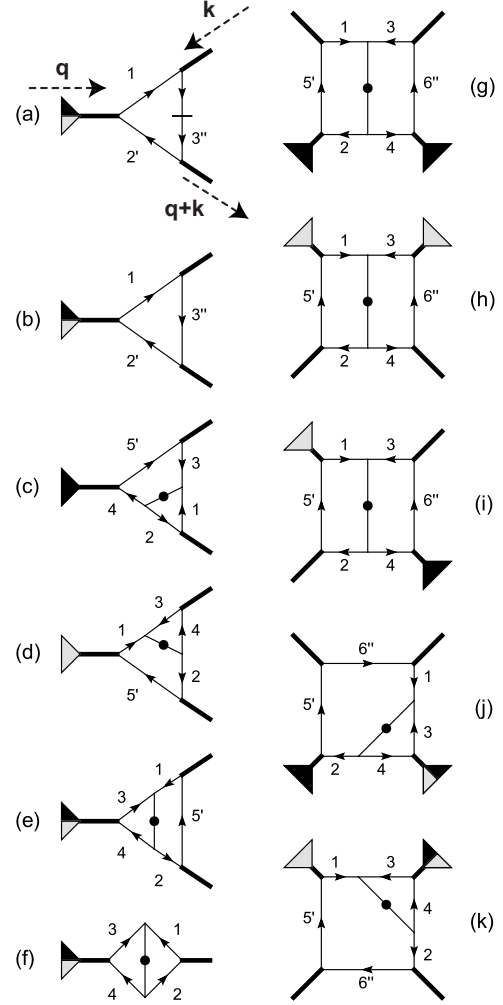

FIG. 8. Feynman rules II: vertices coupling together fast and slow modes arising from the term $S_{F/S}[\hat{Y}, \delta\hat{Q}_S]$ in Eq. (3.13). Vertex $V(\theta)$ is pictured in (θ), with $\theta \in \{a, b, c, \ldots\}$. In this figure, the black and blank triangular terminals indicate $\delta\hat{Q}_s$ and $\delta\hat{Q}_s^\dagger$ slow mode fields, respectively, while the half-black, half-blank terminals indicate linear combinations of these. The unterminated thick lines represent fast mode fields $\hat{Y}$. Vertices $V(a)$ and $V(b)$ are derived from the stiffness and energy terms, respectively, of the noninteracting sigma model action [Eq. (3.2)], while vertices $V(c)$–$V(k)$ arise from the interparticle interactions [Eq. (3.3)]. Momentum labels $\mathbf{q}$, $\mathbf{k}$, and $\mathbf{q}+\mathbf{k}$ have been furnished for the stiffness vertex $V(a)$, as this vertex depends explicitly on these momenta.

quency integration along a closed single fermion line. As with the replica trick, such closed loops vanish in the Keldysh formalism.

The smooth and sublattice staggered interparticle interactions in Eq. (3.16b), characterized by Γ_s and Γ_c, respectively, dress the bare diffuson propagator P_λ [Eq. (3.18a)], giving rise to the propagator components P_S and P_C [Eqs. (3.18c) and (3.18d), respectively]. These equations show that the component P_S (P_C) projects on the propagator channel off-diagonal (diagonal) in $\text{sgn}(\omega)$ space. The kernel

$$\Delta_S^a(|\omega|,\mathbf{k}) \equiv \frac{1}{h}[Dk^2 - i(1-\gamma_s)\xi^a|\omega|]^{-1} \quad (3.20)$$

appears in $\mathsf{P_S}$, the channel of the interaction-dressed propagator off-diagonal in $\mathrm{sgn}(\omega)$ space [Eq. (3.18c)], and is related[2,3] to the diffusion of the physical, conserved electric $U(1)$ charge. In Eqs. (3.20) and (3.18d), we have introduced the relative interaction constants

$$\gamma_s \equiv \frac{4}{\pi h}\Gamma_s = \frac{2}{\pi h}(\Gamma_U + \Gamma_V), \quad (3.21a)$$

$$\gamma_c \equiv \frac{4}{\pi h}\Gamma_c = \frac{2}{\pi h}(\Gamma_U - \Gamma_V), \quad (3.21b)$$

where we have used Eq. (2.54). Finally, the logarithmic function

$$f^a(|\omega|,\mathbf{k}) \equiv \ln\left[\frac{2\Lambda}{|\omega| + i\xi^a Dk^2}\right], \quad (3.22)$$

with Λ a hard frequency cutoff [cf. Eqs. (3.11a), (3.11b), and (3.11c)], appears in $\mathsf{P_C}$, the channel of the interaction-dressed propagator diagonal in $\mathrm{sgn}(\omega)$ space [Eq. (3.18d)]. The structure[3,57,58] of $\mathsf{P_C}$ does *not* follow from any conservation law, as the sublattice staggered electric charge density (the "CDW" order parameter associated with the interaction strength Γ_c) does not represent a conserved quantity. In this paper, we will work only to the lowest nontrivial order in γ_c; practically, this means ignoring[2,57] the logarithmic denominator [Eq. (3.22)] in $\mathsf{P_C}$ [Eq. (3.18d)]. This approximation is adequate for all of the results presented in Sec. V. The sum of the interaction-dressed propagator components $\mathsf{P_S}+\mathsf{P_C}$ will be depicted as a thick line with a black dot, as shown in Fig. 7(c).

The channel of the fast mode propagator diagonal in $\mathrm{sgn}(\omega)$ space, including the components $\mathsf{P_A}$, proportional to the disorder strength λ_A [Eq. (3.18b)], and $\mathsf{P_C}$, proportional to the CDW interaction strength Γ_c [Eq. (3.18d)], is special to a system with sublattice symmetry [Eq. (1.2)]. (Recall from Secs. II A 3 and II A 4 that λ_A measures the strength of quenched orientational fluctuations of bond dimerization in the intersublattice hopping disorder.) The addition of SLS breaking, e.g., in the form of on-site disorder, changes the random matrix class[7] of the (noninteracting version of the) random hopping model studied in this paper, Eqs. (1.1) and (1.9) with $U=V=0$, from the sublattice (chiral) class AIII to the ordinary unitary metal class A. Equivalently, breaking SLS reduces the size of the sigma model target manifold, as discussed in Appendix A. The crossover is marked by the appearance of a "mass" in the FNLσM propagator channel diagonal in $\mathrm{sgn}(\omega)$, which gaps out the propagator components $\mathsf{P_A}$ and $\mathsf{P_C}$ [as well as "half" of the basic diffuson modes $\mathsf{P_\lambda}$ in Eq. (3.18a)]. This is the reason that the coupling strengths λ_A and Γ_c do not appear in the spinless unitary class Finkel'stein NLσM,[3] which retains the parameters λ, h, and Γ_s.

The fast and slow mode fields are coupled together by the term $S_{F/S}[\hat{Y}, \delta\hat{Q}_S]$ in Eq. (3.13). $S_{F/S}[\hat{Y}, \delta\hat{Q}_S]$ gives rise to the Feynman vertices pictured in Fig. 8. We will refer to the

TABLE I. Feynman rules III: factors associated with vertices $\{\mathsf{V(a)},\mathsf{V(b)},\dots\}$, pictured in Fig. 8, coupling together fast and slow modes. Frequency $\{1, 2, 3,\dots\}$ and Keldysh species $\{a,a',a''\}$ indices in the factor $\mathsf{V}(\theta)$ should be matched to those in the corresponding Fig. 8 (θ). Fast mode fields $\hat{Y}$ have been amputated from the vertex factors in this table for brevity; the fast-slow mode coupling structure may be understood from Fig. 8. The (spatial Fourier transform of the) slow mode operator $\mathbf{L}_{S1,2}^{a,a'}(\mathbf{q})$ is defined by Eq. (3.23).

$\mathsf{V(a)}$	$=$	$-(i/2\lambda)\int[d^d\mathbf{q}/(2\pi)^d](2\mathbf{k}+\mathbf{q})\cdot\mathbf{L}_{S1,2}^{a,a'}(\mathbf{q})$
$\mathsf{V(b)}$	$=$	$(ih/2)\int d^d\mathbf{r}(|\omega_2|\xi^{a'}\delta Q_{S1,2}^{a,a'}+|\omega_1|\xi^a\delta Q_{S1,2}^{\dagger a,a'})$
$\mathsf{V(c)}$	$=$	$2i\xi^a\delta_{1+3,2+4}(\Gamma_U s_1 s_3 - \Gamma_V s_2 s_3)\int d^d\mathbf{r}\,\delta Q_{S5,4}^{a',a}$
$\mathsf{V(d)}$	$=$	$2i\xi^a\delta_{1+3,2+4}(\Gamma_U s_2 s_4 - \Gamma_V s_2 s_3)\int d^d\mathbf{r}\,\delta Q_{S1,5}^{\dagger a,a'}$
$\mathsf{V(e)}$	$=$	$i\xi^a\delta_{1+3,2+4}\int d^d\mathbf{r}[\Gamma_s(s_1+s_2)(s_3\delta Q_{S3,4}^{a,a}+s_4\delta Q_{S3,4}^{\dagger a,a})$
		$\qquad +\Gamma_c(s_1-s_2)(s_3\delta Q_{S3,4}^{a,a}-s_4\delta Q_{S3,4}^{\dagger a,a})]$
$\mathsf{V(f)}$	$=$	$2\xi^a\delta_{1+3,2+4}\int d^d\mathbf{r}[\Gamma_s(s_1-s_2)(s_3\delta Q_{S3,4}^{a,a}+s_4\delta Q_{S3,4}^{\dagger a,a})$
		$\qquad +\Gamma_c(s_1+s_2)(s_3\delta Q_{S3,4}^{a,a}-s_4\delta Q_{S3,4}^{\dagger a,a})]$
$\mathsf{V(g)}$	$=$	$2i\xi^a\delta_{1+3,2+4}\Gamma_U s_1 s_3\int d^d\mathbf{r}\,\delta Q_{S5,2}^{a',a}\delta Q_{S6,4}^{a'',a}$
$\mathsf{V(h)}$	$=$	$2i\xi^a\delta_{1+3,2+4}\Gamma_U s_2 s_4\int d^d\mathbf{r}\,\delta Q_{S1,5}^{\dagger a,a'}\delta Q_{S3,6}^{\dagger a,a''}$
$\mathsf{V(i)}$	$=$	$-2i\xi^a\delta_{1+3,2+4}\Gamma_V s_2 s_3\int d^d\mathbf{r}\,\delta Q_{S1,5}^{\dagger a,a'}\delta Q_{S6,4}^{a'',a}$
$\mathsf{V(j)}$	$=$	$i\xi^a\delta_{1+3,2+4}\int d^d\mathbf{r}[\Gamma_U s_1 s_3\delta Q_{S5,2}^{a',a}\delta Q_{S3,4}^{a,a}$
		$\qquad +\Gamma_V s_1 s_4\delta Q_{S5,2}^{a',a}\delta Q_{S3,4}^{\dagger a,a}]$
$\mathsf{V(k)}$	$=$	$i\xi^a\delta_{1+3,2+4}\int d^d\mathbf{r}[\Gamma_U s_2 s_4\delta Q_{S1,5}^{\dagger a,a'}\delta Q_{S3,4}^{a,a}$
		$\qquad +\Gamma_V s_2 s_3\delta Q_{S1,5}^{\dagger a,a'}\delta Q_{S3,4}^{a,a}]$

vertex pictured in Fig. 8 (θ) as "$\mathsf{V}(\theta)$," with $\theta \in \{\mathsf{a},\mathsf{b},\mathsf{c},\dots\}$. In these figures, the vertex corners adorned by thick line "spokes" that split into directed thin lines represent insertions of the slow ($\delta\hat{Q}_S$ and/or $\delta\hat{Q}_S^\dagger$) or fast ($\hat{Y}$) mode matrix fields. Specifically, the triangular black and blank spoke terminals denote the slow mode fields $\delta\hat{Q}_S$ and $\delta\hat{Q}_S^\dagger$, respectively, while the half-black, half-blank terminals denote linear combinations of these. Each unterminated thick line spoke in Fig. 8 represents a fast mode field $\hat{Y}$, which may be interconnected in pairs using the propagators shown in Fig. 7, with amplitudes given by the associated expressions in Eq. (3.18). As in Fig. 7, we use numerical labels to indicate frequency indices, with primes distinguishing independent Keldysh species indices.

The factors associated with the vertices $\{\mathsf{V(a)},\mathsf{V(b)},\dots\}$ are listed in Table I. In this table, the fast mode fields $\hat{Y}$ have been amputated from the vertex expressions; the structure of the fast-slow mode coupling should be understood from Fig. 8. Vertices $\mathsf{V(a)}$ and $\mathsf{V(b)}$ are obtained from the noninteracting sector of the FNLσM action [Eq. (3.2)], while vertices $\mathsf{V(c)}-\mathsf{V(k)}$ are derived from the interparticle interactions [Eq. (3.3)], indicated by the black dots in Figs. 8(c)–8(k). The first entry of Table I gives the factor associated with the "stiffness vertex" $\mathsf{V(a)}$, shown in Fig. 8(a). Here, we have introduced the slow mode vector operator

$$\hat{\mathbf{L}}_S(\mathbf{r}) \equiv \hat{Q}_S(\mathbf{r})\,\boldsymbol{\nabla}\,\hat{Q}_S^\dagger(\mathbf{r}) = [\hat{1} + \delta\hat{Q}_S(\mathbf{r})]\,\boldsymbol{\nabla}\,\delta\hat{Q}_S^\dagger(\mathbf{r}).$$
$$(3.23)$$

Note that all fast-slow vertices pictured in Fig. 8, except V(f), are bilinear in the fast mode fields $\hat{Y}(\mathbf{r})$ (represented by unterminated thick lines); the latter vertex involves only a single fast mode field. Such a vertex would vanish in a pure momentum shell treatment, in which one integrates undetermined fast mode loop momenta over a thin shell while simultaneously integrating undetermined fast mode loop frequencies over the entire real line. In Sec. IV, we show that a diagram involving two copies of V(f) produces the term in the RG flow equations that gives rise to the CDW instability in the clean Hubbard-like model [Eq. (1.1)]. As the CDW term must be present in the advent of sublattice symmetry (e.g., in the ballistic limit $\lambda, \lambda_A \to 0$), we are forced to work with the frequency-momentum shell method in this paper. A similar term responsible for the BCS superconducting instability of the diffusive Fermi liquid also arises in the FNLσM description of normal, TRI metals only in the frequency-momentum shell scheme.[2,3,57,58]

IV. ONE-LOOP CALCULATION

In two dimensions, the disorder parameters λ and λ_A, as well as the ratios γ_s and γ_c, defined by Eqs. (3.21a) and (3.21b), carry zero engineering dimension (demonstrated explicitly in Sec. IV B, below). In the language of the RG, we say that these parameters are marginal (in $d=2$) at tree level. Here, we compute the one-loop RG flow equations for the coupling strengths λ, λ_A, and h, as well as Γ_U and Γ_V, or equivalently, Γ_s and Γ_c [Eq. (2.54)]. The loop expansion is performed in $d=2+\epsilon$ dimensions, with $0 \leq \epsilon \ll 1$, and is formally organized as an expansion in powers of the disorder strength λ, which is inversely proportional to the dimensionless dc conductance. As discussed below Eq. (3.22), we choose to work only to the lowest nontrivial order in the CDW interaction parameter Γ_c (or γ_c); in contrast, the loop expansion incorporates contributions from λ_A, h, and Γ_s to *all* orders. We need make no assumptions about the smallness of these latter three parameters. The diagrammatics appear in Sec. IV A; the results of this section are combined with dimensional analysis in Sec. IV B, yielding the desired one-loop flow equations. The flow equations obtained here are summarized and interpreted in Sec. V.

A. Renormalization

The calculation is performed in the frequency-momentum shell background field formalism established in the previous section. We integrate out the fast modes $Y^{a,a'}_{\omega,\omega'}(\mathbf{k})$ [Eq. (3.7)] lying within the shell defined by Eqs. (3.11a), (3.11b), and (3.11c), where

$$\frac{\Lambda}{\tilde{\Lambda}} \approx 1 + 2dl \qquad (4.1)$$

and $0 < dl \ll 1$, as below Eqs. (3.11a)–(3.11c). The fast mode integration produces corrections to the action S_S [Eq. (3.14)] for the slow mode fields $\delta Q^{a,a'}_{S\omega,\omega'}(\mathbf{k})$ and $\delta Q^{\dagger a,a'}_{S\omega,\omega'}(\mathbf{k})$. Note that in the case of the fast mode field $Y^{a,a'}_{\omega,\omega'}(\mathbf{k})$, *at least* one of
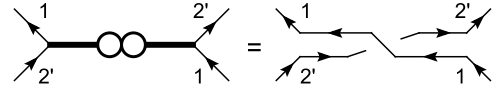

FIG. 9. Basic diffuson propagator P_λ [Fig. 7(a) and Eq. (3.18a)] with a twist.

the three variables $\alpha \in \{D\mathbf{k}^2, |\omega|, |\omega'|\}$ is always fast, lying within the range $\tilde{\Lambda} < \alpha < \Lambda$.

In the pure slow mode sector of the theory, with action S_S defined via Eqs. (3.14), (3.2), and (3.3), all five parameters λ, λ_A, h, Γ_U, and Γ_V couple to local operators which contain nonvanishing terms quadratic in $\delta\hat{Q}_S$ and/or $\delta\hat{Q}_S^\dagger$. In order to renormalize the parameters of the theory, then, we need only consider corrections to terms up to second order in $\delta\hat{Q}_S$ (and its adjoint) in the pure slow mode FNLσM action.

In this subsection, we furnish the set of 83 nonvanishing diagrams that correct the marginal parameters in the FNLσM and/or correspond to the generation of marginal operators not originally present in the FNLσM action. All contributions of the latter type must cancel if the theory is to be renormalizable to one loop; we will show that this is indeed the case. The required diagrams are organized into 14 categories, shown in Figs. 10–22, renormalizing each of the coupling strengths appearing in the FNLσM. To each category of diagrams, we provide the label $\mathfrak{D}m$, with $m \in \{1, \ldots, 14\}$. Category labels $\{\mathfrak{D}1, \mathfrak{D}2, \ldots\}$ appear in the captions of the associated figures $\{10, 11, \ldots\}$. Individual diagrams *and* their associated amplitudes will be referred to by a category label, a letter, and if necessary, a subscript Roman numeral: $\mathfrak{D}1(\mathsf{a})$ refers to the diagram labeled (a) in the left-hand column of Fig. 10 (category $\mathfrak{D}1$), while $\mathfrak{D}2(\mathsf{b})_{iii}$ refers to the diagram labeled (iii) in the right-hand column of Fig. 11 (category $\mathfrak{D}2$). Below, we examine each category of corrections in turn. We also calculate the one-loop renormalization of the single-particle DOS $\nu(\omega)$. Explicit frequency and Keldysh indices (using the same conventions employed in Figs. 7 and 8) distinguish the diagrams in Figs. 10–22 whose detailed evaluation is provided in this section.

The key ingredients for the renormalization process are the fast mode propagators P_λ, P_A, P_S, and P_C, depicted in Figs. 7(a)–7(c), with the associated amplitudes provided by Eq. (3.18), and the vertices $\mathsf{V}(\theta)$ coupling together fast and slow modes, with $\theta \in \{\mathsf{a}, \mathsf{b}, \mathsf{c}, \ldots\}$, cataloged in Table I and pictured in Fig. 8. Explicit formulas for the necessary frequency-momentum shell loop integrations are relegated to Appendix D.

1. Propagator with a twist

The basic diffuson propagator P_λ, given by Eq. (3.18a), is represented as the thick line segment shown in Fig. 7(a). In Fig. 9, we picture the same propagator shown in Fig. 7(a) but with a twist of the right end relative to the left. The twist is represented by the "∞" symbol. We will use this twisted representation of P_λ whenever convenient to simplify the diagrammatics.

2. Renormalization of λ_A

Diagrams $\mathfrak{D}1(\mathsf{a})$–$\mathfrak{D}1(\mathsf{c})$ appearing in Fig. 10 renormalize the disorder parameter λ_A. The associated amplitudes in-
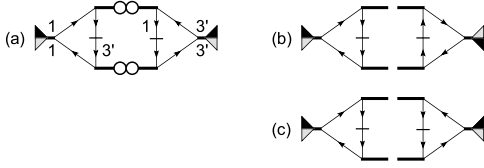
FIG. 10. Category $\mathfrak{D}1$: Diagrams renormalizing λ_A.

volve pure momentum shell integrations since all propagator frequency indices are slow. [See Eqs. (3.11a)–(3.11c) and Fig. 6.] We will compute $\mathfrak{D}1(\mathsf{a})$ explicitly; the labels $1 \rightarrow \{\omega_1, a\}$ and $3' \rightarrow \{\omega_3, a'\}$ in Fig. 10 represent external, slow frequencies (ω_1, ω_3) and Keldysh indices (a, a').

Using the Feynman rules, we find

$$\mathfrak{D}1(\mathsf{a}) = \frac{1}{2!}\left(\frac{-i}{2\lambda}\right)^2 \int \frac{d^d\mathbf{q}}{(2\pi)^d} L^{ia,a}_{\mathsf{S}1,1}(\mathbf{q}) L^{ja',a'}_{\mathsf{S}3,3}(-\mathbf{q}) I^{i,j}_1,$$
(4.2)

where i and j denote vector components, with the pure momentum shell integration

$$I^{i,j}_1 = \int \frac{d^2\mathbf{k}}{(2\pi)^2}(2\mathbf{k}+\mathbf{q})^i(-2\mathbf{k}-\mathbf{q})^j$$
$$\times [\Delta^{a,a'}_{\mathcal{O}}(|\omega_1|,|\omega_3|,\mathbf{k})\Delta^{a,a'}_{\mathcal{O}}(|\omega_1|,|\omega_3|,\mathbf{k}+\mathbf{q})]$$
$$\sim \frac{-4\delta^{i,j}}{2h^2}\frac{1}{2D^2(2\pi)}\int^{\Lambda}_{\tilde{\Lambda}}\frac{dx}{x} = \frac{-\delta^{i,j}\lambda^2}{2\pi}2dl,$$
(4.3)

up to irrelevant slow mode frequency (ω_1, ω_3)- and momentum ($\mathbf{q}$)-dependent terms. On the last line of Eq. (4.3), we have performed the change of integration variables $x \equiv D\mathbf{k}^2$, with $D = 1/\lambda h$ [Eq. (3.9)], and we have used Eq. (4.1). By combining Eqs. (4.2) and (4.3), using Eq. (3.23), and summing over slow mode frequency and Keldysh indices, we obtain

$$\mathfrak{D}1(\mathsf{a}) = \left(\frac{\lambda^2 2dl}{8\pi\lambda_A}\right)\frac{\lambda_A}{2\lambda^2}\int d^d\mathbf{r}[\mathrm{Tr}(\hat{Q}^{\dagger}_{\mathsf{S}}\boldsymbol{\nabla}\,\hat{Q}_{\mathsf{S}})]^2. \quad (4.4)$$

$\mathfrak{D}1(\mathsf{b})$ and $\mathfrak{D}1(\mathsf{c})$ may be similarly evaluated; in fact, these diagrams exactly cancel because of the directional dependence of the stiffness vertex $\mathsf{V}(\mathsf{a})$ on the loop momenta—see Table I. Thus, the complete λ_A renormalization is given by Eq. (4.4).

3. Renormalization of λ and h

The diagrams in category $\mathfrak{D}2$ (Fig. 11) renormalize the disorder parameter λ, proportional to the inverse dimensionless dc conductance. $\mathfrak{D}2(\mathsf{a})_{\mathrm{i}}$–$\mathfrak{D}2(\mathsf{a})_{\mathrm{iv}}$, shown in the left-hand column of Fig. 11, possess no undetermined loop frequencies, and therefore involve pure momentum shell integrations, similar to that in Eq. (4.3). In fact, $\mathfrak{D}2(\mathsf{a})_{\mathrm{i}}$ and $\mathfrak{D}2(\mathsf{a})_{\mathrm{iii}}$ exactly cancel $\mathfrak{D}2(\mathsf{a})_{\mathrm{ii}}$ and $\mathfrak{D}2(\mathsf{a})_{\mathrm{iv}}$. On the other hand, the diagrams in the right-hand column of Fig. 11 involve simultaneous frequency and momentum loop integrations, and their sum indeed yields a nonvanishing renormalization of λ.

Diagrams $\mathfrak{D}2(\mathsf{b})_{\mathrm{i}}$ and $\mathfrak{D}2(\mathsf{b})_{\mathrm{ii}}$ pictured in Fig. 11 give identical contributions, and each involve two copies of the
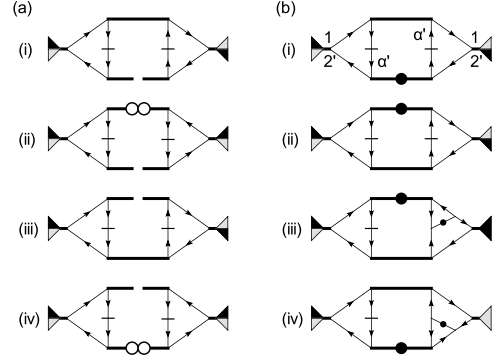
FIG. 11. Category $\mathfrak{D}2$: Diagrams renormalizing λ.

stiffness vertex $\mathsf{V}(\mathsf{a})$, with one basic diffuson P_{λ} and one interacting sector propagator $\mathsf{P}_{\mathsf{S}}+\mathsf{P}_{\mathsf{C}}$. We evaluate

$$\mathfrak{D}2(\mathsf{b})_{\mathrm{i}} = \frac{2i\xi^{a'}(-i)^2}{2!(2\lambda)^2}\int \frac{d^d\mathbf{q}}{(2\pi)^d}L^{ia,a'}_{\mathsf{S}1,2}(\mathbf{q})L^{ja',a}_{\mathsf{S}2,1}(-\mathbf{q})I^{i,j}_2,$$
(4.5)

where the frequency-momentum integral divides into two pieces:

$$I^{i,j}_2 \equiv I^{i,j}_{2\mathsf{S}} + I^{i,j}_{2\mathsf{C}},$$
(4.6)

corresponding to the P_{S} and P_{C} components of the interaction sector propagator, respectively. In the former case, up to irrelevant terms, we have

$$I^{i,j}_{2\mathsf{S}} = \int \frac{d\omega_\alpha d^2\mathbf{k}}{(2\pi)^3}(2\mathbf{k})^i(2\mathbf{k})^j\Gamma_s(s_\alpha - s_2)(s_2 - s_\alpha)$$
$$\times [\Delta^{a,a'}_{\mathcal{O}}(0,|\omega_\alpha|,\mathbf{k})\Delta^{a'}_{\mathsf{S}}(|\omega_\alpha|,\mathbf{k})\Delta^{a',a'}_{\mathcal{O}}(|\omega_\alpha|,0,\mathbf{k})]$$
$$= \frac{-4^2\Gamma_s\delta^{i,j}}{2h^3}\int_{\omega_\alpha>0}\frac{d\omega_\alpha d^2\mathbf{k}}{(2\pi)^3}\{\mathbf{k}^2[D\mathbf{k}^2 - i\xi^{a'}\omega_\alpha]^{-2}$$
$$\times [D\mathbf{k}^2 - i(1-\gamma_s)\xi^{a'}\omega_\alpha]^{-1}\}.$$
(4.7)

The "projection factor" $(s_\alpha - s_2)^2$ appearing in the first line of Eq. (4.7) is inherited from P_{S}. Equation (4.7) yields a result *independent* of the slow frequency ω_2, so we may take $\mathrm{sgn}(\omega_2) < 0$ without loss of generality. As a consequence, the only effect of the aforementioned projection factor in Eq. (4.7) is the restriction of the loop frequency integration to the half-space $\omega_\alpha > 0$. Following a change of variables, Eq. (4.7) gives

$$I^{i,j}_{2\mathsf{S}} = \frac{-4^2\Gamma_s\delta^{i,j}}{2h^3}J_1(\xi^{a'};(1-\gamma_s)\xi^{a'})$$
$$= -\frac{-i\xi^{a'}\delta^{i,j}\lambda^2}{4\pi}2dl\left[1 + \frac{1-\gamma_s}{\gamma_s}\ln(1-\gamma_s)\right]. \quad (4.8)$$

The frequency-momentum shell integral $J_1(z;z')$ in Eq. (4.8) is defined and evaluated in Appendix D [Eq. (D3)]. The CDW channel contribution $I^{i,j}_{2\mathsf{C}}$ to Eq. (4.6) may be similarly computed using the propagator P_{C} and working only to lowest order in Γ_c (i.e., ignoring the logarithmic denominator [Eq. (3.22)] in Eq. (3.18d)). By using Eq. (3.23) and sum-
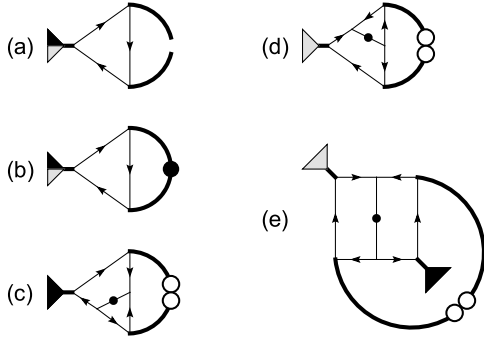
FIG. 12. Category $\mathfrak{D}3$: Diagrams renormalizing h.

ming the identical contributions from $\mathfrak{D}2(\mathsf{b})_\mathrm{i}$ and $\mathfrak{D}2(\mathsf{b})_\mathrm{ii}$, one finds

$$\mathfrak{D}2(\mathsf{b})_\mathrm{i} + \mathfrak{D}2(\mathsf{b})_\mathrm{ii} = \left(\frac{\lambda 2 dl}{4\pi}\right)\left[1 + \frac{1-\gamma_s}{\gamma_s}\ln(1-\gamma_s) - \frac{\gamma_c}{2}\right]$$
$$\times \frac{1}{2\lambda}\int d^d\mathbf{r}\,\mathrm{Tr}[\boldsymbol{\nabla}\hat{Q}_\mathsf{S}^\dagger \cdot \boldsymbol{\nabla}\hat{Q}_\mathsf{S}]. \qquad (4.9)$$

If we set $\gamma_c = 0$ in Eq. (4.9), the remainder is recognized as the usual correction to the "dimensionless dc resistance" λ in the presence of *short-ranged* density-density interparticle interactions.[2,59–61]

The computation of the final two diagrams $\mathfrak{D}2(\mathsf{b})_\mathrm{iii}$ and $\mathfrak{D}2(\mathsf{b})_\mathrm{iv}$ in Fig. 11 is more complicated, as each graph involves *two* loop frequency integrations. We demonstrate the evaluation of a diagram involving two frequency loops appearing in Fig. 15, below. Here, we simply give the result for the sum:

$$\mathfrak{D}2(\mathsf{b})_\mathrm{iii} + \mathfrak{D}2(\mathsf{b})_\mathrm{iv} = \left(\frac{-\lambda 2 dl}{4\pi}\right)\left[2 + \frac{2-\gamma_s}{\gamma_s}\ln(1-\gamma_s)\right]$$
$$\times \frac{1}{2\lambda}\int d^d\mathbf{r}\,\mathrm{Tr}[\boldsymbol{\nabla}\hat{Q}_\mathsf{S}^\dagger \cdot \boldsymbol{\nabla}\hat{Q}_\mathsf{S}]. \quad (4.10)$$

The "anomalous" amplitude in Eq. (4.10) is precisely canceled by other diagrams.

We now turn to the renormalization of h by the diagrams in Fig. 12. $\mathfrak{D}3(\mathsf{a})$ and $\mathfrak{D}3(\mathsf{b})$ involve the symmetry-breaking vertex $\mathsf{V}(\mathsf{b})$, fused with the propagators P_A and $\mathsf{P}_\mathsf{S}+\mathsf{P}_\mathsf{C}$, respectively. $\mathfrak{D}3(\mathsf{a})$ involves a pure momentum shell integration, while $\mathfrak{D}3(\mathsf{b})$ requires the integral $J_2(z,z')$ [Eq. (D4)]. The result is

$$\mathfrak{D}3(\mathsf{a}) + \mathfrak{D}3(\mathsf{b}) = \left(\frac{-2dl}{8\pi}\right)\{\lambda_A + \lambda[\ln(1-\gamma_s) + \gamma_c]\}$$
$$\times ih\int d^d\mathbf{r}\,\mathrm{Tr}[|\hat{\omega}|\hat{\xi}_3(\hat{Q}_\mathsf{S}^\dagger + \hat{Q}_\mathsf{S})]. \quad (4.11)$$

The sum of the remaining diagrams $\mathfrak{D}3(\mathsf{c})$–$\mathfrak{D}3(\mathsf{e})$ gives zero.

To complete the renormalization of λ and h, we must compute the graphs pictured in Fig. 13. $\mathfrak{D}4(\mathsf{a})$ and $\mathfrak{D}4(\mathsf{b})$
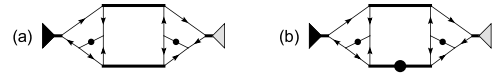
FIG. 13. Category $\mathfrak{D}4$: Diagrams renormalizing λ and h.

involve the cross pairing of the *interaction* vertices $\mathsf{V}(\mathsf{c})$ and $\mathsf{V}(\mathsf{d})$, with both noninteracting P_λ and interacting $\mathsf{P}_\mathsf{S}+\mathsf{P}_\mathsf{C}$ propagator components. These diagrams are quite lengthy to evaluate because they require two $[\mathfrak{D}4(\mathsf{a})]$ and three $[\mathfrak{D}4(\mathsf{b})]$ frequency loop integrations and necessitate Taylor expansions of the fast mode propagators in powers of the external frequencies and momenta. Other diagrams with multifrequency loop integrals will be tackled in detail below. Here, we merely quote the result

$$\mathfrak{D}4(\mathsf{a}) + \mathfrak{D}4(\mathsf{b})$$
$$= -\mathfrak{D}2(\mathsf{b})_\mathrm{iii} - \mathfrak{D}2(\mathsf{b})_\mathrm{iv}$$
$$+ \left(\frac{\lambda 2 dl}{8\pi}\right)[\gamma_s + \ln(1-\gamma_s)]ih\int d^d\mathbf{r}\,\mathrm{Tr}[|\hat{\omega}|\hat{\xi}_3(\hat{Q}_\mathsf{S}^\dagger + \hat{Q}_\mathsf{S})]. \tag{4.12}$$

As promised, the anomalous correction to λ obtained in Eq. (4.10) is completely canceled by the amplitude $\mathfrak{D}4(\mathsf{a}) + \mathfrak{D}4(\mathsf{b})$. In addition, we pick up a crucial renormalization of h from Eq. (4.12).

4. Renormalization of the density of states $\nu(\omega)$

Before we treat the interparticle interaction parameters Γ_U and Γ_V, we pause to consider the local scaling operator

$$\nu^a(\omega,\mathbf{r}) \equiv \int \frac{d\omega'}{2\pi}[Q_{\omega,\omega'}^{a,a}(\mathbf{r}) + Q_{\omega,\omega'}^{\dagger a,a}(\mathbf{r})]. \qquad (4.13)$$

With the aid of Eqs. (2.53a) and (2.53b), it can be seen that the expectation value of $\nu^a(\omega,\mathbf{r})$ in Eq. (4.13) represents a measure of the disorder-averaged, coarse-grained, single-particle DOS $\nu(\omega)$ in the diffusive Fermi liquid, with ω measured relative to the Fermi energy. The scaling behavior of $\nu(\omega)$ as a function of energy scale ω or system size L may be determined through the renormalization of $\nu^a(\omega,\mathbf{r})$. By applying the Wilsonian background field decomposition [Eqs. (3.5) and (3.7)] and the RG program [Eqs. (3.17) and (3.18) and Table I] of the previous section to Eq. (4.13), one encounters the same diagrams responsible for *part* of the renormalization of the frequency rescaling factor h, graphs $\mathfrak{D}3(\mathsf{a})$ and $\mathfrak{D}3(\mathsf{b})$, pictured in Fig. 12.

We obtain the renormalization

$$\langle\nu^a(\omega,\mathbf{r})\rangle_\Lambda \sim \langle\nu^a(\omega,\mathbf{r})\rangle_{\tilde{\Lambda}}\left(1 + \frac{2dl}{8\pi}\{\lambda_A + \lambda[\ln(1-\gamma_s) + \gamma_c]\}\right) \tag{4.14}$$

similar to the amplitude expressed in Eq. (4.11). In Eq. (4.14), the symbols $\langle\cdots\rangle_\Lambda$ and $\langle\cdots\rangle_{\tilde{\Lambda}}$ denote the expectation value taken with respect to the generating functional Z in Eq. (3.12) before and after the elimination of the fast modes $Y_{\omega,\omega'}^{a,a'}(\mathbf{k})$, respectively. In Sec. IV B, we will use Eq. (4.14) to

TABLE II. Slow mode operators that appear in the renormalization of the interaction parameters Γ_U and Γ_V (or, equivalently, Γ_s and Γ_c). The operators in this table are summed over Keldysh species index (a), integrated over position space ($\mathbf{r}$), and integrated over frequency indices $\{1,2,3,4\} \rightarrow \{\omega_1, \omega_2, \omega_3, \omega_4\}$; we have used the compact notation introduced in Eq. (4.15) for this integration. In the interacting sector of the pure slow mode FNLσM action [Eq. (3.14)], the sum $\mathcal{O}_U + \bar{\mathcal{O}}_U$ couples to the same-sublattice interaction strength Γ_U, while $\mathcal{O}_V$ couples to the intersublattice interaction constant Γ_V. The operators $\mathcal{O}_X$, $\bar{\mathcal{O}}_X$, and $\mathcal{O}_Y$ do not correspond to terms occurring in the original FNLσM action [Eq. (3.3), after the saddle point shift in Eq. (3.1)] but are generated at intermediate steps in the renormalization process.

$\mathcal{O}_U$	$\sum_a i\xi^a \int_{1,2,3,4} d^d\mathbf{r}\, s_1 s_3 \delta Q^{a,a}_{S1,2} \delta Q^{a,a}_{S3,4}$
$\bar{\mathcal{O}}_U$	$\sum_a i\xi^a \int_{1,2,3,4} d^d\mathbf{r}\, s_2 s_4 \delta Q^{\dagger a,a}_{S1,2} \delta Q^{\dagger a,a}_{S3,4}$
$\mathcal{O}_V$	$\sum_a i\xi^a \int_{1,2,3,4} d^d\mathbf{r}\, 2 s_2 s_3 \delta Q^{\dagger a,a}_{S1,2} \delta Q^{a,a}_{S3,4}$
$\mathcal{O}_X$	$\sum_a i\xi^a \int_{1,2,3,4} d^d\mathbf{r}\, \delta Q^{a,a}_{S1,2} \delta Q^{a,a}_{S3,4}$
$\bar{\mathcal{O}}_X$	$\sum_a i\xi^a \int_{1,2,3,4} d^d\mathbf{r}\, \delta Q^{\dagger a,a}_{S1,2} \delta Q^{\dagger a,a}_{S3,4}$
$\mathcal{O}_Y$	$\sum_a i\xi^a \int_{1,2,3,4} d^d\mathbf{r}\, 2 \delta Q^{\dagger a,a}_{S1,2} \delta Q^{a,a}_{S3,4}$

derive a flow equation governing the scaling behavior of the DOS.

5. Renormalization of Γ_U and Γ_V

With the renormalization of the disorder-only sector parameters λ_A, λ, and h complete, we now turn to the (much more involved) renormalization of the interparticle interaction parameters Γ_U and Γ_V. It will prove convenient to introduce a set of six slow mode operators $\{\mathcal{O}_U, \bar{\mathcal{O}}_U, \mathcal{O}_V, \mathcal{O}_X, \bar{\mathcal{O}}_X, \mathcal{O}_Y\}$, defined by the expressions given in Table II. In this table, we have introduced the following compact notation for the position and frequency space integral:

$$\int \frac{d\omega_1}{2\pi} \frac{d\omega_2}{2\pi} \frac{d\omega_3}{2\pi} \frac{d\omega_4}{2\pi} d^d\mathbf{r}\, \delta_{1+3,2+4} \equiv \int_{1,2,3,4} d^d\mathbf{r}. \quad (4.15)$$

The operators $\mathcal{O}_U + \bar{\mathcal{O}}_U$ and $\mathcal{O}_V$ correspond to terms in the original FNLσM action [Eq. (3.3)] [*after* the saddle point shift in Eq. (3.1), with the replacement $\hat{Q} \rightarrow \hat{I} + \delta\hat{Q}_S$, as in Eq. (3.14)], coupling to the same-sublattice and intersublattice interaction strengths Γ_U and Γ_V, respectively. The last three operators listed in Table II are new; they do *not* correspond to terms appearing in Eq. (3.3). The structures possessed by the operators $\mathcal{O}_X$, $\bar{\mathcal{O}}_X$, and $\mathcal{O}_Y$ closely parallel those of $\mathcal{O}_U$, $\bar{\mathcal{O}}_U$, and $\mathcal{O}_V$, with a crucial difference: the former lack the frequency-dependent vertex factors $s_1 s_3 \rightarrow \mathrm{sgn}(\omega_1)\mathrm{sgn}(\omega_3)$, etc., appearing in the latter. We will see that $\mathcal{O}_X$, $\bar{\mathcal{O}}_X$, and $\mathcal{O}_Y$ are generated at intermediate steps in the RG process; in order for the theory to be renormalizable, these terms must completely cancel upon summing all one-loop diagrammatic amplitudes. Indeed, this occurs.
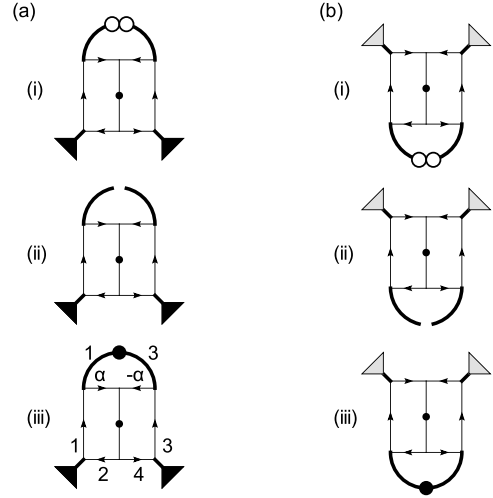

FIG. 14. Category $\mathfrak{D}5$: Diagrams renormalizing Γ_U.

We first consider diagrams that (nominally) renormalize the same-sublattice interaction strength Γ_U, corresponding to operators $\mathcal{O}_U$ and $\bar{\mathcal{O}}_U$ in Table II. We begin with the category $\mathfrak{D}5$ diagrams pictured in Fig. 14. The elements of these diagrams include single copies of the $\mathsf{V}(\mathsf{g})$ and $\mathsf{V}(\mathsf{h})$ vertices and one of each "flavor" of the propagator components P_λ, P_A, and $\mathsf{P}_S + \mathsf{P}_C$. Diagrams $\mathfrak{D}5(\mathsf{a})_i$ and $\mathfrak{D}5(\mathsf{a})_{ii}$ yield pure momentum shell integrations, with the result

$$\mathfrak{D}5(\mathsf{a})_i + \mathfrak{D}5(\mathsf{a})_{ii} = \left[\frac{(\lambda - \lambda_A)2dl}{4\pi}\right]\Gamma_U \mathcal{O}_U. \quad (4.16)$$

$\mathfrak{D}5(\mathsf{a})_{iii}$ involves an undetermined loop frequency; we evaluate this diagram explicitly. Note that in providing the frequency labels for the single fermion lines in $\mathfrak{D}5(\mathsf{a})_{iii}$ (Fig. 14), we have neglected irrelevant small shifts of the loop frequency $\alpha \rightarrow \omega_\alpha$ by the slow mode frequencies $\{1,3\} \rightarrow \{\omega_1, \omega_3\}$, necessary for strict energy conservation. We have

$$\mathfrak{D}5(\mathsf{a})_{iii} = \frac{(2i\xi^a)^2}{2!} \delta_{1+3,2+4} \Gamma_U \int d^d\mathbf{r}\, \delta Q^{a,a}_{S1,2} \delta Q^{a,a}_{S3,4} I_3,$$
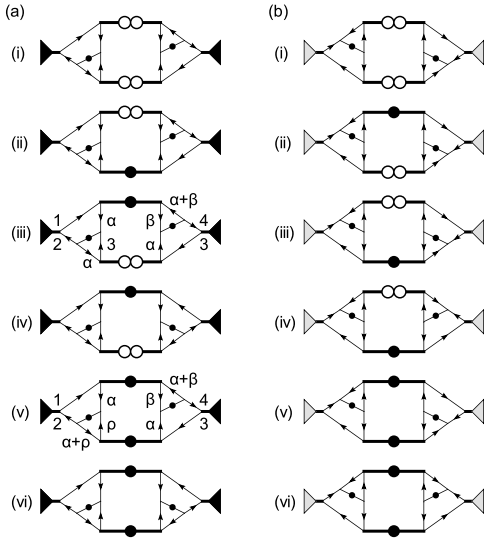
$$(4.17)$$

where the frequency-momentum integral divides into the pieces

$$I_3 \equiv I_{3S} + I_{3C}. \quad (4.18)$$

We calculate I_{3C}; up to irrelevant terms,

$$I_{3C} = \int \frac{d\omega_\alpha d^2\mathbf{k}}{(2\pi)^3} (-s_\alpha^2)\Gamma_c(s_1 + s_\alpha)(s_3 - s_\alpha)[\Delta^{a,a}_{\mathcal{O}}(0, |\omega_\alpha|, \mathbf{k})]^2. \quad (4.19)$$

P_C yields the projection factor $(s_1 + s_\alpha)(s_3 - s_\alpha)$ in Eq. (4.19); this factor gives a nonzero contribution only for $s_1 = -s_3 = s_\alpha$. We therefore obtain

FIG. 15. Category $\mathfrak{D}6$: Diagrams renormalizing Γ_U.

$$I_{3C} = \frac{\Gamma_c(s_1 - s_3)^2}{h^2} \int_{\omega_\alpha > 0} \frac{d\omega_\alpha d^2\mathbf{k}}{(2\pi)^3} [D\mathbf{k}^2 - i\xi^a \omega_\alpha]^{-2}$$

$$= \frac{\Gamma_c(s_1 - s_3)^2}{h^2} J_3(\xi^a) = \frac{\lambda i\xi^a 2dl}{32\pi} \gamma_c(s_1 - s_3)^2, \quad (4.20)$$

where we have used Eqs. (3.21b) and (D5). Evaluating I_{3S} [Eq. (4.18)], in a similar fashion using Eq. (D4), and combining this with Eqs. (4.17) and (4.20), we find the result

$$\mathfrak{D}5(a)_{iii} = \left(\frac{\lambda 2dl}{8\pi}\right)[\gamma_c - \ln(1 - \gamma_s)]\Gamma_U(\mathcal{O}_U - \mathcal{O}_X).$$
$$(4.21)$$

The amplitude in Eq. (4.21) renormalizes the same-sublattice interaction operator $\mathcal{O}_U \leftrightarrow \Gamma_U$ but also generates its "evil twin," $\mathcal{O}_X$, which does not appear in the original theory [Eqs. (3.2) and (3.3)].

The amplitudes for $\mathfrak{D}5(b)_i$–$\mathfrak{D}5(b)_{iii}$ mirror those found in Eqs. (4.16) and (4.21):

$$\mathfrak{D}5(b)_i + \mathfrak{D}5(b)_{ii} = \frac{(\lambda - \lambda_A)2dl}{4\pi}\Gamma_U\bar{\mathcal{O}}_U \qquad (4.22)$$

and

$$\mathfrak{D}5(b)_{iii} = \left(\frac{\lambda 2dl}{8\pi}\right)[\gamma_c - \ln(1 - \gamma_s)]\Gamma_U(\bar{\mathcal{O}}_U - \bar{\mathcal{O}}_X).$$
$$(4.23)$$

We next direct our attention to the large array of diagrams shown in Fig. 15, denoted as category $\mathfrak{D}6$. The diagrams in subcategory $\mathfrak{D}6(a)$ [$\mathfrak{D}6(b)$] pair together two copies of the vertex $V(c)$ [$V(d)$]. Moreover, as suggested by the figure, diagrams $\mathfrak{D}6(a)_m$ and $\mathfrak{D}6(b)_m$, with $m \in \{i, \ldots, vi\}$, give structurally similar results that renormalize same-sublattice [Eqs. (2.53a) and (2.53b)] local operators involving

$\delta Q_{S1,2}^{a,a} \delta Q_{S3,4}^{a,a}$ ($\mathcal{O}_U$ or $\mathcal{O}_X$) and $\delta Q_{S1,2}^{\dagger a,a} \delta Q_{S3,4}^{\dagger a,a}$ ($\bar{\mathcal{O}}_U$ or $\bar{\mathcal{O}}_X$), respectively. We therefore evaluate the subcategories $\mathfrak{D}6(a)$ and $\mathfrak{D}6(b)$ simultaneously.

$\mathfrak{D}6(a)_i$ and $\mathfrak{D}6(b)_i$ each possess a single frequency loop, which may be evaluated using Eq. (D5) giving the result

$$\mathfrak{D}6(a)_i + \mathfrak{D}6(b)_i = \left(\frac{-\lambda 2dl}{8\pi}\right)\left[\begin{array}{l}\Gamma_U(\gamma_s + \gamma_c)(\mathcal{O}_U + \bar{\mathcal{O}}_U) \\ + \Gamma_V(\gamma_s - \gamma_c)(\mathcal{O}_X + \bar{\mathcal{O}}_X)\end{array}\right].$$
$$(4.24)$$

$\mathfrak{D}6(a)_{ii}$ and $\mathfrak{D}6(a)_{iii}$ give identical contributions. We evaluate $\mathfrak{D}6(a)_{iii}$ as an example of a diagram with two frequency loop integrations over $\alpha \to \omega_\alpha$ and $\beta \to \omega_\beta$. Using the Feynman rules, we have

$$\mathfrak{D}6(a)_{iii} = \frac{(2i\xi^a)^3}{2!}\delta_{1+3,2+4}\int d^d\mathbf{r}\,\delta Q_{S1,2}^{a,a}\delta Q_{S3,4}^{a,a}I_4,$$
$$(4.25)$$

where the frequency-momentum integral again separates into

$$I_4 \equiv I_{4S} + I_{4C}, \qquad (4.26)$$

corresponding to the P_S and P_C components of the interaction sector propagator in $\mathfrak{D}6(a)_{iii}$ (Fig. 15). We first compute I_{4S}; up to irrelevant terms, one finds

$$I_{4S} = \int \frac{d\omega_\alpha d\omega_\beta d^2\mathbf{k}}{(2\pi)^4}\Gamma_s(s_1 - s_\alpha)(s_{\alpha+\beta} - s_\beta)s_\alpha^2(\Gamma_U s_3 - \Gamma_V s_\alpha)$$
$$\times (\Gamma_U s_\beta - \Gamma_V s_{\alpha+\beta})[\Delta_{\mathcal{O}}^{a,a}(0,|\omega_\alpha|,\mathbf{k})]^2\Delta_S^a(|\omega_\alpha|,\mathbf{k}). \quad (4.27)$$

Although this expression entails two frequency loop integrations, the propagator kernels $\Delta_{\mathcal{O}}$ and Δ_S in Eq. (4.27) depend exclusively on a single frequency variable, ω_α. The integral over ω_β yields only a kinematical factor of $|\omega_\alpha|$: the projector $s_{\alpha+\beta} - s_\beta$ in Eq. (4.27) gives a nonzero contribution as a function of ω_β only over a frequency segment of length $|\omega_\alpha|$; over this range, $\Gamma_U s_\beta - \Gamma_V s_{\alpha+\beta} = s_\beta 2\Gamma_s$. The factor $s_1 - s_\alpha$ limits the range of the ω_α integration to the half-line (as usual); one obtains

$$I_{4S} = \frac{-4\Gamma_s^2}{\pi h^3}(\Gamma_U s_1 s_3 + \Gamma_V)\int_{\omega_\alpha > 0} \frac{d\omega_\alpha d^2\mathbf{k}}{(2\pi)^3}\omega_\alpha$$
$$\times [D\mathbf{k}^2 - i\xi^a\omega_\alpha]^{-2}[D\mathbf{k}^2 - i(1 - \gamma_s)\xi^a\omega_\alpha]^{-1}.$$
$$(4.28)$$

We use Eq. (D6) to evaluate the integral, and we find the result

$$I_{4S} = \frac{-4\Gamma_s^2}{\pi h^3}(\Gamma_U s_1 s_3 + \Gamma_V)J_4(\xi^a; (1 - \gamma_s)\xi^a)$$
$$= \frac{-\lambda 2dl}{32\pi}(\Gamma_U s_1 s_3 + \Gamma_V)[\gamma_s + \ln(1 - \gamma_s)]. \quad (4.29)$$

What we have found here is well known (see, e.g., Ref. 41) from other Finkel'stein NLσMs: in a one-loop calculation, a given diagram may involve $n = \{0, 1, 2, \ldots\}$ undetermined frequency loops; however, for $n \geq 2$, $n-1$ of the associated frequency integrations typically give simple kinematical fac-

tors, and the final diagrammatic amplitude can almost always be expressed in terms of an integration over a single loop frequency and a single loop momentum, as in Eq. (4.28) (but see the evaluation of $\mathfrak{D}9(\mathsf{b})_i$ [Eq. (4.45)] and $\mathfrak{D}13$ [Eq. (4.51)]).

We can try to evaluate $I_{4\mathsf{C}}$ in a similar fashion, but the associated amplitude goes like $\lambda\Gamma_c^2[1+O(\Gamma_c)]$. In our one-loop results [Eqs. (4.57a)-(4.57e), (5.3a)-(5.3e)], we keep only terms to second homogeneous order in λ and Γ_c in the flow equations for the interaction constants γ_s and γ_c; therefore, we neglect the contribution of $I_{4\mathsf{C}}$.

By combining Eqs. (4.25) and (4.29) and accounting for the identical contribution from $\mathfrak{D}6(\mathsf{a})_{ii}$, we have

$$\mathfrak{D}6(\mathsf{a})_{ii}+\mathfrak{D}6(\mathsf{a})_{iii}=\left(\frac{\lambda 2dl}{4\pi}\right)[\gamma_s+\ln(1-\gamma_s)](\Gamma_U\mathcal{O}_U+\Gamma_V\mathcal{O}_X)$$

$$(4.30)$$

and, similarly,

$$\mathfrak{D}6(\mathsf{b})_{ii}+\mathfrak{D}6(\mathsf{b})_{iii}=\left(\frac{\lambda 2dl}{4\pi}\right)[\gamma_s+\ln(1-\gamma_s)](\Gamma_U\bar{\mathcal{O}}_U+\Gamma_V\bar{\mathcal{O}}_X).$$

$$(4.31)$$

Diagrams $\mathfrak{D}6(\mathsf{a})_{iv}$ and $\mathfrak{D}6(\mathsf{b})_{iv}$ each contain two frequency loops; the result obtained is

$$\mathfrak{D}6(\mathsf{a})_{iv}+\mathfrak{D}6(\mathsf{b})_{iv}=\left(\frac{-\lambda 2dl}{8\pi}\right)\left\{\Gamma_s[\gamma_s+\ln(1-\gamma_s)]-\Gamma_c\frac{\gamma_s^2}{2}\right\}$$

$$\times(\mathcal{O}_U-\mathcal{O}_X+\bar{\mathcal{O}}_U-\bar{\mathcal{O}}_X).\qquad(4.32)$$

$\mathfrak{D}6(\mathsf{a})_v$ and $\mathfrak{D}6(\mathsf{a})_{vi}$ provide examples of the most complicated type of diagram that appears to one loop, involving three loop frequencies each. The computation nonetheless proceeds similar to the above, and one finds that

$$\mathfrak{D}6(\mathsf{a})_v+\mathfrak{D}6(\mathsf{b})_v=\left(\frac{-\lambda 2dl}{8\pi}\right)\Gamma_s\left[\gamma_s\left(\frac{2-\gamma_s}{1-\gamma_s}\right)+2\ln(1-\gamma_s)\right]$$

$$\times(\mathcal{O}_U+\mathcal{O}_X+\bar{\mathcal{O}}_U+\bar{\mathcal{O}}_X).\qquad(4.33)$$

Finally, we give the result for the last two diagrams in Fig. 15,

$$\mathfrak{D}6(\mathsf{a})_{vi}+\mathfrak{D}6(\mathsf{b})_{vi}=\left(\frac{\lambda 2dl}{8\pi}\right)\left\{\Gamma_s\left[\gamma_s\left(\frac{2-\gamma_s}{1-\gamma_s}\right)+2\ln(1-\gamma_s)\right]\right.$$

$$-\Gamma_c\left[\ln(1-\gamma_s)+\gamma_s+\frac{\gamma_s^2}{2}\right]\right\}$$

$$\times(\mathcal{O}_U-\mathcal{O}_X+\bar{\mathcal{O}}_U-\bar{\mathcal{O}}_X).\qquad(4.34)$$

We denote the sum of the amplitudes in each of the diagram categories evaluated above using the category symbols $\mathfrak{D}5$ and $\mathfrak{D}6$. We express our results in terms of the interaction parameters Γ_s and Γ_c, defined via Eq. (2.54), as well as the relative versions γ_s and γ_c, introduced in Eqs. (3.21a) and (3.21b). We drop terms higher than first order in Γ_c (or γ_c).
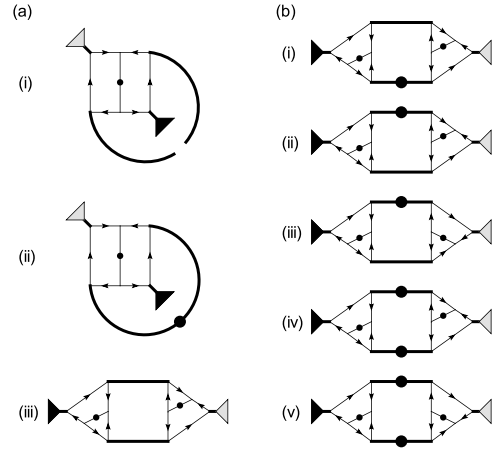

FIG. 16. Category $\mathfrak{D}7$: Diagrams renormalizing Γ_V.

By summing results from Eqs. (4.16), (4.21)–(4.24), and (4.30)–(4.34), a large number of nontrivial cancellations occur, and we find the results

$$\mathfrak{D}5+\mathfrak{D}6=\left(\frac{-2dl}{8\pi}\right)[2(\lambda_A-\lambda)(\Gamma_s+\Gamma_c)](\mathcal{O}_U+\bar{\mathcal{O}}_U)$$

$$+\left(\frac{-2dl}{8\pi}\right)\left[\frac{2\lambda\Gamma_s\gamma_s}{1-\gamma_s}\right](\mathcal{O}_X+\bar{\mathcal{O}}_X).\qquad(4.35)$$

The diagrams in category $\mathfrak{D}7$ (Fig. 16) nominally renormalize the intersublattice interaction strength Γ_V, corresponding to the operator $\mathcal{O}_V$ in Table II. The computation of these graphs closely parallels the results we have obtained above in Eq. (4.35). By summing the diagrams in category $\mathfrak{D}7$, we obtain

$$\mathfrak{D}7=\left(\frac{-2dl}{8\pi}\right)[-2\lambda_A(\Gamma_s-\Gamma_c)]\mathcal{O}_V+\left(\frac{-2dl}{8\pi}\right)\left[\frac{2\lambda\Gamma_s\gamma_s}{1-\gamma_s}\right]\mathcal{O}_Y.$$

$$(4.36)$$

In the partial results given by these equations, observe the almost complete cancellation of all "junk" terms involving the operators $\mathcal{O}_X$, $\bar{\mathcal{O}}_X$, and $\mathcal{O}_Y$, not present in the original FNLσM action [Eqs. (3.2) and (3.3)]. In fact, the remaining terms proportional to $\mathcal{O}_X+\bar{\mathcal{O}}_X$ and $\mathcal{O}_Y$ in Eqs. (4.35) and (4.36), respectively, exactly cancel up to terms fourth order in the slow mode fluctuations $\delta\hat{Q}_\mathsf{S}$ and $\delta\hat{Q}_\mathsf{S}^\dagger$. To see this, we use Eqs. (3.5) and (3.6) to write

$$\delta\hat{Q}_\mathsf{S}+\delta\hat{Q}_\mathsf{S}^\dagger=-\delta\hat{Q}_\mathsf{S}\delta\hat{Q}_\mathsf{S}^\dagger.\qquad(4.37)$$

Repeated applications of Eq. (4.37) prove the identification

$$\mathcal{O}_Y=-(\mathcal{O}_X+\bar{\mathcal{O}}_X)+(\delta\hat{Q}_\mathsf{S}\delta\hat{Q}_\mathsf{S}^\dagger)^2.\qquad(4.38)$$

Thus, to our working order in the slow mode fields, the FNLσM appears (so far) to be renormalizable.[62] We must complete the one-loop calculation to verify this.

6. (Further) renormalization of Γ_s and Γ_c

The interaction sector renormalizations described by the remaining diagrams in Figs. 17–22 are most compactly
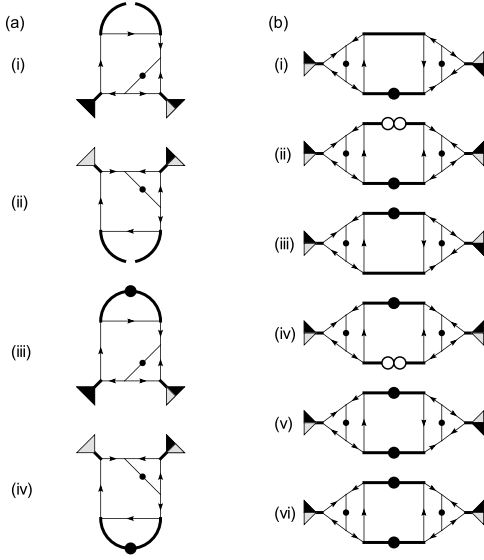
FIG. 17. Category $\mathfrak{D}8$: Diagrams renormalizing Γ_s and Γ_c.

stated in terms of corrections to the linear combinations Γ_s and Γ_c [Eq. (2.54)], which couple to the slow mode operators

$$\mathcal{O}_s \equiv \mathcal{O}_U + \bar{\mathcal{O}}_U + \mathcal{O}_V$$

$$\mathcal{O}_c \equiv \mathcal{O}_U + \bar{\mathcal{O}}_U - \mathcal{O}_V, \qquad (4.39)$$

respectively [Eq. (3.14)].

Category $\mathfrak{D}8$ diagrams are shown in Fig. 17. The diagrams in subcategory $\mathfrak{D}8(\mathsf{a})$ involve vertices $\mathsf{V}(\mathsf{j})$ and $\mathsf{V}(\mathsf{k})$, with propagator components P_A and $\mathsf{P}_\mathsf{S}+\mathsf{P}_\mathsf{C}$. The sum of these four graphs gives

$$\mathfrak{D}8(\mathsf{a}) = \left(\frac{-2dl}{8\pi} \right) \{2\lambda_A + 2\lambda[\gamma_c + \ln(1 - \gamma_s)]\}(\Gamma_s\mathcal{O}_s + \Gamma_c\mathcal{O}_c).$$

$$(4.40)$$

The diagrams in subcategory $\mathfrak{D}8(\mathsf{b})$ each pair together two copies of the vertex $\mathsf{V}(\mathsf{e})$, with various combinations of the propagator components P_λ and $\mathsf{P}_\mathsf{S}+\mathsf{P}_\mathsf{C}$. Graphs $\mathfrak{D}8(\mathsf{b})_\mathsf{i}$–$\mathfrak{D}8(\mathsf{b})_\mathsf{vi}$ each encompass two frequency loops, and their evaluation proceeds along the lines of $\mathfrak{D}6(\mathsf{a})_\mathsf{iii}$ [Eqs. (4.25)–(4.30)]. Diagrams $\mathfrak{D}8(\mathsf{b})_\mathsf{v}$ and $\mathfrak{D}8(\mathsf{b})_\mathsf{vi}$ precisely cancel. The sum of all six graphs in $\mathfrak{D}8(\mathsf{b})$ gives

$$\mathfrak{D}8(\mathsf{b}) = \left(\frac{\lambda 2dl}{8\pi} \right)(2\Gamma_c\gamma_s^2)\mathcal{O}_s. \qquad (4.41)$$

The eight diagrams in category $\mathfrak{D}9$ (pictured in Fig. 18) represent only two discernible amplitudes. These diagrams also involve two copies of the vertex $\mathsf{V}(\mathsf{e})$, with the λ_A propagator component P_A in combination with P_λ or $\mathsf{P}_\mathsf{S}+\mathsf{P}_\mathsf{C}$. The four graphs in subcategory $\mathfrak{D}9(\mathsf{a})$ each give identical contributions, with the sum

$$\mathfrak{D}9(\mathsf{a}) = \left(\frac{\lambda_A 2dl}{8\pi} \right)\Gamma_s\gamma_s\mathcal{O}_s. \qquad (4.42)$$
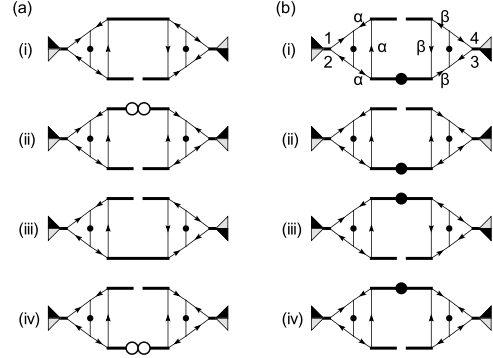
FIG. 18. Category $\mathfrak{D}9$: Diagrams renormalizing $\Gamma_s = \frac{\Gamma_U + \Gamma_V}{2}$.

Likewise, each of the four diagrams in subcategory $\mathfrak{D}9(\mathsf{b})$ gives the same amplitude. Each of these graphs involves two undetermined frequency loops. We explicitly evaluate $\mathfrak{D}9(\mathsf{b})_\mathsf{i}$ because the structure of the two frequency loop integration is quite different from that of Eq. (4.27), studied in the previous subsection. By using the Feynman rules, we write
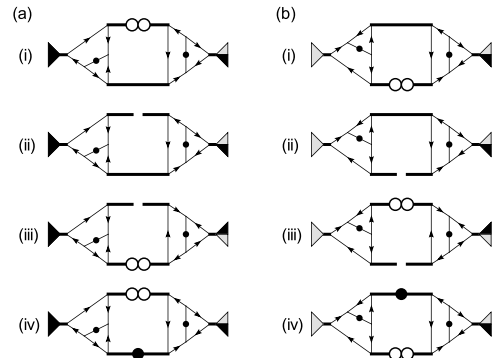
$$\mathfrak{D}9(\mathsf{b})_\mathsf{i} = \frac{2(i\xi^a)^3}{2!}\left(\frac{-\lambda_A\Gamma_s^2}{\lambda^2} \right)\delta_{1+3,2+4} \int d^d\mathbf{r}[(s_1\delta Q_{\mathsf{S}1,2}^{a,a}$$
$$+ s_2\delta Q_{\mathsf{S}1,2}^{\dagger a,a})(s_3\delta Q_{\mathsf{S}3,4}^{a,a} + s_4\delta Q_{\mathsf{S}3,4}^{\dagger a,a})]I_5. \qquad (4.43)$$

In this equation, note that both of the two $\mathsf{V}(\mathsf{e})$ vertices contribute only the portions of the associated vertex amplitudes (Table I) proportional to Γ_s; all other terms vanish. The integral I_5 separates into parts:

$$I_5 \equiv I_{5\mathsf{S}} + I_{5\mathsf{C}}, \qquad (4.44)$$

corresponding to interacting propagator components P_S and P_S, respectively. From the figure and given the structure of P_S [Eq. (3.18c)], it can be seen that $I_{5\mathsf{S}}=0$. On the other hand, $I_{5\mathsf{C}}$ may be written as

$$I_{5\mathsf{C}} = \int \frac{d\omega_\alpha d\omega_\beta d^2\mathbf{k}}{(2\pi)^4}\Gamma_c(2s_\alpha)^2(2s_\beta)^2\mathbf{k}^2[\Delta_{\mathcal{O}}^{a,a}(|\omega_\alpha|,|\omega_\alpha|,\mathbf{k})$$
$$\times\Delta_{\mathcal{O}}^{a,a}(|\omega_\beta|,|\omega_\beta|,\mathbf{k})]^2. \qquad (4.45)$$

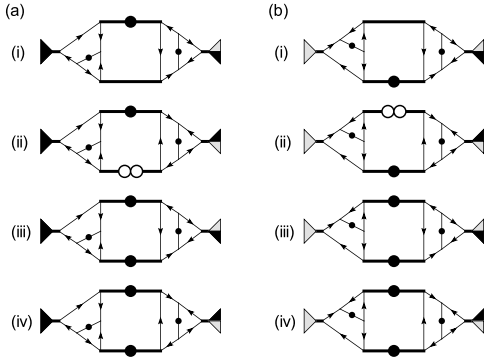FIG. 19. Category $\mathfrak{D}10$: Diagrams renormalizing $\Gamma_s = \frac{\Gamma_U + \Gamma_V}{2}$.

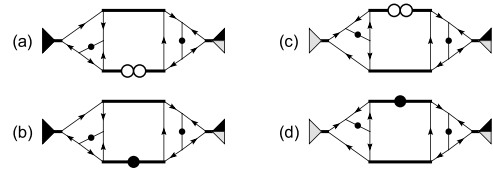FIG. 20. Category $\mathfrak{D}11$: Diagrams renormalizing $\Gamma_s = \frac{\Gamma_U + \Gamma_V}{2}$.

FIG. 21. Category $\mathfrak{D}12$: Additional nonzero diagrams, which cancel in pairs. Contributions from individual diagrams correspond to the generation of local operators not present in the original model.

Distinct from the two frequency loop integration previously evaluated [Eq. (4.27)], the propagator kernels $\Delta_{\mathcal{O}}$ in Eq. (4.45) depend on *either* of the two loop frequencies ω_α or ω_β. Equation (4.45) should be understood as an integration over the full frequency-momentum shell, [Eqs. (3.11a)-(3.11c)], pictured in Fig. 6, in the space $(|\omega_\alpha|, |\omega_\beta|, Dk^2)$. It may be evaluated using Eq. (D7):

$$I_{5C} = \frac{2^6 \Gamma_c}{h^4} J_5(2\xi^a) = \frac{-\lambda^2 2dl}{\pi(\pi h)^2}\Gamma_c. \qquad (4.46)$$

By summing identical contributions from all four diagrams in $\mathfrak{D}9(\mathsf{b})$, we obtain

$$\mathfrak{D}9(\mathsf{b}) = \left(\frac{-\lambda_A 2dl}{8\pi}\right)(2\Gamma_c\gamma_s^2)\mathcal{O}_s. \qquad (4.47)$$

The eight category $\mathfrak{D}10$ diagrams depicted in Fig. 19 pair $\mathsf{V}(\mathsf{e})$ with the other "triangular" interaction vertices, $\mathsf{V}(\mathsf{c})$ and $\mathsf{V}(\mathsf{d})$. The evaluation of these graphs proceeds as in Sec. IV A 5; we give only the result for the entire category:

$$\mathfrak{D}10 = \left(\frac{-2dl}{8\pi}\right)\Gamma_s\{\lambda[2\gamma_c - 2\ln(1-\gamma_s)] - 4\lambda_A\gamma_c\}\mathcal{O}_s. \qquad (4.48)$$

Categories $\mathfrak{D}11$ and $\mathfrak{D}12$ appear in Figs. 20 and 21, respectively. The diagrams in these categories share the same structural elements as those in $\mathfrak{D}10$, but there is no net contribution to the RG from either $\mathfrak{D}11$ or $\mathfrak{D}12$. The graphs in Fig. 20 cancel pairwise:

$$\mathfrak{D}11(\mathsf{a})_i + \mathfrak{D}11(\mathsf{a})_{ii} = \mathfrak{D}11(\mathsf{a})_{iii} + \mathfrak{D}11(\mathsf{a})_{iv}$$
$$= \mathfrak{D}11(\mathsf{b})_i + \mathfrak{D}11(\mathsf{b})_{ii} = \mathfrak{D}11(\mathsf{b})_{iii}$$
$$+ \mathfrak{D}11(\mathsf{b})_{iv} = 0. \qquad (4.49)$$

The individual diagrams in category $\mathfrak{D}12$ correspond to the generation of new operators, not present in the original FNLσM action [Eqs. (3.2) and (3.3)]. Fortunately, their sum gives zero [up to terms $O(\delta\hat{Q}_\mathsf{S}^3)$, the cancellation of which we have not checked in detail].

Finally, we evaluate the single diagram in $\mathfrak{D}13$ (Fig. 22). In this figure, two copies of the vertex $\mathsf{V}(\mathsf{f})$ are connected by a single, basic diffuson propagator P_λ. $\mathfrak{D}13$ is unique among the graphs presented in this paper in that it involves a pure frequency loop integration since the momentum carried by P_λ between the slow mode fields at the vertices is necessarily slow. We will see that $\mathfrak{D}13$ drives the CDW instability in the clean limit, $\lambda, \lambda_A \rightarrow 0$. Such a contribution appears naturally in the frequency-momentum shell RG but not in a pure momentum shell scheme.[2,3,57,58] Using the Feynman rules, we write

$$\mathfrak{D}13 = \frac{(2\xi^a)^2}{2!}\delta_{1+3,2+4}\Gamma_c^2 \int d^d\mathbf{r}[(s_1\delta Q_{\mathsf{S}1,2}^{a,a} - s_2\delta Q_{\mathsf{S}1,2}^{\dagger a,a})$$
$$\times(s_3\delta Q_{\mathsf{S}3,4}^{a,a} - s_4\delta Q_{\mathsf{S}3,4}^{\dagger a,a})]I_6. \qquad (4.50)$$

In writing the amplitude for $\mathfrak{D}13$ [Eq. (4.50)], we have exactly the *opposite* of the situation we had with $\mathfrak{D}9(\mathsf{b})i$ [Eq. (4.43)]: both of the two $\mathsf{V}(\mathsf{f})$ vertices in Eq. (4.50) contribute only the portions of the associated vertex amplitudes (Table I) proportional to Γ_c; all other terms vanish. The pure frequency integral I_6 may be evaluated as

$$I_6 = \int \frac{d\omega_\alpha}{2\pi}(2s_\alpha)^2 \Delta_{\mathcal{O}}^{a,a}(|\omega_\alpha|, |\omega_\alpha|, \mathbf{q})$$
$$= \frac{4}{\pi h}\int_{\tilde{\Lambda}}^{\Lambda} d\omega_\alpha[D\mathbf{q}^2 - 2i\xi^a\omega_\alpha]^{-1} \approx \frac{4i\xi^a}{2\pi h}2dl. \qquad (4.51)$$

By combining Eqs. (4.50) and (4.51), we obtain the result

$$\mathfrak{D}13 = \Gamma_c\gamma_c 2dl\mathcal{O}_c. \qquad (4.52)$$

This expression is second order in Γ_c but *zeroth* order in the disorder strength λ.

B. Dimensional analysis

We obtain the flow equations for the FNLσM parameters in the usual way, by re-exponentiating the diagrammatic corrections derived in the previous subsection and subtracting them from the pure slow mode action S_S [Eq. (3.14)] and by rescaling position $\mathbf{r}$ and time t via
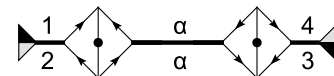
$$\mathbf{r} \rightarrow b\mathbf{r}, \qquad (4.53a)$$

FIG. 22. Category $\mathfrak{D}13$: Diagram renormalizing $\Gamma_c = \frac{\Gamma_U - \Gamma_V}{2}$.

$$t \to b^z t, \qquad (4.53b)$$

where $b \approx 1 + dl$ is the change in length scale, and z is the (so far undetermined, possibly scale-dependent) dynamic critical exponent. Equivalently, Eqs. (4.53a) and (4.53b) imply that momentum **k** and frequency ω carry the engineering dimensions

$$[\mathbf{k}] = 1, \qquad (4.54a)$$

$$[\omega] = z, \qquad (4.54b)$$

both stated in inverse length units. A similar analysis of the FNLσM action, Eqs. (2.49) and (2.50) [or (3.2) and (3.3)], gives the engineering dimensions of the field matrix elements:

$$[Q^{a,a'}_{\omega,\omega'}(\mathbf{r})] = -z, \quad [Q^{a,a'}_{t,t'}(\mathbf{r})] = z, \qquad (4.55)$$

and of the model coupling constants,

$$[\lambda] = [\lambda_A] = 2 - d, \qquad (4.56a)$$

$$[h] = [\Gamma_s] = [\Gamma_c] = d - z, \qquad (4.56b)$$

and

$$[\gamma_s] = [\gamma_c] = 0, \qquad (4.56c)$$

where Γ_s and Γ_c (γ_s and γ_c) were defined in Eq. (2.54) [Eqs. (3.21a) and (3.21b)].

By combining the above dimensional analysis with the diagrammatic results [Eqs. (4.4), (4.9)–(4.12), (4.35), (4.36), (4.40)–(4.42), (4.47), (4.48), and (4.52)], we obtain the one-loop RG equations

$$\frac{d\lambda}{dl} = -\epsilon\lambda - \frac{\lambda^2}{4\pi}\gamma_c + \frac{2\lambda^2}{4\pi}\left[1 + \frac{1-\gamma_s}{\gamma_s}\ln(1-\gamma_s)\right]$$
$$+ \mathbf{O}(\lambda^2\gamma_c^2, \lambda^3), \qquad (4.57a)$$

$$\frac{d\lambda_A}{dl} = \epsilon\lambda_A + \frac{\lambda^2}{4\pi} + 2\frac{\lambda_A}{\lambda}\frac{d\lambda}{dl} + \mathbf{O}(\lambda^3), \qquad (4.57b)$$

$$\frac{d\Gamma_s}{dl} = (d-z)\Gamma_s + \frac{1}{4\pi}(2\lambda_A - \lambda)(\Gamma_s + \Gamma_c) + \frac{1}{4\pi}[2(\lambda - \lambda_A)$$
$$\times (2 - \gamma_s)\Gamma_s\gamma_c - \lambda_A\Gamma_s\gamma_s]$$
$$+ \mathbf{O}(\lambda\Gamma_c\gamma_c, \lambda_A\Gamma_c\gamma_c, \lambda^2\Gamma_{s/c}, \lambda\lambda_A\Gamma_{s/c}), \qquad (4.57c)$$

$$\frac{d\Gamma_c}{dl} = (d-z)\Gamma_c + \frac{1}{4\pi}(2\lambda_A - \lambda)(\Gamma_s + \Gamma_c)$$
$$+ \frac{1}{4\pi}[2\lambda\Gamma_c\ln(1-\gamma_s)] - 2\Gamma_c\gamma_c$$
$$+ \mathbf{O}(\lambda\Gamma_c\gamma_c, \lambda_A\Gamma_c\gamma_c, \lambda^2\Gamma_{s/c}, \lambda\lambda_A\Gamma_{s/c}), \quad (4.57d)$$

$$\frac{d\ln h}{dl} = (d-z) + \frac{1}{4\pi}[\lambda_A + \lambda(\gamma_c - \gamma_s)] + \mathbf{O}(\lambda\gamma_c^2, \lambda^2, \lambda\lambda_A).$$
$$(4.57e)$$

In Eqs. (4.57a) and (4.57b), we have set $d = 2 + \epsilon$ explicitly.

The flow equations (4.57a)-(4.57e) are given to the lowest nontrivial orders in both the dimensionless dc resistance parameter λ and the CDW interaction strength Γ_c (or γ_c). Specifically, we retain terms in Eq. (4.57a)-(4.57c) and (4.57e) only to first order in Γ_c, i.e., terms $\mathbf{O}(\lambda^2\gamma_c)$ [Eq. (4.57a)] and terms $\mathbf{O}(\lambda\Gamma_c, \lambda_A\Gamma_c)$ [Eqs. (4.57c) and (4.57e)]. In principle, since we make no assumption about the smallness of λ_A, we should retain terms $\mathbf{O}(\lambda_A^n\Gamma_c)$, with $n \in \{1,2,3\ldots\}$, but only $n=1$ appears in the RG equations. The second order pure CDW self-interaction, $(-2\Gamma_c\gamma_c)$ in Eq. (4.57d), is the sole exception to the rule; this term is tied to the ballistic Fermi liquid physics in the presence of sublattice symmetry (and therefore nesting) and must be retained in the weakly disordered limit. We have checked by numerical integration that all of the results presented in Sec. V, including the identification of a disorder-driven, interaction-mediated instability of the diffusive Fermi liquid phase in $d = 2 + \epsilon$ dimensions, are unmodified (within the perturbatively accessible coupling strength regime) by the inclusion of higher order terms in Γ_c.

By using Eq. (4.14), one may also obtain a flow equation governing the scaling behavior of the disorder-averaged DOS $\nu(\omega)$. In the (Keldysh) sigma model formalism, Eqs. (4.13) and (4.55) imply that the DOS carries zero engineering dimension, so that Eq. (4.14) implies the flow equation

$$\frac{d\ln\nu}{dl} = -\frac{1}{4\pi}[\lambda_A + \lambda\ln(1-\gamma_s) + \lambda\gamma_c]. \qquad (4.58)$$

V. RESULTS AND DISCUSSION

In this section, we summarize and interpret the results of the RG calculation, set up in Sec. III and performed in Sec. IV, for the FNLσM originally defined by Eqs. (2.48)–(2.50), in Sec. II. The FNLσM action given by Eqs. (2.49) and (2.50) is parametrized by five coupling constants: λ, proportional to the dimensionless dc resistance of the system; λ_A, which gives a second measure of the hopping disorder (associated with quenched orientational fluctuations of bond strength dimerization, as discussed in Secs. II A 3 and II A 4); h, which tracks the relative scaling of length and time in the theory; Γ_U and Γ_V, which characterize the strengths of generic short-ranged same-sublattice and inter-sublattice interparticle interactions, respectively, in the coarse-grained FNLσM description. Alternatively, we have introduced the interaction parameters Γ_s and Γ_c [the sum and difference of Γ_U and Γ_V, see Eq. (2.54)], which couple to the square of the smooth and of the sublattice staggered local charge densities, respectively. As discussed below Eq. (2.54), a staggered interaction $\Gamma_c < 0$ is expected to promote the CDW instability in the clean limit [i.e., we identify $\Gamma_c \sim W_c$, with W_c defined by Eq. (1.8) for the Hubbard-like model given by Eq. (1.1)]. The RG calculation has been performed with the aid of an epsilon expansion in $d = 2 + \epsilon$ spatial dimensions, with $0 \leq \epsilon \leq 1$.

The one-loop RG flow equations for the coupling strengths λ, λ_A, Γ_s, Γ_c, and h were obtained at the end of the previous section, in Eqs. (4.57a)-(4.57e). We restate them below in a slightly more streamlined form. We will need the

"relative interaction parameters" γ_s and γ_c, defined in Eqs. (3.21a) and (3.21b), repeated here for convenience:

$$\gamma_s \equiv \frac{4}{\pi h} \Gamma_s = \frac{2}{\pi h}(\Gamma_U + \Gamma_V), \qquad (5.1a)$$

$$\gamma_c \equiv \frac{4}{\pi h} \Gamma_c = \frac{2}{\pi h}(\Gamma_U - \Gamma_V). \qquad (5.1b)$$

Next, we perform a trivial rescaling of the coupling constants appearing in Eqs. (2.49), (4.57a)-(4.57e),

$$\lambda \rightarrow 4\pi\lambda, \quad \lambda_A \rightarrow 4\pi\lambda_A, \qquad (5.2)$$

after which the one-loop RG flow equations for the couplings λ, λ_A, γ_s, γ_c, and h take the following form in $d=2+\epsilon$ dimensions:

$$\frac{d\lambda}{dl} = -\epsilon\lambda - \lambda^2\gamma_c + 2\lambda^2\left[1 + \frac{1-\gamma_s}{\gamma_s}\ln(1-\gamma_s)\right], \qquad (5.3a)$$

$$\frac{d\lambda_A}{dl} = \epsilon\lambda_A + \lambda^2 + 2\frac{\lambda_A}{\lambda}\frac{d\lambda}{dl}, \qquad (5.3b)$$

$$\frac{d\gamma_s}{dl} = \lambda_A(1-\gamma_s)(\gamma_s + 2\gamma_c - 2\gamma_s\gamma_c)$$
$$- \lambda(1-\gamma_s)(\gamma_s + \gamma_c - 2\gamma_s\gamma_c), \qquad (5.3c)$$

$$\frac{d\gamma_c}{dl} = \lambda_A(\gamma_c + 2\gamma_s) - \lambda(\gamma_s + \gamma_c)$$
$$+ \lambda[2\gamma_c\ln(1-\gamma_s) + \gamma_s\gamma_c] - 2\gamma_c^2, \qquad (5.3d)$$

$$\frac{d\ln h}{dl} = (d-z) + \lambda_A + \lambda(\gamma_c - \gamma_s), \qquad (5.3e)$$

where l is the logarithm of the spatial length scale. The parameter z in Eq. (5.3e) is the (as yet undetermined, possibly scale-dependent) "dynamic critical exponent."[63] We have also calculated the scale dependence of the disorder-averaged, single-particle DOS $\nu(\omega)$. By implementing the rescaling of Eq. (5.2) in Eq. (4.58), the one-loop flow equation for ν is

$$\frac{d\ln\nu}{dl} = -[\lambda_A + \lambda\ln(1-\gamma_s) + \lambda\gamma_c]. \qquad (5.4)$$

Flow equations (5.3a)-(5.3e) and (5.4) are given to the lowest nontrivial order in the parameters λ and γ_c but contain contributions from λ_A and γ_s to *all* orders. This is an advantage of the Finkel'stein NLσM formulation, which provides[3] a loop expansion that is controlled perturbatively by the (small) dimensionless resistance λ, but which does not require the coupling strengths λ_A or γ_s to be small. We will discuss the physics that emerges from an analysis of our results [Eqs. (5.3a)-(5.3e)] in turn for $d=2$ and $d>2$ dimensions.

A. Structure of the one-loop flow equations

To gain an understanding of the competing mechanisms driving the RG flow, we isolate the effects of the various terms in Eqs. (5.3a)-(5.4). Fortunately, the most important structures in these equations either occur generically in the perturbative description of interacting, diffusive Fermi liquids[2,3,59–61] or can be tied specifically to the special SLS [Eq. (1.2)] and its effects on the well-understood limits of (i) disorder with vanishing interparticle interactions[9,12,13] and (ii) interactions with vanishing disorder.[23,24]

1. Noninteracting limit

We first consider the noninteracting limit. In $d=2$ spatial dimensions, the FNLσM [Eqs. (2.48)–(2.50)] with $\Gamma_U = \Gamma_V = 0$ ($\gamma_s = \gamma_c = 0$) and nonzero-disorder couplings λ and λ_A describes an unusual low-dimensional delocalized state,[9,12,13] analogous in many ways to the type of critical state[40,64,65] that occurs at a continuous, *three-dimensional* (Anderson) MIT of noninteracting diffusive electrons in the *absence* of SLS. At such an ordinary Anderson transition, the single-particle wave functions at the Fermi energy are extended, and thus capable of transporting charge, heat, etc., across the system, but these states are also very far from the plane waves of a clean Fermi gas and exhibit so-called multifractal scaling[64,65] (due to the presence of the disorder). In $d=2$, the extended single-particle wave functions reside only at the band center (energy $\omega=0$) for arbitrarily weak disorder [i.e., wave functions *are* exponentially localized, with a localization length that diverges upon approaching the band center $(\omega\rightarrow0)$],[9,12] so that the critical state appears only at half-filling [a necessary but not sufficient condition for SLS, Eq. (1.2)]. The critical state at the band center ($\omega=0$) described above characterizes the 2D noninteracting random hopping model defined by the Hamiltonian in Eqs. (1.1) and (1.9), with $U=V=0$.[9,12,13] This delocalized state turns into a somewhat more conventional metallic one in $d>2$, but it is still distinguished by SLS (and broken TRI). (See also the discussion in the Introduction, Sec. I B, especially Figs. 3 and 4.)

These conclusions follow from the fact that a variety of aspects of the class AIII non-interacting sigma model, argued in Sec. II and in Refs. 9, 12, and 13 to capture the low-energy physics of the sublattice symmetric random hopping model lacking TRI, can be solved[13] exactly in $d=2$ using conformal field theory techniques. In particular, in the absence of interactions, it is possible[13] to obtain the *exact* renormalization group equations (to all orders in λ and λ_A) in two dimensions for the disorder-only sector sigma model parameters λ and λ_A and for the average density of states ν in a particular RG scheme. These are of the following forms:[66]

$$\frac{d\lambda}{dl} = 0, \qquad (5.5a)$$

$$\frac{d\lambda_A}{dl} = f_1(\lambda) + 2\frac{\lambda_A}{\lambda}\frac{d\lambda}{dl}, \qquad (5.5b)$$

$$= f_1(\lambda)$$

$$\frac{d \ln \nu}{dl} = -\lambda_A f_2(\lambda) - f_3(\lambda), \tag{5.5c}$$

with $f_i(\lambda)$, $i \in \{1,2,3\}$, real analytic (RG-scheme-dependent) functions of λ. By using the results of our perturbative analysis [Eqs. (5.3a), (5.3b), and (5.4)] and setting $\epsilon = 0$, we find agreement with Eqs (5.5a), (5.5b), and (5.5c), obtaining the lowest order terms in the expansions

$$f_1(\lambda) = \lambda^2 + \boldsymbol{O}(\lambda^3), \tag{5.6a}$$

$$f_2(\lambda) = 1 + \boldsymbol{O}(\lambda), \tag{5.6b}$$

$$f_3(\lambda) = 0 + \boldsymbol{O}(\lambda^2). \tag{5.6c}$$

The lowest order (one-loop) results in Eqs. (5.5a)-(5.6c), are universal and were originally obtained via perturbative methods by Gade and Wegner in Ref. 9. Equation (5.5a) states that the dimensionless dc resistance λ is exactly marginal in $d=2$; equivalently, the dimensionless conductance g scales classically since all quantum corrections to it vanish. The exact marginality of λ demonstrates that Anderson localization effects are "disabled" by SLS at the band center in the 2D random hopping model. We can extend these results for the one-loop RG equations of the NLσM to $d=2+\epsilon$ dimensions by simply adding the appropriate engineering dimension terms, i.e., $-\epsilon\lambda$ to Eq. (5.5a) and $-\epsilon\lambda_A$ to the second line of Eq. (5.5b).[67] [See Eq. (4.56a).] Moreover, this procedure yields[68,69] the exact result for the RG equation for λ, which [from Eq. (5.5a)] reads in $d=2+\epsilon$ dimensions as $d\lambda/dl = -\epsilon\lambda$. We conclude from this field theory treatment of the system that, in the absence of interactions and in dimensions $d \geq 2$, the delocalized phase, characterized by a finite conductivity, persists even for "strong" disorder; in particular, even the strongly disordered system exhibits no transition into a localized phase (as already mentioned in the Introduction).

The behavior of the system in $d=2$ is special in that the dimerization disorder[70] parameter λ_A is (logarithmically) driven to strong coupling at a rate determined by $f_1(\lambda)$ [Eq. (5.5b)]. The running λ_A feeds into the average density of states $\nu(\omega)$, as shown in Eq. (5.5c). This equation in turn implies the divergence of the low-energy DOS upon approaching the band center, taken to reside at $\omega=0$. Specifically, one finds that in two dimensions,[9,12,13]

$$\nu(\omega) \sim \frac{1}{\omega} \exp(-c|\ln \omega|^\alpha) \tag{5.7}$$

in the limit as $\omega \to 0$, where $c=c(\lambda)$ is a scale-independent constant and the exponent α is $1/2$.[71] Note that the DOS divergence in Eq. (5.7) that occurs in the 2D random hopping model has nothing to do with Fermi surface van Hove singularities, which may appear only in the clean limit,[73] e.g., in the case of pure nearest-neighbor hopping on the square lattice, where such a singularity at half-filling gives a weaker, logarithmic divergence. Returning to the random hopping model, in $d>2$, the low-energy DOS is finite but parametrically enhanced at the band center. (See Figs. 3 and 4 in Sec. I B.) By contrast, the density of states in a noninteracting ordinary diffusive metal (lacking SLS and being in one of the

three Wigner–Dyson classes) is typically not renormalized by the disorder.[40]

2. Interparticle interactions: Diffusive Fermi liquid and clean Hubbard-like model physics

We now turn to the interpretation of various pieces of Eqs. (5.3a)-(5.3e) involving the interparticle interactions. We first consider the term in square brackets on the right-hand side of Eq. (5.3a). This term can be recognized as the usual perturbative correction to the inverse conductance in a diffusive Fermi liquid in the presence of short-ranged interparticle interactions[2,59,60] and may be interpreted[61] as coherent backscattering of carriers off of disorder-induced Friedel oscillations in the background electronic charge density. Background density fluctuations become a source of *on-site* disorder in the presence of electron-electron interactions, so that we may attribute this nontrivial correction to "dynamic SLS breaking."

Next, we note the nontrivial zero of the one-loop RG equation (5.3c) at $\gamma_s = 1$. [A factor of $(1-\gamma_s)$ is expected in all orders.] This zero follows from the established representation of the thermodynamic compressibility $\partial n/\partial \mu \equiv \kappa$ in terms of the Finkel'stein model parameters,[3]

$$\kappa \sim h(1-\gamma_s) = h - \frac{4}{\pi}\Gamma_s, \tag{5.8}$$

valid in the diffusive Fermi liquid regime, where we have used Eqs. (5.1a) and (5.1b) and where we set $z=d$ [see Eq. (5.3e)]. Equation (5.8) shows that the incompressible limit $\kappa \to 0$ is attained by sending $\gamma_s \to 1$ (for finite h). From the definition Eq. (5.1a), we have

$$\frac{d\gamma_s}{dl} = -\frac{1}{h}\frac{d}{dl}\left(h - \frac{4}{\pi}\Gamma_s\right) + (1-\gamma_s)\frac{d \ln h}{dl}$$

$$\sim -\frac{1}{h}\frac{d\kappa}{dl} + (1-\gamma_s)\frac{d \ln h}{dl}. \tag{5.9}$$

In an interacting, disordered normal metal, κ receives no divergent corrections,[3] so that the condition $(d\gamma_s/dl)(\gamma_s=1) = 0$ is satisfied automatically. In the advent of sublattice symmetry, however, κ does renormalize, so that the first term on the right-hand side of Eq. (5.9) is typically nonzero. This can be seen from the noninteracting limit, where κ is equivalent to the single-particle density of states ν; as shown in Eq. (5.7) for the 2D case, $\nu(\omega)$ is strongly renormalized upon approaching the band center ($\omega \to 0$). Regardless of this, it is plausible to expect that in the limit $\gamma_s = 1$ and $\kappa = 0$, the incompressibility of the diffusive Fermi liquid is preserved under the RG flow, so that $d\kappa/dl(\gamma_s=1) = 0$, and therefore $(d\gamma_s/dl)(\gamma_s=1) = 0$, as we have found in Eq. (5.3c).

Finally, we note that the last term on the second line of Eq. (5.3d) drives the CDW instability, which is a remnant of the clean Hubbard-like model (recall that in our conventions, $\gamma_c < 0$ signals this instability).

B. Results (i): No metallic phase in $d=2$

Finally, we analyze our results considering first the 2D case. As discussed above in Sec. V A 1, the noninteracting

NLσM describes in $d=2$ an unusual critical, delocalized state of the random hopping model in Eqs. (1.1) and (1.9) with $U=V=0$. Other noninteracting models of disordered electrons are also known to possess delocalized states in $d=2$, such as the spin-orbit ("symplectic") normal metal class, where, e.g., a delocalized (metallic) phase occurs for sufficiently weak disorder.[40] The latter delocalized phase is, however, destabilized[3] by the introduction of (in this case, *long-ranged*) 3D Coulomb interactions, yielding an insulator in the presence of both disorder and interactions in $d=2$. What is the analogous outcome in the presence of sublattice symmetry, i.e., for the Hubbard-like models which are the focus of this work? The answer may be obtained by specializing Eqs. (5.3a)-(5.3d) to the vicinity of $\gamma_s=\gamma_c=0$. The linearized flow equations are given by (5.5a) and (5.5b) with (5.6a), and

$$\frac{d\gamma_U}{dl} \sim (3\lambda_A - 2\lambda)\gamma_U, \tag{5.10a}$$

$$\frac{d\lambda_V}{dl} \sim -\lambda_A \gamma_V, \tag{5.10b}$$

where we have introduced the relative same-sublattice (intersublattice) interaction strength $\gamma_U \equiv \gamma_s + \gamma_c$ ($\gamma_V \equiv \gamma_s - \gamma_c$) [cf. Eqs. (2.54), (5.1a), and (5.1b)]. (Note that while this result is valid only to first order in λ, no such restriction is placed on λ_A.) Equation (5.10a) shows that the same-sublattice interaction strength γ_U positively feeds back upon itself via the special sublattice class disorder coupling $\lambda_A \geq 0$. Since the latter is always driven to strong coupling [see Eqs. (5.5b) and (5.6a)] in $d=2$ for any $\lambda > 0$, we see that same-sublattice interactions are rapidly enhanced as we renormalize the FNLσM. At the very least, our result implies that the noninteracting description is unsuitable for describing the ground state of the 2D version of the full interacting, disordered Hubbard-like lattice model. This should be compared to an analogous result[18] previously obtained for a TRI, interacting random hopping model on the honeycomb lattice. In both models, the noninteracting phase is initially destabilized by the growth of short-ranged same-sublattice interparticle interactions, as in Eq. (5.10a), and this growth is mediated by a special disorder coupling, here λ_A, which occurs in general in the description of a random lattice model with an underlying SLS.[74]

Turning to an analysis of the full flow equations (5.3a)-(5.3e), we observe that Eq. (5.3b) precludes the existence of *any* perturbatively accessible, nontrivial fixed points occurring at nonzero resistance $\lambda > 0$ for small $\epsilon \geq 0$ ($d \geq 2$). By numerically integrating Eqs. (5.3a)-(5.3e) for generic initial conditions in $d=2$, we observe that either $\gamma_c \to -\infty$, signaling CDW formation, or that $\lambda, \lambda_A \to \infty$ and $\gamma_c \to +\infty$, indicating a flow toward *simultaneously* strong disorder and strong interactions. We demonstrate below that in $d>2$ dimensions, these two flow directions away from the noninteracting state evolve into two distinguishable instabilities of the diffusive Fermi liquid, which exists as a stable phase throughout a region of finite volume in the four-dimensional ($\lambda, \lambda_A, \gamma_s, \gamma_c$) coupling constant space. By contrast, since we find no stable
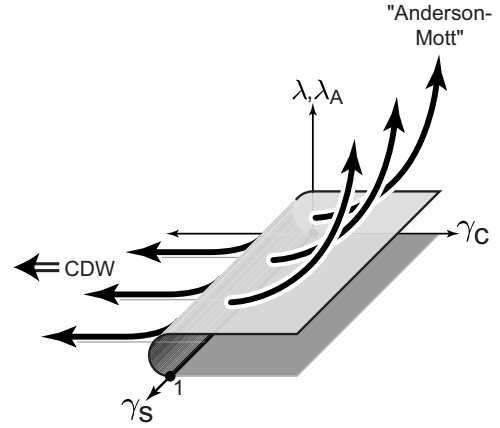

FIG. 23. Schematic phase diagram in $d=2+\epsilon$ dimensions, with $0 < \epsilon \ll 1$. λ and λ_A are both measures of the disorder, whereas γ_s and γ_c characterize the interaction strengths. The full phase diagram resides in the 4D ($\lambda, \lambda_A, \gamma_s, \gamma_c$) coupling constant space; this figure can be thought of as a 3D projection of this space, where the vertical axis (perpendicular to the interaction axes) measures the total disorder strength for some fixed ratio of λ/λ_A. The stable metallic phase resides between the ballistic plane ($\lambda=\lambda_A=0$) and the shaded sheath; the thick arrows indicate the two instabilities of the (metallic) diffusive Fermi liquid discussed in the text.

metallic region for $\epsilon=0$, we expect that the 2D disordered and interacting Hubbard-like model in Eqs. (1.1) and (1.9) is always an insulator at zero temperature.

We see that in two dimensions, sublattice symmetry is both the genesis of delocalized (critical) behavior in the absence of interactions, as well as the doom of such behavior in the presence of interactions. Moreover, in the Hubbard-like model studied in this work, SLS is also responsible for the Mott insulating charge density wave ground state in the clean limit. The physics that we have found is consistent with numerical studies[38,39] of the half-filled spin-1/2 Hubbard model in $d=2$, which have shown that TRI random hopping disorder *preserves* the charge compressibility gap of the clean Mott insulator, and that the disordered and interacting system shows no signs of metallic behavior.

C. Results (ii): Fermi liquid instability in $d=2+\epsilon$

The situation in $d=(2+\epsilon)>2$ dimensions is more interesting. Upon increasing ϵ from zero, a narrow, irregularly shaped sliver corresponding to a *stable* metallic, diffusive Fermi liquid opens up in the four-dimensional (4D) ($\lambda, \lambda_A, \gamma_s, \gamma_c$) coupling constant space. (A metallic, diffusive Fermi liquid is a state characterized by the condition that both disorder parameters λ and λ_A tend to zero at large length scales, whereas the interaction parameters approach $\gamma_s \to$ const and $\gamma_c \to 0$ in the same limit; see Fig. 24. In this limit, the FNLσM discussed in Sec. III becomes a simple, weakly coupled Gaussian theory.[3]) The sliver encloses the line $\lambda=\lambda_A=\gamma_c=0$, with $-\infty < \gamma_s < 1$, the entirety of which is perturbatively accessible because the FNLσM does not require the interaction strength γ_s to be small. A highly schematic 3D "projected" phase diagram is depicted in Fig. 23.

In this figure, the interaction constants (γ_s, γ_c) reside in the horizontal plane, while the vertical direction schematically represents (both) disorder strengths, (λ, λ_A). For example, we could take the vertical direction to measure the geometric average $\sqrt{\lambda \lambda_A}$ while fixing the ratio λ/λ_A to a constant. The shaded sheath in Fig. 23 is a cartoon for the boundary of the stable metallic volume, which resides between it and the ballistic $(\lambda = \lambda_A = 0)$ plane. Over the range of perturbatively small values of γ_c, the stable metallic, diffusive Fermi liquid phase resides in the region $\gamma_c \gtrsim 0$, terminating near $\gamma_c = 0$. For $\gamma_c > 0$, the "height" of the stable metallic volume in the vertical "disorder" direction is controlled by ϵ and is approximately independent of γ_c (as indicated in Fig. 23), although the precise shape and size of the phase boundary do vary with the ratio λ/λ_A and with γ_s, making it difficult to characterize analytically.

The flow equations (5.3a)-(5.3d) possess no nontrivial RG fixed points in dimensions $d > 2$, which would be accessible in an epsilon expansion about $d = 2$. Thus, no continuous metal-insulator transition can be identified. However, the two instabilities described in the previous subsection for the $d = 2$ case persist for $d > 2$ and become clearly distinct roads out of the metallic state. The conventional CDW instability is found to always occur for initial $\gamma_c < 0$ and sufficiently weak disorder, i.e., when $\lambda, \lambda_A \ll \epsilon$, and is represented by the flow $\gamma_c \to -\infty$. [Recall Eqs. (2.47), (5.1a), and (5.1b) and Sec. I A.] This flow is accompanied by a decay in both disorder strengths λ, λ_A, indicative of the clean limit. In Fig. 23, the CDW instability is schematically indicated by the thick arrows that emanate from the terminating surface of the metallic phase near $\gamma_c = 0$, running off toward large negative γ_c.

The primary result of this paper is the identification of a *second* route out of the diffusive Fermi liquid phase of the class AIII FNLσM in $d = 2 + \epsilon > 2$ dimensions, different from the Mott CDW instability, arising solely from the competition of disorder and interaction effects. As in $d = 2$ dimensions, this second route is characterized by a flow off to simultaneously strong disorder $(\lambda, \lambda_A \to \infty)$ and strong interactions $(\gamma_c \to +\infty)$, as indicated by the thick arrows emerging from the $\gamma_c > 0$ portion of the phase boundary shown in Fig. 23; we therefore dub it an Anderson–Mott instability.[4] Even though there is no perturbatively accessible fixed point, this second instability is nonetheless perturbatively controlled in $d = 2 + \epsilon$ over a wide range of initial conditions when $\epsilon \ll 1$; in particular, it is accessible over the entire range $0 \leq \gamma_s < 1$.[75] Numerically integrating Eqs. (5.3a), (5.3b), (5.3c), and (5.3d) for small $\epsilon \ll 1$, we find that the Anderson–Mott instability[4] can apparently always be reached by increasing *only* the "dimensionless resistance" λ beyond some small threshold value λ_T, while keeping the other three parameters λ_A, γ_s, and γ_c fixed. The threshold value λ_T is a function of ϵ (and of the other coupling strengths) which vanishes continuously in the limit $\epsilon \to 0$. In contrast, we find that it is difficult to access the Anderson–Mott route out of the Fermi liquid phase by varying the CDW interaction strength γ_c alone, despite the fact that the ensuing instability is characterized by the rapid flow of $\gamma_c \to +\infty$. We therefore interpret the boundary separating the flow toward the stable metallic regime from that toward the regime of the Anderson–Mott instability as a disorder-driven, first-order MIT. We emphasize

that a MIT does not exist in the noninteracting random hopping model, which possesses only a delocalized phase at half-filling for finite disorder in $d \geq 1$,[8,9,12,13] while the clean spinless Hubbard model possesses only the Mott CDW instability.

We demonstrate the physical picture described in the previous paragraph with a selection of RG flow trajectory plots. We have numerically integrated Eqs. (5.3a)-(5.3d) for the case of $d = 2 + \epsilon$ dimensions, with $\epsilon \equiv 0.01$, for a variety of initial conditions lying within the perturbatively accessible volume of the four-dimensional coupling constant space $(\lambda, \lambda_A, \gamma_s, \gamma_c)$. Figure 24 shows the results.

It is interesting to speculate on the nature of the insulating state ultimately obtained upon breaching the boundary of the stable, metallic diffusive Fermi liquid along the Anderson–Mott route. Although we cannot rule out the possibility that both this and the CDW instability, while clearly distinct along the boundary of the diffusive Fermi liquid, eventually terminate into the *same* insulating phase, it is important to stress that this need not be the case. As shown in Fig. 24, the Anderson–Mott instability is characterized by a rapid flow to large λ_A and large positive γ_c. Since λ_A describes quenched orientational fluctuations in bond strength dimerization (as discussed in Secs. II A 3 and II A 4), while γ_c is responsible for the Mott CDW instability $(\gamma_c \to -\infty)$, we might expect the insulator reached by the Anderson–Mott instability to possess local Mott insulating order, broken up on longer length scales into randomly oriented domains pinned by the strong bond dimerization disorder. Note that a flow to large positive γ_c is *not* consistent with local CDW formation [i.e., order at a nesting wave vector $\mathbf{K_N}$, as in Eq. (1.4)], but other types of Mott insulating order may occur in the limit of strong interparticle interactions $(\gamma_c \to +\infty)$. For example, sending the same-sublattice interaction strength $U \to +\infty$, for fixed V in the 2D square lattice version of the clean Hubbard-like model defined via Eq. (1.1), favors charge "stripes," i.e., order at $\mathbf{K} = (0, \pi)$ rather than at $\mathbf{K_N} = (\pi, \pi)$. [Recall from Eqs. (2.47), (3.21a), and (3.21b) that this limit corresponds to $\gamma_c \to +\infty$. In the same model, large negative values of γ_c would arise, e.g., from the different limit $V \to +\infty$ for fixed U.]

Finally, let us put the Anderson–Mott instability and the associated first-order metal-insulator transition that we have found into some context. As we have stressed, the SLS possessed by the Hubbard-like model in Eqs. (1.1) and (1.9) leads to special properties in both the noninteracting but disordered limit (delocalized phase at band center in $d \geq 1$),[8,9,12,13] and in the interacting but nondisordered (ballistic) limit (Mott insulating ground state at half-filling due to nesting for any $V > U \geq 0$). In the simultaneous presence of interactions and random hopping, we have a stable metallic phase and have found an interaction-stabilized, disorder-driven MIT in $d = 2 + \epsilon > 2$. These features mutate if we break SLS, e.g., either by allowing diagonal (on-site) disorder or by tuning the filling fraction away from $1/2$. In the case of broken SLS (keeping broken TRI, for simplicity), we recover the usual unitary metal symmetry class (for spinless electrons),[40] described by an appropriate Finkel'stein NLσM characterized by three coupling strengths, analogous to λ, γ_s, and h appearing in Eqs. (2.49) and (2.50). [Analogs of the dimerization disorder[70] parameter λ_A, as well as the CDW
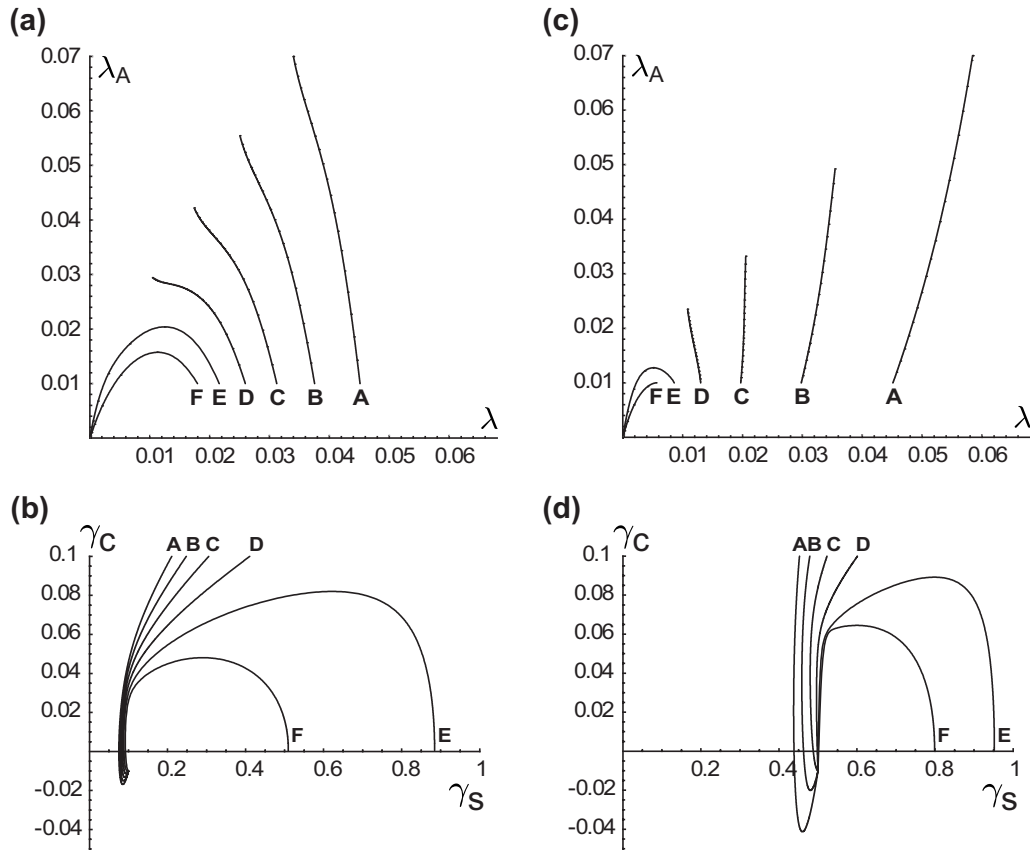
FIG. 24. RG flow trajectories in $d=2+\epsilon$ dimensions. (a) depicts six trajectories projected into the disorder (λ,λ_A) plane. The trajectories are distinguished by different initial conditions (ICs) for the resistance parameter λ, indicated by the labels A, ..., F (locating the *initial conditions* of the RG flow). (b) shows the same trajectories as in (a), now projected into the interaction (γ_s,γ_c) plane. In contrast to (a), the trajectory labels A, ..., F here demarcate the *end points* of the RG flow. The chosen λ ICs tune through the phase boundary enclosing the stable diffusive Fermi liquid state, demonstrating the disorder-driven instability discussed in the text. In (a) and (b), the trajectories labeled E and F flow into the diffusive metal. As for the other coupling strengths, all trajectories in (a) and (b) share the ICs $\lambda_A=-\gamma_c=\epsilon=0.01$, with $\gamma_s=0.1$. (c) and (d) depict a different set of RG flow trajectories possessing the same ICs for λ_A and γ_c but with $\gamma_s=0.5$.

interaction strength γ_c, do *not* appear in the unitary class Finkel'stein sigma model;[3] see the discussion in Sec. III following Eq. (3.22) for details.] In the case of short-ranged interparticle interactions, the FNLσM predicts[3] that the unitary metal class is an insulator in $d=2$ regardless of the presence of interactions, while the MIT in $d=2+\epsilon$ dimensions is actually in the same universality class as the noninteracting, continuous (pure Anderson) transition, i.e., the interparticle interactions are irrelevant at the transition. (Recall that we consider the spinless case.)

D. Conclusion

As we have already summarized our main results in the Introduction (Sec. I C), we conclude with a brief discussion of applications and extensions of our work, and we comment on some very recent results[36] for spin-1/2 fermion systems subject to the effects of both disorder and interactions.

Let us first revisit possible connections to spin-1/2 fermion models. As discussed in Sec. II B and elaborated in Appendixes B and C, the Finkel'stein NLσM calculation presented in this paper also applies to (i) a spin-1/2 Hubbard

lattice model with SLS, broken TRI, and strong spin-orbit coupling, and to (ii) a continuum model of fermionic quasi-particles, native to a superconducting phase, possessing TRI and a remnant $U(1)$ of spin $SU(2)$ rotational symmetry (i.e., invariance under rotations about one axis in spin space), preserved in every realization of the disorder (polar p-wave superconductor—see Appendix C). In the absence of interactions, both systems are realizations of the (quantum disorder) symmetry class AIII, within the classification scheme of Ref. 7.

Consider first the interpretation in terms of the *spin-1/2* random (sublattice) hopping model mentioned above. Disorder may be realized, e.g., via the application of a random orbital magnetic field to the otherwise clean model. (As discussed in Sec. II B and Appendix B, a random Zeeman field, on the other hand, realizes the *completely different* disorder class C, while the combination of random orbital and Zeeman fields gives the ordinary unitary metal symmetry class A.) The calculation presented in this paper also applies to such a spin-1/2 random hopping model, subject to generic short-ranged interparticle interactions and to strong (homogeneous or random) spin-orbit coupling. Spin-orbit coupling suppresses the hydrodynamic spin diffusion channel in the

Finkel'stein NLσM low-energy field theory, without modifying the symmetry class (AIII) of the disordered system in the absence of interactions. (Without spin-orbit coupling, an additional interaction term between the spin densities would appear, which does not exist in the spinless case and which is therefore not included in our treatment here.)

On the other hand, the superconductor quasiparticle interpretation of the AIII NLσM, mentioned above, provides a very different realization of our results. In particular, the superconductor interpretation does not require the disorder to take any special form (i.e., pure potential scattering will work) but requires only TRI and a remnant $U(1)$ of spin $SU(2)$ rotational symmetry to be preserved in every disorder realization. As discussed in Appendix C, such a situation "naturally" arises in the description of a spin-triplet, p-wave superconductor (lacking intrinsic spin-orbit coupling) in its polar, TRI phase.[53,54] This tantalizing but so far speculative connection could prove a more readily attainable connection to experiment.

As already mentioned, very recently, Dell'Anna[36] has independently studied several universality classes of Finkel'stein NLσMs including realizations of both the particle-hole symmetric class C and the sublattice symmetric class AIII for spin-1/2 fermions. In the AIII case, Dell'Anna included the spin diffusion channel (i.e., assumed no spin-orbit coupling). We have compared our one-loop RG results Eqs. (5.3a)-(5.4) to his, and we find agreement if we suppress the interactions associated with the spin degrees of freedom by hand.

APPENDIX A: SCHWINGER–KELDYSH SYMMETRY STRUCTURE

In this appendix, we examine the symmetry content of the lattice fermion Keldysh action in Eqs. (2.2) and (2.3). We establish a link between the noninteracting sector [Eq. (2.2); see also Eqs. (2.7) and (2.8)] and the transformation introduced in Eq. (2.17), justifying the promotion of the latter to a spatially varying "Goldstone fluctuation" in Eqs. (2.36a) and (2.36b).

For a given realization of the complex random hopping amplitudes $\{\delta t_{i,j}\}$, the only "physical" invariance possessed by Eqs. (2.2) and (2.3) is the discrete SLS, defined by Eq. (1.2). Nevertheless, the noninteracting sector of the Keldysh action [Eq. (2.2)] is actually invariant under a large group of *continuous* transformations, to be defined below. The full, interacting Finkel'stein NLσM, defined by Eqs.

(2.48)–(2.50), further incorporates the interparticle interactions of Eq. (2.3), which formally obliterate this symmetry.

Adopting the matrix notations introduced in the paragraph preceding Eq. (2.5), we recast the noninteracting Keldysh action in Eqs. (2.7) and (2.8):

$$S_1 \equiv S_1^h + S_1^\eta + S_1^\omega, \qquad (A1)$$

where

$$S_1^h = \sum_{\langle ij \rangle} (\bar{c}_{Ai} t_{i,j} c_{Bj} + \bar{c}_{Bj} t_{i,j}^* c_{Ai}), \qquad (A2a)$$

$$S_1^\eta = i\eta \sum_{i \in A} \bar{c}_{Ai} \hat{\Sigma}_3 \hat{\xi}_3 c_{Ai} + i\eta \sum_{j \in B} \bar{c}_{Bj} \hat{\Sigma}_3 \hat{\xi}_3 c_{Bj}, \qquad (A2b)$$

and

$$S_1^\omega = \sum_{i \in A} \bar{c}_{Ai} \hat{\Sigma}_3 |\hat{\omega}| c_{Ai} + \sum_{j \in B} \bar{c}_{Bj} \hat{\Sigma}_3 |\hat{\omega}| c_{Bj}, \qquad (A2c)$$

with $t_{i,j} \equiv t + \delta t_{i,j}$, as in Eq. (2.2).

Consider a general, spatially uniform unitary transformation in $|\omega| \otimes \Sigma \otimes \xi$ (frequency $\otimes$ Keldysh) space:

$$c_{Ai} \rightarrow \hat{U}_A c_{Ai}, \quad \bar{c}_{Ai} \rightarrow \bar{c}_{Ai} \hat{V}_A,$$

$$c_{Bj} \rightarrow \hat{U}_B c_{Bj}, \quad \bar{c}_{Bj} \rightarrow \bar{c}_{Bj} \hat{V}_B, \qquad (A3)$$

where

$$\hat{U}_A^\dagger \hat{U}_A = \hat{V}_A^\dagger \hat{V}_A = \hat{U}_B^\dagger \hat{U}_B = \hat{V}_B^\dagger \hat{V}_B = \hat{1}_{|\omega| \otimes \Sigma \otimes \xi}. \qquad (A4)$$

We now examine the symmetry content of the noninteracting Keldysh action S_1 [Eq. (A1)] assembled in stages from the three pieces defined in Eqs. (A2a)–(A2c).

Invariance of the "Hamiltonian" piece S_1^h [Eq. (A2a)] under the transformation in Eq. (A3) requires that

$$\hat{V}_A = \hat{U}_B^\dagger, \quad \hat{V}_B = \hat{U}_A^\dagger. \qquad (A5)$$

If we imagine discretizing and truncating the continuum of allowed absolute energies to a set of n discrete values, $|\omega| \rightarrow |\omega|_\alpha$, with $\alpha \in \{1, \ldots, n\}$, then we can say that the conditions in Eqs. (A4) and (A5) imply that the action S_1^h is invariant under transformations belonging to the space $U(4n) \times U(4n)$.

Next, we consider the Hamiltonian plus "pole prescription" pieces [Eqs. (A2a) and (A2b), respectively]. Invariance of $S_1^h + S_1^\eta$ requires the restriction given by Eq. (A5), as well as

$$\hat{\Sigma}_3 \hat{\xi}_3 \hat{U}_A \hat{\Sigma}_3 \hat{\xi}_3 = \hat{U}_B. \qquad (A6)$$

Taken together, Eqs. (A5) and (A6) imply that the $U(4n) \times U(4n)$ symmetry of S_1^h is broken down to the diagonal subgroup $U(4n)$ by the pole prescription term S_1^η.

Finally, the full noninteracting action is assembled by

TABLE III. Symmetry content of the noninteracting Keldysh action [Eqs. (A1) and (A2a)–(A2c)]. The target space of the NLσM is set by the quotient of the first and second entries, below.

Imposed condition	Implied invariance
(1) Invc. of S_1^h	$U(4n) \times U(4n)$
(2) Invc. of $S_1^h + S_1^\eta$	$U(4n)$
(3) Invc. of $S_1 = S_1^h + S_1^\eta + S_1^\omega$	$[U(2) \times U(2)]^n$

adding the "energy" piece, defined by Eq. (A2c). Under the transformation given by Eq. (A3), invariance of $S_1 \equiv S_1^h + S_1^\eta + S_1^\omega$ requires the conditions provided in Eqs. (A5) and (A6), as well as

$$[\hat{\xi}_3, \hat{U}_A] = 0 \qquad (A7)$$

and

$$[|\hat{\omega}|, \hat{U}_A] = 0, \qquad (A8)$$

with $[\hat{A}, \hat{B}] \equiv \hat{A}\hat{B} - \hat{B}\hat{A}$. The noninteracting Keldysh action admits symmetry transformations off diagonal in $\Sigma [\text{sgn}(\omega)]$ space but necessarily diagonal in both $|\omega|$ and ξ (Keldysh) spaces, implying the (much smaller) symmetry group $[U(2) \times U(2)]^n$.

The pattern of symmetry-breaking that we have found is summarized in Table III. The symmetry content of the Hamiltonian piece S_1^h of the Keldysh action is broken down into successively smaller remnants via the addition of the pole prescription and energy terms. We interpret the pole prescription piece S_1^η [Eq. (A2b) with $\eta \to 0^+$] as an infinitesimal source, analogous to an external field in an $O(N)$ ferromagnet; in the diffusive metallic phase, this source selects a particular ground state from the $U(4n) \times U(4n)$ saddle point manifold of the system. [The magnitude of the saddle point configuration is given by the elastic scattering rate $1/\tau$ due to the disorder, evaluated in the self-consistent Born approximation.[40] See, e.g., Eqs. (2.32) and (2.33).] The (noninteracting) NLσM retains only the quantum Goldstone fluctuations about this symmetry-broken minimum. We retain modes (weakly) off diagonal in both the $|\omega|$ and Keldysh (ξ) spaces. As a result, the noninteracting Keldysh NLσM, appropriate to the complex random hopping model defined in Eqs. (1.1) and (1.9), with $U = V = 0$, possesses the target manifold $U(4n) \times U(4n)/U(4n) \sim U(4n)$. The NLσM with target manifold of the Lie group $U(4n)$, for *finite*, integer n, is termed the unitary principal chiral model in the field theory literature. An analogous result for the noninteracting, class AIII random hopping model, formulated in terms of bosonic replicas, was originally obtained by Gade and Wegner.[9]

Consider tuning the fermion density away from half-filling in the noninteracting random hopping model, which necessitates the addition of a finite chemical potential term to the Hamiltonian piece of the Keldysh action [Eq. (A2a)]. Going through the above analysis, one finds a smaller NLσM target manifold $U(4n)/U(2n) \times U(2n)$, characteristic of the TRI-broken, unitary normal metal class, as expected.

APPENDIX B: DISORDERED, BIPARTITE LATTICE MODELS FOR SPIN-1/2 ELECTRONS

In this appendix, we identify the quantum disorder symmetry classes appropriate to models of noninteracting spin-1/2 fermions, with nearest-neighbor hopping on a bipartite lattice at half-filling, subject to random orbital or random Zeeman magnetic fields. Our starting point is the general bipartite lattice Hamiltonian

$$H = \sum_{\alpha,\beta} \left[\sum_{i,j} c_{Ai}^{\dagger\alpha}(\hat{t}_{AB})_{i,j}^{\alpha,\beta} c_{Bj}^{\beta} + \text{H.c.} + \sum_{i,i'} c_{Ai}^{\dagger\alpha}(\hat{t}_{AA})_{i,i'}^{\alpha,\beta} c_{Ai'}^{\beta} + \sum_{j,j'} c_{Bj}^{\dagger\alpha}(\hat{t}_{BB})_{j,j'}^{\alpha,\beta} c_{Bj'}^{\beta} \right], \qquad (B1)$$

where $c_{Ai}^{\dagger\alpha}$ and c_{Bj}^{β} are creation and annihilation operators for fermions on the A and B sublattices, respectively, with $\alpha, \beta \in \{\uparrow, \downarrow\}$ spin-1/2 component indices. In Eq. (B1), indices $\{i, i'\}$ and $\{j, j'\}$ denote, respectively, sites on the A and B sublattices, so that the sum on (i, j) runs over *all* (not just nearest-neighbor) pairs of A and B sites, while the sums on (i, i') and (j, j') run over all same-sublattice pairs of sites. Particle hopping is facilitated by the spin-dependent intersublattice $\{\hat{t}_{AB}, \hat{t}_{AB}^\dagger\}$ and same-sublattice $\{\hat{t}_{AA}, \hat{t}_{BB}\}$ complex connectivity matrices. The same sublattice matrices are constrained by Hermiticity:

$$\hat{t}_{AA}^\dagger = \hat{t}_{AA}, \quad \hat{t}_{BB}^\dagger = \hat{t}_{BB}. \qquad (B2)$$

Let us adopt a compact matrix notation reminiscent of that implemented in Eq. (2.7), in Sec. II A 1. We rewrite Eq. (B1) as

$$H \equiv c^\dagger \hat{h} c, \qquad (B3)$$

where c ($c^\dagger$) is a column (row) vector, with indices in position, sublattice flavor, and spin-1/2 spaces, i.e., $c \to c_{Ai/Bj}^\alpha$ with all indices displayed. The single-particle Hamiltonian $\hat{h}$ in Eq. (B3) has the sublattice flavor space decomposition

$$\hat{h} = \begin{bmatrix} \hat{t}_{AA} & \hat{t}_{AB} \\ \hat{t}_{AB}^\dagger & \hat{t}_{BB} \end{bmatrix}. \qquad (B4)$$

If we assume that the model in Eq. (B1) resides upon a d-dimensional bipartite lattice of $2N$ sites, then $\hat{h}$ is a $4N \times 4N$ Hermitian matrix.

In the presence of disorder, the elements of $\hat{h}$ will be random variables. The structure of $\hat{h}$ can then be classified[7,42] using random matrix theory (RMT) according to the constraints imposed by any symmetry preserved in every realization of the static disorder. Consider the clean case of real, homogeneous, spin-independent nearest-neighbor hopping on a bipartite lattice at half-filling. We will refer to this situation as pure sublattice hopping. Pure sublattice hopping corresponds to Eq. (B1) with

$$\hat{t}_{AA} = \hat{t}_{BB} = 0 \qquad (B5)$$

and

$$(\hat{t}_{AB})_{i,j}^{\alpha,\beta} = t\delta_{\langle i,j\rangle}\delta^{\alpha,\beta}, \tag{B6}$$

where $t=t^*$, and $\delta_{\langle i,j\rangle}$ gives 1 for i and j nearest neighbors, and vanishing otherwise. We introduce two commuting sets of Pauli matrices: the matrix $\hat{\sigma}_m$ acts in sublattice flavor space, while the matrix $\hat{J}_n$ acts in the spin-1/2 space, with $m,n \in \{1,2,3\}$. We use the conventional basis for all Pauli matrices. In addition to symmetries implied by the lattice space group, the single-particle Hamiltonian with pure sublattice hopping [Eqs. (B4)–(B6)] possesses spin $SU(2)$ rotational invariance

$$\hat{J}_m\hat{h}\hat{J}_m = \hat{h} \tag{B7}$$

for $m=\{1,2,3\}$, as well as three discrete symmetries: TRI, SLS, and PH symmetry, defined as invariance under the following operations:

$$c \rightarrow -i\hat{J}_2 c, \quad c^\dagger \rightarrow c^\dagger i\hat{J}_2 \quad \text{(TRI)}, \tag{B8a}$$

$$c \rightarrow \hat{\sigma}_3(c^\dagger)^\mathsf{T}, \quad c^\dagger \rightarrow c^\mathsf{T}\hat{\sigma}_3 \quad \text{(SLS)}, \tag{B8b}$$

$$c \rightarrow -i\hat{J}_2\hat{\sigma}_3(c^\dagger)^\mathsf{T}, \quad c^\dagger \rightarrow c^\mathsf{T} i\hat{J}_2\hat{\sigma}_3 \quad \text{(PH)}. \tag{B8c}$$

In these equations, "T" denotes the matrix transpose operation. The TRI and SLS operations are antiunitary; the PH operation as defined in Eq. (B8c) is a *product* of TRI and SLS, and is therefore unitary. The PH operation so defined is unconventional in that it involves a spin flip. Equations (B8a)–(B8c) equivalently imply the following conditions on $\hat{h}$:

$$\hat{J}_2\hat{h}^\mathsf{T}\hat{J}_2 = \hat{h} \quad \text{(TRI)}, \tag{B9a}$$

$$-\hat{\sigma}_3\hat{h}\hat{\sigma}_3 = \hat{h} \quad \text{(SLS)}, \tag{B9b}$$

$$-\hat{J}_2\hat{\sigma}_3\hat{h}^\mathsf{T}\hat{J}_2\hat{\sigma}_3 = \hat{h} \quad \text{(PH)}. \tag{B9c}$$

Equation (B9b) demonstrates that SLS translates into a chiral condition on $\hat{h}$: invariance under SLS forces $\hat{h}$ to be purely off diagonal in sublattice flavor space (this condition provides an equivalent definition of SLS in the absence of interactions).

For the case of disorder that breaks all of the "internal" symmetries detailed in Eqs. (B7) and (B9a)–(B9c), the only constraint placed on $\hat{h}$ is Hermiticity. The most precise statement that we can make, independent of the details of a particular disorder realization, is that $\hat{h}$ belongs to a matrix representation[77] of the Lie algebra $u(4N)$ of the unitary group: we say that $\hat{h} \in u(4N)$. This places the model in Eq. (B1) into the ordinary "unitary" (Wigner–Dyson) class A.[7] Adding one or more of the symmetry constraints in Eqs. (B7) and (B9a)–(B9c) will allow us to refine this statement, potentially altering the random matrix class.

Consider first the addition of a random orbital field to the pure sublattice hopping model defined by Eqs. (B4)–(B6). The presence of a random orbital field modifies only Eq. (B6), which now reads

$$(\hat{t}_{AB})_{i,j}^{\alpha,\beta} \rightarrow te^{i\theta_{i,j}}\delta_{\langle i,j\rangle}\delta^{\alpha,\beta}, \tag{B10}$$

with $\theta_{i,j}$ a bond-dependent real phase. By using Eqs. (B5) and (B10) in Eq. (B4), we see that $\hat{h}$ preserves spin $SU(2)$ rotational symmetry [Eq. (B7)], breaks TRI and PH [Eqs. (B9a) and (B9c)], and preserves SLS [Eq. (B9b)]. Imposing Eq. (B7) alone implies that $\hat{h} \in u(2N)$; subsequently enforcing the "anti-SLS" constraint

$$\hat{\sigma}_3\hat{h}\hat{\sigma}_3 = \hat{h} \tag{B11}$$

further reduces the space to which $\hat{h}$ belongs to $u(N) \times u(N)$. Since the conditions in Eqs. (B9b) and (B11) are complementary, enforcing instead spin $SU(2)$ and SLS leads to the identification $\hat{h} \in u(2N)/u(N) \times u(N)$, associated with the chiral random matrix class AIII.[7] Thus, adding a random orbital magnetic field [Eq. (B10)] to the spin-1/2 pure sublattice hopping model yields a system in the same class as the (noninteracting) spinless random hopping model [Eqs. (1.1) and (1.9) with $U=V=0$], discussed in Secs. I B and V A 1 of this paper.

We may also consider imposing only SLS, i.e., removing the spin $SU(2)$ constraint given by Eq. (B7). This is consistent with the addition of spin-orbit coupling to the orbital magnetic field case analyzed above. Using Eq. (B9b), we find $\hat{h} \in u(4N)/u(2N) \times u(2N)$, so that $\hat{h}$ belongs to the same space of matrices (and therefore the same random matrix class AIII) regardless of whether spin $SU(2)$ rotational symmetry is preserved or destroyed (completely). As discussed in Secs. II B and V D, the Finkel'stein NLσM formulated in Sec. II, defined by Eqs. (2.48)–(2.50), also applies to a spin-1/2 Hubbard model with sublattice hopping, subject to a random orbital magnetic field and possessing spin-orbit coupling.

Next, we turn to the case of a random Zeeman field. Given the assumption of pure sublattice hopping [Eqs. (B4)–(B6)], the introduction of a Zeeman field modifies Eq. (B5) as follows:

$$(\hat{t}_{AA})_{i,i'}^{\alpha,\beta} \rightarrow \mathbf{b}_{Ai}\cdot\mathbf{J}^{\alpha,\beta}\delta_{i,i'},$$

$$(\hat{t}_{BB})_{j,j'}^{\alpha,\beta} \rightarrow \mathbf{b}_{Bj}\cdot\mathbf{J}^{\alpha,\beta}\delta_{j,j'}, \tag{B12}$$

where $\hat{\mathbf{J}}=\{\hat{J}_m\}\rightarrow\{J_m^{\alpha,\beta}\}$, with $m \in \{1,2,3\}$, is a vector of spin-1/2 space Pauli matrices, and where $\mathbf{b}_{Ai}$ and $\mathbf{b}_{Bj}$ denote real three-component vectors with sublattice site-dependent orientations and magnitudes. By using Eqs. (B12) and (B6) in Eq. (B4), we see that a random Zeeman field breaks spin $SU(2)$ rotational symmetry [Eq. (B7)] (completely), TRI [Eq. (B9a)], and SLS [Eq. (B9b)] while preserving PH [Eq. (B9c)] in every static realization of disorder.[78] Equation (B9c) provides a symplectic condition on $\hat{h}$; in isolation, PH therefore implies that $\hat{h} \in sp(4N)$. The Lie algebra $sp(4N)$ of the symplectic group is associated with the random matrix class C.[7,42] Class C is also realized by a spin-1/2 fermionic quasiparticle system native to a superconductor with singlet pairing, broken TRI, and spin $SU(2)$ rotational symmetry preserved in every realization of disorder.[7,37,42,47–50]

In summary, given the assumption of a clean system of spin-1/2 fermions with pure sublattice hopping [Eqs. (B4)–(B6)], the introduction of a random orbital magnetic field, as in Eq. (B10), gives a noninteracting quantum disordered system with SLS, lacking TRI and PH, belonging to the random matrix class AIII; the introduction of a random Zeeman field, as in Eq. (B12), gives a system with PH, lacking spin $SU(2)$ rotational symmetry, TRI, and SLS, belonging to class C. The application of both random orbital and random Zeeman fields to a spin-1/2 system with pure sublattice hopping breaks TRI, SLS, PH, and spin $SU(2)$ rotational symmetry (completely), in which case the ordinary unitary (Wigner–Dyson) class A is recovered.

APPENDIX C: POLAR SUPERCONDUCTOR INTERPRETATION

By using the same type of RMT symmetry analysis[42] applied in Appendix B to classify systems of spin-1/2 lattice fermions, we demonstrate here a completely different microscopic interpretation of the Finkel'stein NLσM studied in this paper, which provides a view of our results alternative to the spinless Hubbard model physics espoused in the main text. The microscopic view adopted in this appendix concerns the fermionic quasiparticles associated with a particular type of superconductor, subject to quenched disorder. (These quasiparticles are initially taken to be noninteracting, within a mean field theory treatment of pairing; subsequently, quasiparticle interactions are added.)

Fermionic quasiparticles in a superconductor do not carry well-defined quantities of physical electric charge.[25] In the presence of disorder, this means that electric charge is not a slow, hydrodynamic variable; a low-energy nonlinear sigma model description of such a disordered noninteracting quasiparticle system therefore cannot describe any kind of conventional metal-insulator transition, as might be observed experimentally through electric transport measurements. Disorder may yet dramatically influence other properties of the system, however, including thermal and spin transport coefficients [the latter only if at least a $U(1)$ subgroup of spin $SU(2)$ rotational symmetry is preserved], as well as the behavior of the low-energy, single-particle (tunneling) density of states.[79] In particular, it is possible in principle to observe a "thermal metal" to "thermal insulator" transition,[47,48,50,80] indicative of Anderson localization of the single quasiparticle states due to the disorder. This transition is described by a random Bogoliubov–De Gennes equation and may possibly be accessible[48] by tuning, e.g., the impurity concentration in a superconducting sample. To build a more realistic model of such a system, one should also include the effects of interactions[36,37,49] between the quasiparticles of the superconductor; near $d=2$, both disorder and interaction effects may be reliably described within the Finkel'stein NLσM framework.

In this appendix, we first show that a noninteracting, spin-1/2 quasiparticle system, native, e.g., to a certain spin-triplet p-wave superconductor and subject to quenched disorder satisfying certain additional symmetry constraints, falls into the same random matrix class (the chiral class AIII in the scheme

of Ref. 7) as the noninteracting spinless random hopping model [Eqs. (1.1) and (1.9) with $U=V=0$] discussed in Secs. I B and V A 1. To obtain a superconductor quasiparticle system in the chiral class AIII, in every static realization, the disorder must preserve TRI, as well as a remnant $U(1)$ of the spin $SU(2)$ rotational symmetry. Such a situation is expected to occur "naturally" for pure potential scattering (i.e., nonmagnetic impurities and no spin-orbit scattering), in a spin-triplet p-wave superconducting host residing in its TRI, "polar" phase.[53,54] We emphasize that, in contrast to the Hubbard model, this quasiparticle system may be defined directly in the continuum, without reference to a lattice or an additional sublattice symmetry. After demonstrating the equivalence of the noninteracting superconductor quasiparticle and spinless random hopping (normal) particle or electron systems at the level of RMT, we will briefly discuss the interpretation of the disorder and interaction parameters of the corresponding FNLσM [Eqs. (2.48)–(2.50)], studied in this paper, in the superconductor quasiparticle context.

In order to motivate the basic underlying idea, consider first the system of quasiparticles in a *two-dimensional spinless* (or *spin-polarized*) p_x superconductor,[54,81] which is subject to static short-ranged disorder[82] (in the potential and pair field). Weak disorder, acting on the pair of Dirac fermions at the two nodal points and preserving the TRI of the p_x superconducting state,[83] is known[13] to place this system in the (orthogonal) chiral[7] symmetry class BDI.[84,85] In the low-energy Dirac theory, the disorder occurs in two varieties: intra- and internode scatterings. The intranode randomness[13] takes the form of a random $U(1)$ vector potential.[82,86] In the p_x superconductor realization, quenched random $U(1)$ vector potential fluctuations correspond to small random shifts of the positions of the nodal points, and thus, in particular, to small random fluctuations of the *orientation* of the Cooper pair wave function away from the x axis. Internode scattering appears as a pair of random masses for the Dirac quasiparticles.[13,82] In the disorder-averaged Dirac theory, it is necessary to specify two parameters g_A and g in order to quantify the strength of intra- and internode scatterings, respectively. As shown in Ref. 13, g_A and g each play a role in the class BDI disordered Dirac theory described above that is analogous to the parameters λ_A and λ, respectively, in the NLσM formulation of the (different) chiral disorder class AIII, as defined by Eqs. (2.48), (2.49), and (2.51) in Sec. II. We demonstrate below that this analogy reflects a concrete realization of class AIII in terms of quasiparticles of a certain p-wave superconductor, with spin 1/2 rather than spin 0. The strength g_A of the vector potential randomness in the spinless case is analogous to λ_A in the sigma model description of the spin-1/2 quasiparticle system.

We now turn to the random matrix symmetry analysis. Consider a clean p-wave, spin-triplet Bogoliubov–De Gennes (pairing) Hamiltonian of the form

$$H = \int d^d\mathbf{r}\, c^\dagger(\mathbf{r})[-\nabla^2 - \mu]c(\mathbf{r})$$

$$+ \frac{1}{2}\int d^d\mathbf{r}\, d^d\mathbf{r}'[\mathbf{b}^\dagger(\mathbf{r},\mathbf{r}') \cdot \boldsymbol{\Delta}(\mathbf{r}-\mathbf{r}') + \text{H.c.}], \quad \text{(C1)}$$

where we define the spin-triplet pair field operator

$$\mathbf{b}(\mathbf{r},\mathbf{r}') \equiv c^{\mathsf{T}}(\mathbf{r})\hat{J}_2\hat{\mathbf{J}}c(\mathbf{r}'). \tag{C2}$$

In Eq. (C1), $c^{\dagger}$ and c denote two-component fermion creation and annihilation operators, i.e., $c \to c^{\alpha}$, where $\alpha \in \{\uparrow,\downarrow\}$ is a spin-1/2 component index; μ is the chemical potential. In the absence of disorder and quasiparticle interactions, the gap $\mathbf{\Delta}(\mathbf{r})$ in Eq. (C1) is a static, spatially antisymmetric vector-valued function. In Eq. (C2), the superscript "T" denotes the matrix transpose operation, and we denote the vector of Pauli matrices acting in spin-1/2 space by $\hat{\mathbf{J}} = \{\hat{J}_m\}$ $\to \{J_m^{\alpha,\beta}\}$, with $m \in \{1,2,3\}$. The pair field operator defined by Eq. (C2) carries electric charge $2e$ and transforms like an $O(3)$ vector under $SU(2)$ spin rotations. In the polar phase of a spin-triplet, p-wave superfluid, the gap function takes the form[53,54] (ignoring dynamical fluctuations)

$$\mathbf{\Delta}(\mathbf{r}) = \zeta\phi(\mathbf{r}), \tag{C3}$$

where the fixed unit vector ζ and the spatially antisymmetric scalar function $\phi(\mathbf{r})$ are both purely real. We take $\zeta = (0,0,1)$. The Hamiltonian in Eq. (C1) then possesses TRI and a remnant $U(1)$ of spin rotational symmetry (about the $m=3$ axis), defined as invariance under the transformations

$$c \to -i\hat{J}_2 c, \quad c^{\dagger} \to c^{\dagger}i\hat{J}_2 \quad \text{(TRI)}, \tag{C4a}$$

$$c \to e^{i\hat{J}_3\theta}c, \quad c^{\dagger} \to c^{\dagger}e^{-i\hat{J}_3\theta} \quad [\text{spin } U(1)]. \tag{C4b}$$

The time-reversal operation [Eq. (C4a)] is antiunitary.

We implement the following compact notation: first, we construct the Majorana spinor

$$\chi \equiv \begin{bmatrix} c \\ \hat{J}_2(c^{\dagger})^{\mathsf{T}} \end{bmatrix}, \tag{C5}$$

which carries indices in particle-hole $\{\mathfrak{p}=1,2\}$, spin-1/2 $\{\alpha = \uparrow,\downarrow\}$, and position space $\mathbf{r}$, i.e., $\chi_{\mathfrak{p}=1}^{\alpha}(\mathbf{r}) = c^{\alpha}(\mathbf{r})$ and $\chi_{\mathfrak{p}=2}^{\alpha}(\mathbf{r}) = [\hat{J}_2(c^{\dagger})^{\mathsf{T}}]^{\alpha}(\mathbf{r})$ with all indices displayed. Note that χ transforms like c under spin space transformations. Next, we introduce a second set standard of Pauli matrices $\{\hat{\Pi}_m\}$, $m \in \{1,2,3\}$, acting in the particle-hole space of χ. The definition Eq. (C5) implies that

$$\chi^{\dagger} = \chi^{\mathsf{T}}i\hat{\Pi}_2\hat{J}_2. \tag{C6}$$

Using Eqs. (C5) and (C6), we rewrite Eq. (C1) as

$$H = \frac{1}{2}\chi^{\dagger}\hat{h}\chi, \tag{C7}$$

where we have introduced the single-particle Hamiltonian

$$\hat{h} = \begin{bmatrix} \hat{t} & \hat{\mathbf{\Delta}} \cdot \hat{\mathbf{J}} \\ \hat{\mathbf{J}} \cdot \hat{\mathbf{\Delta}}^{\dagger} & -\hat{J}_2\hat{t}^{\mathsf{T}}\hat{J}_2 \end{bmatrix}, \tag{C8}$$

with

$$\hat{t} \to t^{\alpha,\beta}(\mathbf{r},\mathbf{r}') = [(-\nabla^2 - \mu)\delta^d(\mathbf{r}-\mathbf{r}')]\delta^{\alpha,\beta},$$

$$\hat{\mathbf{\Delta}} \cdot \hat{\mathbf{J}} \to \hat{\mathbf{\Delta}}(\mathbf{r}-\mathbf{r}') \cdot \hat{\mathbf{J}}^{\alpha,\beta} \tag{C9}$$

(α and β are spin-1/2 component indices.)

By combining Eqs. (C6) and (C7) and noting that the components of χ mutually anticommute up to irrelevant additive constants, we see that the single-particle Hamiltonian $\hat{h}$ may be taken without loss of generality to satisfy the "Majorana" condition

$$-\hat{\Pi}_2\hat{J}_2\hat{h}^{\mathsf{T}}\hat{J}_2\hat{\Pi}_2 = \hat{h}. \tag{C10}$$

The transformations defined by Eqs. (C4a) and (C4b) may be reexpressed in the χ language using Eq. (C5); doing so shows that TRI and spin $U(1)$ rotational symmetry translate into the following conditions upon $\hat{h}$ [via Eq. (C7) and using Eq. (C10)]:

$$-\hat{\Pi}_1\hat{h}\hat{\Pi}_1 = \hat{h} \quad \text{(TRI)}, \tag{C11a}$$

$$\hat{J}_3\hat{h}\hat{J}_3 = \hat{h} \quad [\text{spin}U(1)]. \tag{C11b}$$

Equation (C11a) shows that time-reversal invariance appears as a chiral[7] condition [see Eq. (B9b)] on the Bogoliubov–De Gennes single-particle Hamiltonian $\hat{h}$.

As discussed in Appendix B, in the presence of disorder, we may classify the noninteracting quasiparticle system introduced in Eq. (C1) by examining the algebraic structure of the Hamiltonian $\hat{h}$ [Eqs. (C7) and (C8)], arising in the presence of an arbitrary, static realization of impurities. If we imagine discretizing position space into a lattice of N sites, then $\hat{h}$ is a $4N \times 4N$ Hermitian square matrix. In the absence of both TRI and spin $U(1)$ rotational invariance, the only constraint upon this matrix is the Majorana condition [Eq. (C10)], which implies that $\hat{h}$ belongs to a matrix representation of the Lie algebra $so(4N)$ [in the defining (vector) representation]. We write this condition as $\hat{h} \in so(4N)$. This space of matrices $\hat{h}$ is associated with the random matrix class D.[7,42,80]

Let us turn to the situation of interest, a quasiparticle system, subject to (e.g., pure potential) disorder, that preserves the symmetry conditions native to the polar phase of a p-wave, spin-triplet superconducting host:[53,54] TRI and spin $U(1)$ rotational invariance. The Majorana [Eq. (C10)] and spin $U(1)$ [Eq. (C11b)] conditions imply the following decomposition in spin-1/2 space:

$$\hat{h} = \begin{bmatrix} \hat{h}_{2N} & 0 \\ 0 & -\hat{\Pi}_2\hat{h}_{2N}^{\mathsf{T}}\hat{\Pi}_2 \end{bmatrix}, \tag{C12}$$

where $\hat{h}_{2N} \in u(2N)$. Further imposing the "anti-TRI" condition

$$\hat{\Pi}_1\hat{h}\hat{\Pi}_1 = \hat{h} \tag{C13}$$

would identify $\hat{h}_{2N} \in u(N) \times u(N)$. Equations (C11a) and (C13) are exact complements, so that, instead, imposing the Majorana condition, spin $U(1)$ rotational invariance, and TRI leads to $\hat{h} \in u(2N)/u(N) \times u(N)$. This space of matrices is

associated with the chiral random matrix class AIII.[7] The same space of matrices also applies to the noninteracting, spinless random hopping model discussed in Secs. I B and V A 1 of this paper.[9,12] [See also the discussion below Eq. (B11) in Appendix B.]

At the level of random matrix theory, we have succeeded in identifying (i) the system of noninteracting spin-1/2 quasiparticles (treated within the mean field theory of pairing) native to a superconducting host and subject to quenched disorder preserving TRI and a remnant $U(1)$ of the $SU(2)$ spin rotational symmetry, with (ii) the noninteracting limit of the spinless Hubbard-like model with random hopping, defined by Eqs. (1.1) and (1.9) with $U=V=0$. We have shown how such a system might naturally arise in the context of a p-wave, spin-triplet superconductor in its TRI, polar phase,[53,54] subject to pure potential scattering due to nonmagnetic impurities.

We can extend the analogy between these two systems to the detailed NLσM formulation, incorporating residual quasiparticle interactions à la Finkel'stein.[2] In contrast to the 2D case of Dirac quasiparticles in the spinless p_x superconductor mentioned in the paragraph above Eq. (C1), we now restrict our discussion to the case $d>2$, for which our RG calculation of Sec. V C predicts a metal-insulator transition due to the interplay of both disorder and interactions, as we will now explain.

In Sec. II, we derived the class AIII FNLσM using the Hubbard-like model [Eqs. (1.1) and (1.9)] as our microscopic starting point. The action for the FNLσM was defined in Sec. II A 4 by Eqs. (2.49) and (2.50). In order to understand the relevance of Sec. V C in the superconductor context, we need to explain the reinterpretation of the FNLσM parameters appropriate to the p-wave superconductor quasiparticle view, which we will now do.[87] The parameter λ still plays the role of the dimensionless resistance, now proportional to the $U(1)$ spin conductivity, associating positive and negative spin $U(1)$ charges to particles with "up" and "down" $m=3$ components of spin, respectively.[37,47,48] The second disorder strength λ_A was attributed in Sec. II A 4 to quenched bond dimerization fluctuations in the random (sublattice) hopping model. As discussed in the paragraph above Eq. (C1), in the superconductor, λ_A measures the strength of quenched random orientational fluctuations of the p-wave Cooper pairing wave function induced by the disorder.

Turning to the interaction sector of the FNLσM action [Eq. (2.50)], we now reinterpret the interaction strengths Γ_s and Γ_c [Eq. (2.54)] within the context of the quasiparticles of the superconductor. The parameter Γ_s arises from the S_z-S_z component of spin-triplet[88] interactions (in the particle-hole channel) inherited from the normal Fermi liquid phase adjacent to the BCS superconductor, and modifies the effective spin diffusion constant in the presence of the interactions.[37] The parameter Γ_c, on the other hand, characterizes the residual interaction in the particle-particle Cooper channel and may be interpreted for $\Gamma_c<0$ as an attractive BCS interaction in a different, spin-singlet (e.g., s-wave) pairing channel.[89] Summarizing, the interaction sector of the Finkel'stein NLσM defined by Eq. (2.50) can be reexpressed as follows:

$$S_I = i \sum_{a=1,2} \xi^a \int dt d^d\mathbf{r} (\Gamma_s [Q_{t,t}^{a,a}(\mathbf{r}) + Q_{t,t}^{\dagger a,a}(\mathbf{r})]^2$$
$$+ \Gamma_c [Q_{t,t}^{a,a}(\mathbf{r}) - Q_{t,t}^{\dagger a,a}(\mathbf{r})]^2)$$
$$= i \sum_{a=1,2} \xi^a \int dt d^d\mathbf{r} (\Gamma_s [S_Z^a(t,\mathbf{r})]^2 + \Gamma_c \bar{\Delta}_S^a(t,\mathbf{r}) \Delta_S^a(t,\mathbf{r})),$$
(C14)

where the fields $S_Z^a(t,\mathbf{r})$, $\Delta_S^a(t,\mathbf{r})$, and $\bar{\Delta}_S^a(t,\mathbf{r})$ may be written in terms of $Q_{t,t}^{a,a}(\mathbf{r})$ and $Q_{t,t}^{\dagger a,a}(\mathbf{r})$, and represent the electron bilinear operators

$$S_Z^a(t,\mathbf{r}) \sim \xi^a [\bar{c}_\uparrow^a(t,\mathbf{r}) c_\uparrow^a(t,\mathbf{r}) - \bar{c}_\downarrow^a(t,\mathbf{r}) c_\downarrow^a(t,\mathbf{r})], \quad (C15)$$

$$\Delta_S^a(t,\mathbf{r}) \sim \xi^a c_\downarrow^a(t,\mathbf{r}) c_\uparrow^a(t,\mathbf{r}), \quad (C16)$$

$$\bar{\Delta}_S^a(t,\mathbf{r}) \sim \xi^a \bar{c}_\uparrow^a(t,\mathbf{r}) \bar{c}_\downarrow^a(t,\mathbf{r}). \quad (C17)$$

As written, $\Delta_S^a(t,\mathbf{r})$ represents the simplest singlet channel pairing amplitude, $a \in \{1,2\}$ is the Keldysh index, and ξ^a was defined by Eq. (2.4).

APPENDIX D: FREQUENCY-MOMENTUM SHELL INTEGRALS

The frequency-momentum loop integrations needed in the RG calculation described in Sec. IV are cataloged in this appendix. All integrations listed below are taken over a portion of the frequency-momentum shell [Eqs. (3.11a), (3.11b), and (3.11c) and Fig. 6],

$$\int \frac{d\omega d^2\mathbf{k}}{(2\pi)^3} = \frac{1}{2D(2\pi)^2} \int d\omega dx$$
$$\equiv \frac{1}{2D(2\pi)^2} \left[\int_0^\Lambda d\omega \int_{\tilde{\Lambda}}^\Lambda dx + \int_0^\Lambda dx \int_{\tilde{\Lambda}}^\Lambda d\omega \right],$$
(D1)

unless stated otherwise. In this equation, we have made the change of integration variables $D\mathbf{k}^2 \equiv x$. [D is the (heat) diffusion constant defined by Eq. (3.9).] The ratio of the cutoffs in Eq. (D1) is given by the expression

$$\frac{\Lambda}{\tilde{\Lambda}} \approx 1 + 2dl, \quad (D2)$$

with $0<dl\ll1$.

The integrals are as follows:

$$J_1(z;z') \equiv \frac{1}{2(2\pi D)^2} \int d\omega dx x \frac{1}{(x-iz\omega)^2} \frac{1}{x-iz'\omega}$$
$$= \frac{1}{2(2\pi D)^2} \frac{i2dl}{z-z'} \left[1 - \frac{z'}{z-z'} \ln\left(\frac{z}{z'}\right) \right], \quad (D3)$$

$$J_2(z,z') \equiv \frac{1}{2D(2\pi)^2} \int d\omega dx \frac{1}{x-iz\omega} \frac{1}{x-iz'\omega} = \frac{1}{2D(2\pi)^2} \frac{i2dl}{z-z'} \ln\left(\frac{z}{z'}\right), \tag{D4}$$

$$J_3(z) \equiv \frac{1}{2D(2\pi)^2} \int d\omega dx \frac{1}{(x-iz\omega)^2} = \frac{1}{2D(2\pi)^2} \frac{i2dl}{z}, \tag{D5}$$

$$J_4(z;z') \equiv \frac{1}{2D(2\pi)^2} \int d\omega dx \omega \frac{1}{(x-iz\omega)^2} \frac{1}{x-iz'\omega} = \frac{1}{2D(2\pi)^2} \frac{2dl}{z-z'} \left[\frac{1}{z} - \frac{1}{z-z'} \ln\left(\frac{z}{z'}\right)\right], \tag{D6}$$

$$J_5(z) = \frac{1}{2D^2(2\pi)^3} \left[\int_0^\Lambda d\omega \int_0^\Lambda d\omega' \int_{\tilde{\Lambda}}^\Lambda dx + \int_0^\Lambda dx \int_0^\Lambda d\omega \int_{\tilde{\Lambda}}^\Lambda d\omega' + \int_0^\Lambda dx \int_0^\Lambda d\omega' \int_{\tilde{\Lambda}}^\Lambda d\omega \right] x \frac{1}{(x-iz\omega)^2} \frac{1}{(x-iz\omega')^2}$$

$$= \frac{-1}{2D^2(2\pi)^3} \frac{2dl}{z^2}. \tag{D7}$$

*foster@phys.columbia.edu

[1] For a recent account, see: S. V. Kravchenko and M. P. Sarachik, Rep. Prog. Phys. **67**, 1 (2004); A. Punnoose and A. M. Finkel'stein, Science **310**, 289 (2005).

[2] A. M. Finkel'stein, Zh. Eksp. Teor. Fiz. **84**, 168 (1983) [Sov. Phys. JETP **57**, 97 (1983)].

[3] For a review, see, e.g., D. Belitz and T. R. Kirkpatrick, Rev. Mod. Phys. **66**, 261 (1994).

[4] We will employ the term "Anderson–Mott" insulator in this work to describe an insulating state dominated by *both* strong disorder and strong interactions.

[5] M. S. Foster and A. W. W. Ludwig, Phys. Rev. B **74**, 241102(R) (2006).

[6] For a recent discussion, see, e.g., A. Auerbach, *Interacting Electrons and Quantum Magnetism* (Springer-Verlag, New York, 1994).

[7] M. R. Zirnbauer, J. Math. Phys. **37**, 4986 (1996).

[8] For recent references that treat the one-dimensional case, see, e.g., L. Balents and M. P. A. Fisher, Phys. Rev. B **56**, 12970 (1997); M. Bocquet, Nucl. Phys. B **546**, 621 (1999).

[9] R. Gade and F. Wegner, Nucl. Phys. B **360**, 213 (1991); R. Gade, *ibid.* **398**, 499 (1993).

[10] P. A. Lee and D. S. Fisher, Phys. Rev. Lett. **47**, 882 (1981).

[11] A. Furusaki, Phys. Rev. Lett. **82**, 604 (1999).

[12] M. Fabrizio and C. Castellani, Nucl. Phys. B **583**, 542 (2000).

[13] S. Guruswamy, A. LeClair, and A. W. W. Ludwig, Nucl. Phys. B **583**, 475 (2000).

[14] S. Ryu and Y. Hatsugai, Phys. Rev. B **65**, 033301 (2001).

[15] O. Motrunich, K. Damle, and D. A. Huse, Phys. Rev. B **65**, 064206 (2002).

[16] M. Bocquet and J. T. Chalker, Phys. Rev. B **67**, 054204 (2003); Ann. Henri Poincare **4**, S539 (2003).

[17] C. Mudry, S. Ryu, and A. Furusaki, Phys. Rev. B **67**, 064202 (2003).

[18] M. S. Foster and A. W. W. Ludwig, Phys. Rev. B **73**, 155104 (2006).

[19] The presence of a Fermi surface with a finite extent, i.e., of codimension 1, is a model-dependent detail. If a particular lattice model possesses an extended Fermi surface, then the advent of SLS guarantees that that surface is nested [Eq. (1.5)]. See, e.g., Refs. 18, 20, and 21 for 2D counterexamples involving massless Dirac-like Fermi points.

[20] M. P. A. Fisher and E. Fradkin, Nucl. Phys. B **251**, 457 (1985); E. Fradkin, Phys. Rev. B **33**, 3257 (1986).

[21] Y. Hatsugai, X.-G. Wen, and M. Kohmoto, Phys. Rev. B **56**, 1061 (1997).

[22] J. E. Hirsch, Phys. Rev. Lett. **51**, 1900 (1983); Phys. Rev. B **31**, 4403 (1985).

[23] J. E. Gubernatis, D. J. Scalapino, R. L. Sugar, and W. D. Toussaint, Phys. Rev. B **32**, 103 (1985).

[24] R. Shankar, Rev. Mod. Phys. **66**, 129 (1994).

[25] See, e.g., J. R. Schrieffer, *Theory of Superconductivity*, Revised printing (Westview, Boulder, CO, 1999).

[26] R. T. Scalettar, E. Y. Loh, J. E. Gubernatis, A. Moreo, S. R. White, D. J. Scalapino, R. L. Sugar, and E. Dagotto, Phys. Rev. Lett. **62**, 1407 (1989).

[27] A. Moreo, D. J. Scalapino, R. L. Sugar, S. R. White, and N. E. Bickers, Phys. Rev. B **41**, 2313 (1990).

[28] Note that for $U<0$ in Eqs. (1.1) and (1.8), we will also have an additional, competing superconducting instability; in this case, although the critical Fermi liquid phase is expected to be unstable, we cannot determine the actual ground state without more detailed arguments.

[29] R. Staudt, M. Dzierzawa, and A. Muramatsu, Eur. Phys. J. B **17**, 411 (2000); P. R. C. Kent, M. Jarrell, T. A. Maier, and T. Pruschke, Phys. Rev. B **72**, 060411(R) (2005).

[30] R. Vlaming, G. S. Uhrig, and D. Vollhardt, J. Phys.: Condens. Matter **4**, 7773 (1992).

[31] G. S. Uhrig and R. Vlaming, J. Phys.: Condens. Matter **5**, 2561 (1993).

[32] R. Berkovits, J. W. Kantelhardt, Y. Avishai, S. Havlin, and A. Bunde, Phys. Rev. B **63**, 085102 (2001).

[33] M. Ma, Phys. Rev. B **26**, 5097 (1982).

[34] C. Huscroft and R. T. Scalettar, Phys. Rev. B **55**, 1185 (1997); R. T. Scalettar, N. Trivedi, and C. Huscroft, *ibid.* **59**, 4364 (1999).

[35] D. Heidarian and N. Trivedi, Phys. Rev. Lett. **93**, 126401 (2004).

[36] L. Dell'Anna, Nucl. Phys. B **758**, 255 (2006).

[37] M. Jeng, A. W. W. Ludwig, T. Senthil, and C. Chamon, Bull. Am. Phys. Soc. **46**, 231 (2001); arXiv:cond-mat/0112044 (unpublished); M. Jeng, Ph.D. thesis, University of California, Santa Barbara, 2002.

[38] M. Ulmke and R. T. Scalettar, Phys. Rev. B **55**, 4149 (1997).

[39] P. J. H. Denteneer, R. T. Scalettar, and N. Trivedi, Phys. Rev. Lett. **87**, 146401 (2001).

[40] For a review, see, e.g., P. A. Lee and T. V. Ramakrishnan, Rev. Mod. Phys. **57**, 287 (1985).

[41] M. L. Horbach and G. Schoen, Ann. Phys. **2**, 51 (1993); A. Kamenev and A. Andreev, Phys. Rev. B **60**, 2218 (1999); C. Chamon, A. W. W. Ludwig, and C. Nayak, *ibid.* **60**, 2239 (1999).

[42] A. Altland and M. R. Zirnbauer, Phys. Rev. B **55**, 1142 (1997).

[43] Invariance of the action in Eqs. (2.2) and (2.3) under the path integral version of the sublattice symmetry transformation prevents the appearance of terms linear in $n^a_{Ai/Bj}$ in these equations. We take the SLS transformation of the Grassmann fields to be identical in form to the operator-level deformation given by Eq. (1.2), with the replacement $c^\dagger_{Ai/Bj} \to \bar{c}^a_{Ai/Bj}(t)$, etc. Normal-ordering issues are most simply resolved with this convention.

[44] In Eq. (2.7), for simplicity of presentation, we have assumed sublattice inversion symmetry: $\varepsilon(-\mathbf{k}) = \varepsilon(\mathbf{k})$.

[45] Recall that, even at the level of the effective field theory [Eqs. (2.28)–(2.30)], the Keldysh construction assures us that the generating functional Z [Eq. (2.27)] is normalized to 1.

[46] We do not provide a precise relationship between λ and $\lambda^{(m)}$ since such a connection depends on various nonuniversal lattice-scale details.

[47] T. Senthil, M. P. A. Fisher, L. Balents, and C. Nayak, Phys. Rev. Lett. **81**, 4704 (1998); T. Senthil and M. P. A. Fisher, Phys. Rev. B **60**, 6893 (1999).

[48] S. Vishveshwara, T. Senthil, and M. P. A. Fisher, Phys. Rev. B **61**, 6966 (2000).

[49] M. Fabrizio, L. Dell'Anna, and C. Castellani, Phys. Rev. Lett. **88**, 076603 (2002).

[50] V. Kagalovsky, B. Horovitz, Y. Avishai, and J. T. Chalker, Phys. Rev. Lett. **82**, 3516 (1999); T. Senthil, J. B. Marston, and M. P. A. Fisher, Phys. Rev. B **60**, 4245 (1999); I. A. Gruzberg, A. W. W. Ludwig, and N. Read, Phys. Rev. Lett. **82**, 4524 (1999); E. J. Beamond, J. Cardy, and J. T. Chalker, Phys. Rev. B **65**, 214301 (2002).

[51] S. Hikami, Phys. Lett. **98B**, 208 (1981); A. M. Polyakov, *Gauge Fields and Strings* (Harwood, London, 1988); F. Wegner, Nucl. Phys. B **316**, 663 (1989).

[52] For a review, see *The Quantum Hall Effect*, 2nd ed., edited by R. E. Prange and S. M. Girvin (Springer-Verlag, New York, 1990).

[53] See, e.g., T.-L. Ho, Phys. Rev. Lett. **81**, 742 (1998).

[54] See, e.g., D. Vollhardt and P. Woelfle, *The Superfluid Phases of Helium 3* (Taylor & Francis, New York, 1990).

[55] M. A. Baranov, A. M. M. Pruisken, and B. Škorić, Phys. Rev. B **60**, 16821 (1999).

[56] It can be easily shown that the one-loop, Wilsonian background field calculation requires the expansion of Eqs. (3.2) and (3.3) only to second order in the $\hat{Y}$.

[57] G. Kotliar and S. Sorella, in *Field Theory in Condensed Matter Physics*, edited by Z. Tesanovic (Addison-Wesley, Redwood

CA, 1990).

[58] T. R. Kirkpatrick and D. Belitz, Phys. Rev. B **50**, 8272 (1994).

[59] B. L. Altshuler and A. G. Aronov, in *Electron-Electron Interactions in Disordered Systems*, edited by A. L. Efros and M. Pollak (North-Holland, Amsterdam, 1985).

[60] E. P. Nakhmedov, V. Prigodin, S. Çalışkan, and E. Şaşıoglu, Phys. Rev. B **66**, 233105 (2002).

[61] A. M. Rudin, I. L. Aleiner, and L. I. Glazman, Phys. Rev. B **55**, 9322 (1997); I. L. Aleiner, B. L. Altshuler, and M. E. Gershenson, Waves Random Media **9**, 201 (1999).

[62] Similar cancellations must occur at fourth order in $\delta\hat{Q}_S$ and $\delta\hat{Q}^\dagger_S$, although we have not checked this in detail.

[63] At a critical point, z may be uniquely determined through the condition $d\ln h/dl \equiv 0$ (Refs. 3 and 18).

[64] F. Wegner, Nucl. Phys. B **280**, 210 (1987).

[65] For a review, see, e.g., A. D. Mirlin, Phys. Rep. **326**, 259 (2000).

[66] Exact expressions for $f_1(\lambda)$ and $f_2(\lambda)$ to all orders in λ were obtained in Ref. 13 in a particular RG scheme.

[67] Note that in Eq. (5.3b), the engineering dimension term $-\epsilon\lambda_A$ arises through the sum of the first and third terms on the right-hand side of this equation.

[68] In the dimensional regularization with minimal subtraction RG scheme, the RG equation for λ in $d = 2 + \epsilon$ can be obtained in this way from that in $d = 2$ dimensions (Ref. 69). Furthermore, the vanishing of the RG function for λ in one scheme implies the same in another scheme. (Moreover, λ_A cannot feed into the RG equation for λ.)

[69] See, e.g., J. Zinn-Justin, *Quantum Field Theory and Critical Phenomena* (Clarendon, Oxford, 1993).

[70] The physical interpretation of the coupling strength λ_A was discussed in Secs. II A 3 and II A 4.

[71] In the asymptotic low-energy regime of the closely related, noninteracting class BDI NLσM (Refs. 9 and 12) in $d = 2$, appropriate to 2D random hopping models for spinless fermions possessing both SLS and TRI (Ref. 13), a "freezing" transition (Refs. 15 and 17) occurs in the dynamic scaling relationship between energy and length, yielding a low-energy density of states as in Eq. (5.7) but with the "typical" exponent $\alpha = 2/3$ (Ref. 72). A similar phenomenon will occur in the broken TRI, sublattice symmetric class AIII model studied in this paper. In this work, we do not discuss such a "frozen" regime because we show in Sec. V B that the interactions flow very rapidly to strong coupling in two dimensions as we renormalize to lower energy scales. We note, however, that if the frozen regime could be reached before interactions destabilize the noninteracting description, a previous result (Ref. 18) for a disordered Dirac (Refs. 15, 17, 20, and 21) realization of class BDI suggests that this regime would also be unstable to interaction effects.

[72] See also, e.g., L. Dell'Anna, Nucl. Phys. B **750**, 213 (2006).

[73] Sharp band structure features (such as van Hove singularities) appearing in the clean limit are typically smeared out in the presence of arbitrarily weak disorder, as can be seen in the self-consistent Born approximation [Eq. (2.33)].

[74] We note that Eqs. (5.10a) and (5.10b) may be alternatively obtained from an analysis performed in the (much simpler) noninteracting 2D (but disordered) theory (using, e.g., replicas or supersymmetry) since these equations describe only the scaling of the interaction operators near the noninteracting fixed point (i.e., are of linear order in the interaction strengths).

[75] Here, we do not consider the regime $\gamma_s < 0$, which corresponds to the condition $U + V < 0$, i.e., where at least one of the micro-

scopic interactions is attractive in the Hubbard-like model defined by Eqs. (1.1) and (1.9).

[76] D. Binosi and L. Theussl, Comput. Phys. Commun. **161**, 76 (2004).

[77] In this case, $\hat{h}$ belongs to the fundamental matrix representation of $u(4N)$.

[78] In the standard basis for the spin-1/2 space Pauli matrices $\hat{\mathbf{J}}$, the condition $-\hat{J}_2\hat{\mathbf{J}}^*\hat{J}_2=\hat{\mathbf{J}}$ follows from the pseudoreality of the fundamental representation of $su(2)$.

[79] In contrast to the ordinary Wigner–Dyson classes typically associated with dirty normal metals, the symmetry classes of quantum disordered systems realized by superconductor quasiparticles often exhibit density of states singularities (Refs. 47 and 80).

[80] T. Senthil and M. P. A. Fisher, Phys. Rev. B **61**, 9690 (2000).

[81] The 2D superconductor is treated within the mean field approximation of pairing and formed from a Fermi liquid with circular Fermi surface.

[82] A. A. Nersesyan, A. M. Tsvelik, and F. Wenger, Nucl. Phys. B **438**, 561 (1995).

[83] TRI dictates that the Dirac nodes always appear in pairs.

[84] P. Fendley and R. M. Konik, Phys. Rev. B **62**, 9359 (2000).

[85] The disorder assumed in Ref. 84, which excludes internode scattering, actually leads to the different random vector potential universality class of Ref. 86. Incorporation of internode scattering, consistent with TRI for the spinless electronic system, recovers the full chiral class BDI.

[86] A. W. W. Ludwig, M. P. A. Fisher, R. Shankar, and G. Grinstein, Phys. Rev. B **50**, 7526 (1994).

[87] In the superconductor context, the FNLσM may be derived by embedding the clean Hamiltonian in Eqs. (C1) and (C7), augmented with a source of quenched disorder (e.g., pure potential scattering) consistent with TRI and spin $U(1)$ symmetries [Eqs. (C11a) and (C11b)], in a Keldysh path integration analogous to that defined by Eqs. (2.1) and (2.2). Residual quasiparticle interactions are encoded as in Eq. (2.3). (See also the discussion at the end of Appendix C.) The structure of the FNLσM is almost entirely determined by Eq. (2.51), which in turn follows from the symmetry structure of the Keldysh action, as detailed in Appendix A. A corresponding analysis in terms of transformations on the Majorana spinor in Eq. (C5) gives the same constraint.

[88] In the polar p-wave state (Refs. 53 and 54) spin $SU(2)$ rotational symmetry is broken down to a $U(1)$ subgroup; as a result, spin-triplet interactions will typically contain anisotropy in spin space, being either easy-axis (z) or easy-plane (xy) dominated; in other words, there will be two interaction coupling constants. In the diffusive FNLσM description of the disordered system, however, only the easy-axis interactions enter (up to irrelevant perturbations) because easy-axis spin is conserved, in analogy to the situation with uniaxial spin symmetry discussed in Ref. 37.

[89] The spin singlet nature of the residual pairing channel characterized by Γ_c is encoded at the coarse level of the FNLσM; other details, especially the orbital pairing symmetry, are not.